NOTE TO USERS

Radiation Pattern of Aperture Coupled Prolate Hemispheroidal Dielectric Resonator Antenna

Yunpeng Song

A Thesis

in

The Department

of

Electrical and Computer Engineering

Presented in Partial Fulfillment of the Requirements
for the Degree of Master of Applied Science(Electrical Engineering) at
Concordia University
Montreal, Quebec, Canada

December 2004

Your file Votre référence
ISBN: 0-494-04400-4
Our file Notre référence
ISBN: 0-494-04400-4

ABSTRACT

Radiation Pattern of Aperture Coupled Prolate Hemispheroidal
Dielectric Resonator Antenna

Yunpeng Song

A detailed analysis and study of a prolate hemispheroidal dielectric resonator antenna (DRA) excited by a rectangular slot aperture are developed. The method used is based on the dyadic Green's function technique in the spheroidal coordinates. In this work, the dyadic Green's functions pertaining to a magnetic-current source located in a dielectric spheroid is derived and expressed in a form convenient for numerical computations. The dyadic Green's functions are then employed to formulate the electromagnetic fields radiated by the DRA. The electromagnetic far field is expressed analytically in a compact form.

The antenna radiation patterns and directivities are computed for different design parameters. The accuracy of the solution is attested by both comparing with HFSS simulation results and with published data for the corresponding hemispherical dielectric resonator antenna. Furthermore, efficient algorithms for calculating the prolate spheroidal wave functions are developed using the software package MATLAB. The algorithm developed here for calculating the prolate spheroidal function is compact, fast, and efficient, and compared well with other results in the literature.

Acknowledgement

I would like to express my sincere gratitude to Professor A. R. Sebak, my supervisor, for his instruction, advice, and helpful discussion throughout the course of this research.

Special thanks to my wife for her patience, constant encouragements and understanding.

Contents

List of Figures

List of Tables

Chapter 1
Introduction

1.1 Survey of dielectric resonator antennas

Since the early experimental study of dielectric resonator antenna (DRA) by Long, McAllister and others [1]-[3], the dielectric resonator antennas have been studied extensively. Much of the early work focused on characterizing the basic properties of DRAs for a variety of simple shapes and feed configurations. It has been shown that dielectric resonator antennas can be used as effective radiators at microwave frequencies where ohmic losses become a serious problem for conventional metallic antennas. DRAs offer a number of advantages such as small size, light weight, low cost, ease of excitation, and ease of integration with active circuitry. Furthermore, they offer wider bandwidth than the microstrip patch antennas commonly used at the same frequency [4].

1.1.1 Cylindrical and half cylindrical dielectric resonator antennas

The first cylindrical dielectric resonator antenna excited by a coaxial probe was investigated by Long *et al.* [1] in 1983. An experimental investigation of the radiation and circuit properties of cylindrical DRAs has been undertaken in their work. Kishk *et al.* [5] studied the cylindrical dielectric resonator antenna excited by a narrow slot in

the ground plane of a microstrip line. The resonance frequencies for various resonators are predicted numerically, and radiation characteristics are verified theoretically. Leung *et al.* [6] investigated an aperture-coupled DRA loaded by a low-profile dielectric resonator disk of a very high permittivity. The antenna bandwidth is increased from 8% to 25%. Other studies have presented different methodologies to obtain circular polarization [7]-[9]. A half cylindrical DRA was investigated by Mongia *et al.* [10]. A microstrip line slot feed scheme is reported in their work.

1.1.2 Hemispherical dielectric resonator antennas

Leung *et al.* [11] studied the hemispherical DRA excited by a coaxial probe both theoretically and experimentally. In their work, the Green's function and method of moment technique are used to derive probe current and input impedance. The input impedance of aperture coupled DRA and cross-polarization characteristic of a probe-fed DRA were well investigated by Leung *et al.* [12], [13]. Other researchers like Kishk *et al.* [14] presented radiation characteristics of a DRA excited by coaxial probe or slot.

1.1.3 Rectangular dielectric resonator antennas

The earliest rectangular DRA was investigated experimentally by McAllister *et al.* [2]. Salameh *et al.* [15] presented a coplanar-waveguide-fed slot-coupled rectangular

dielectric resonator antenna. They have obtained linear polarization patterns with very low-cross polarization components. Oliver *et al.* [16] investigated circular polarized DRA excited by a single slot. The antenna element was mutually orthogonal nearly degenerate modes to generate circular polarization with a low axial ratio over a wide frequency band and a wide beam width.

1.1.4 Triangular dielectric resonator antennas

The triangular DRA is more compact in size than rectangular and circular disk DRAs. They were investigated recently by several researchers. Kishk [17] examined numerically and experimentally a truncated tetrahedron dielectric resonator antenna. The tetrahedron base is an equilateral triangular over a ground plane and excited by a coaxial probe to provide a broad side radiation pattern. The tetrahedron with narrow base attached to the ground plane achieves a wide-band performance, about 40% for the impedance matching and the radiation patterns. In [18] a aperture-coupled equilateral triangular DRA of very high permittivity (ε_r = 82) was investigated experimentally. The impedance matching, radiation patterns and antenna gain were presented.

1.2 Survey of spheroidal geometry applications

Concomitant with the development of the important properties of the spheroidal functions and the development of computer facilities, there have been an increasing number of applications of these functions in computational electromagnetics. Antenna mounted on aircrafts, rockets, satellites, and guided missiles can be considered to have part of a spheroidal shape. Related EM wave scattering problems to these shapes have been studied for many years [25]-[29]. With the development of mobile communications, spheroidal dipoles and monopoles have been investigated intensively [21]-[24]. Also, electromagnetic interaction between the human head and a cellular antenna has been a hot topic in recent years where the human head can be approximated as a dielectric prolate spheroid [36].

1.2.1 Spheroidal antennas

Chu and Stratton [19] investigated the boundary problem of the forced EM oscillations of a conducting prolate spheroid which was fed by a gap of infinitesimal width across the central section of the spheroid. Schelkunoff [20] analyzed the prolate spheroidal antenna where the voltage is applied symmetrically between two halves of the spheroid by means of a biconical transmission line.

Weeks [21] analyzed the prolate spheroidal antenna from a different angle. Instead of having the excitation gap in the centre of the antenna, he allowed the gap to be located arbitrarily along the antenna without disturbing the symmetry in the direction. Some other researchers, such as Jen and Hu [22] presented the radiated field and input admittance of a metallic prolate spheroid excited by a circumferential slot, and Zhang and Sebak [23] studied the radiation characteristics of an asymmetrical slot antenna on a conducting prolate spheroid.

In some practical applications or to widen the beam width of microstrip antenna, the antennas are normally mounted on curved surfaces. Tauchi *et al.* [24] analyzed the radiation characteristics of a circular microstrip antennas inserted at the center of an oblate spheroidal conductor.

1.2.2 Electromagnetic scattering by spheroids

Electromagnetic scattering by a single spheroid or two spheroids have been well investigated, and many analytical solutions have been obtained. Asano and Yamamato [25] studied the EM scattering by a homogeneous prolate (or oblate) spheroidal particle with arbitrary size and refractive index at any angle of incidence. Sinha and Macphie [26], [27] analyzed the scattering of plane wave with arbitrary polarization and angle of incidence by conducting prolate spheroids. Cooray and Ciric [28], [29]

have presented solutions of EM wave scattering by a system of two perfectly conducting or dielectric spheroids of arbitrary orientation.

1.2.3 Electromagnetic waves inside dielectric spheroids

Uzunoglu and Angelikas [30] studied the electromagnetic fields in a three-layered prolate spheroidal human body model due to a loop antenna that is used as an EM therapy apparatus. This investigation of the radiated fields inside a prolate spheroidal human body model due to loop antenna was limited to the scalar analysis and the $\hat{\phi}$-component of fields only. Iskander *et al.* [31-32] investigated the exposure of a prolate spheroidal model to the near field of a short dipole or a small loop antenna, using the extended boundary condition method. Ruppin [33] calculated the electromagnetic power absorption in tissue prolate spheroids irradiated by a plane wave using point-matching method. The calculation is restricted to prolate spheroids of small eccentricities.

1.3 Overview of this report

In this thesis we present an analytical solution for the radiation by a prolate hemispheroidal DRA using dyadic Green's function technique. The aperture-coupled prolate hemispheroidal DRA excited at the fundamental broadside TE_{10} mode is shown in figure 1.1. Radiation patterns are calculated and presented for different

design parameters. The input impedance is also investigated by using Ansoft HFSS. The primary motivation for this study is that no study of hemispheroidal DRA has been found so far, and hemispheroidal DRA has more design freedom than hemispherical DRA. The analysis of the radiation characteristics of a hemispheroidal DRA is very complicated. The difficulty is mainly due to two aspects. One is the very complicated calculation of the spheroidal angular and radial functions; the other is lack of orthogonality of spheroidal vector wave functions. This is part of the reason that there have been fewer reports about the applications of spheroidal wave functions in computational electromagnetics than those related to other canonical geometries.

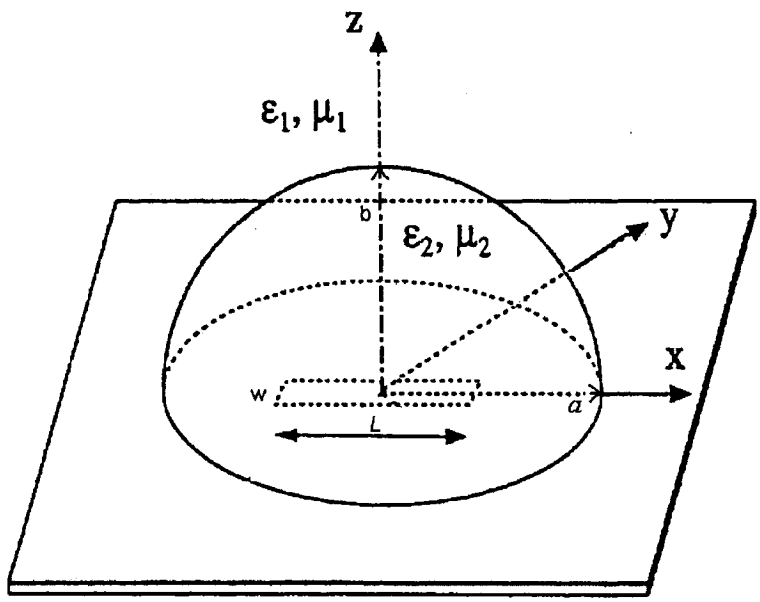

Fig. 1.1 The geometry of a hemispheroidal dielectric resonator antenna excited by a slot aperture

In Chapter 2, the prolate spheroidal wave functions are reviewed and calculated. An efficient algorithm for computing prolate spheroidal wave functions and their eigenvalues is developed with the Matlab software, and numerical results calculated are compared with results in the literature. The numerical results have a better accuracy than other results in the literature.

In Chapter 3, the dyadic Green's functions pertaining to a magnetic-current source located in a dielectric prolate spheroid is formulated. The modal series is represented as a sum of unbounded and scattering solutions. The unbounded solution alone represents the source radiating in the unbounded dielectric medium, while the scattering solution accounts for the presence of the dielectric discontinuity.

In Chapter 4, the unknown scattering coefficients of the dyadic Green's functions are obtained by enforcing the boundary conditions. The scattering coefficients of each of the scattering dyadic Green's functions are coupled with one another. The coupled system of linear equations satisfied by these coefficients is obtained. The point source information is included in the coupled equations. The unknown scattering coefficients cannot be obtained analytically from the equations without calculating the integrals of current source. This is different from the spherical case, where the transmitting and scattering coefficients are independent of integrals of source currents and decoupled from each other. However, for a given source excitation in a spheroidal structure, the current distribution is assumed and the source point does not appear after integration

over the entire source region. Also in Chapter 4, the formulation of electromagnetic far fields are simplified according to the asymptotic form of the spheroidal radial function when $c\xi \to \infty$. The electric far field is expressed in a very simple and compact form.

In Chapter 5, the antenna radiation patterns and directivities are computed numerically for different design parameters. The accuracy of the solution is checked by both comparing with HFSS simulation results and comparing with published data for a corresponding hemispherical dielectric resonator antenna [14] when the axial ratio *b/a* of the hemispheroid approaches one. Also, the input impedance of the hemispheroidal DRA is studied using HFSS.

Finally, in Chapter 6, conclusions are summarized and some recommendations for future research are presented.

Chapter 2
Spheroidal Wave Functions

2.1 Introduction

Spheroidal wave functions are the solutions of the Helmholtz equation in a spheroidal coordinate system. In the evaluation of electromagnetic fields in spheroidal structures, spheroidal wave functions are frequently encountered. Theoretically, the formulation of these functions is well documented by J. A. Stratton *et al.* [34] in 1956 and C. Flammer [35] in 1957. Computation of the spheroidal functions is very complicated, which requires the eigenvalue computation and the forward and backward recursion formulations. There are two kinds of spheroidal coordinate systems: prolate spheroidal coordinates and oblate spheroidal coordinates. In this work, only prolate spheroidal wave functions are computed, because the geometry of the dielectric resonator antenna discussed in this project is a prolate hemispheroid. The oblate spheroidal wave functions can be computed similarly. An efficient algorithm for computing spheroidal prolate wave functions and their eigenvalues is developed with the Matlab software, and the numerical results calculated are compared with results in the literature [36]-[38]. The numerical results agree very well with other results in the literature.

2.2 Prolate spheroidal coordinates

A 3-D prolate spheroid and the prolate spheroidal coordinates (η, ξ, ϕ) are shown in figure 2.1. The prolate spheroidal coordinates are related to the rectangular coordinates (x, y, z) by

$$x = \frac{d}{2}\sqrt{(1-\eta^2)(\xi^2-1)}\cos\phi \tag{2.1a}$$

$$y = \frac{d}{2}\sqrt{(1-\eta^2)(\xi^2-1)}\sin\phi \tag{2.1b}$$

$$z = \frac{d}{2}\eta\xi \tag{2.1c}$$

where

$$-1 \le \eta \le 1,\ 1 \le \xi \le \infty,\ 0 \le \phi \le 2\pi. \tag{2.1d}$$

Eliminating (η, ϕ) and (ξ, ϕ) respectively, we obtain

$$\frac{z^2}{\xi^2} + \frac{x^2+y^2}{\xi^2-1} = (\frac{d}{2})^2 \tag{2.2a}$$

$$\frac{z^2}{\eta^2} - \frac{x^2+y^2}{\eta^2-1} = (\frac{d}{2})^2 \tag{2.2b}$$

It can be seen from equations (2.2a) and (2.2b) that ξ = constant defines a family of confocal ellipses revolving around the major axis, which is the z-axis, and η =

constant defines a family of confocal hyperbolas revolving around the z-axis. In the formulas given above,

$$d = 2 \times \sqrt{b^2 - a^2} \tag{2.2c}$$

is the interfocal distance of the ellipses, with a being the semi-minor axis and b being the semi-major axis of the ellipses.

A prolate spheroidal coordinate system is a curvilinear orthogonal system. Its metric coefficients are given by

$$h_\eta = \sqrt{(\frac{\partial x}{\partial \eta})^2 + (\frac{\partial y}{\partial \eta})^2 + (\frac{\partial z}{\partial \eta})^2} = \frac{d}{2}\sqrt{\frac{\xi^2 - \eta^2}{1 - \eta^2}} \tag{2.3a}$$

$$h_\xi = \sqrt{(\frac{\partial x}{\partial \xi})^2 + (\frac{\partial y}{\partial \xi})^2 + (\frac{\partial z}{\partial \xi})^2} = \frac{d}{2}\sqrt{\frac{\xi^2 - \eta^2}{\xi^2 - 1}} \tag{2.3b}$$

$$h_\phi = \sqrt{(\frac{\partial x}{\partial \phi})^2 + (\frac{\partial y}{\partial \phi})^2 + (\frac{\partial z}{\partial \phi})^2} = \frac{d}{2}\sqrt{(1 - \eta^2)(\xi^2 - 1)} \tag{2.3c}$$

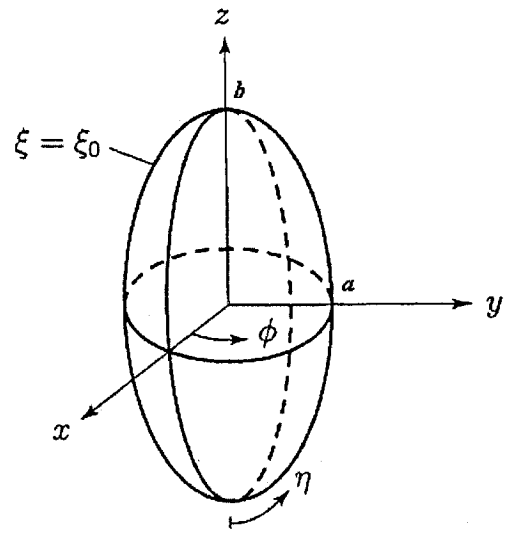

(a)

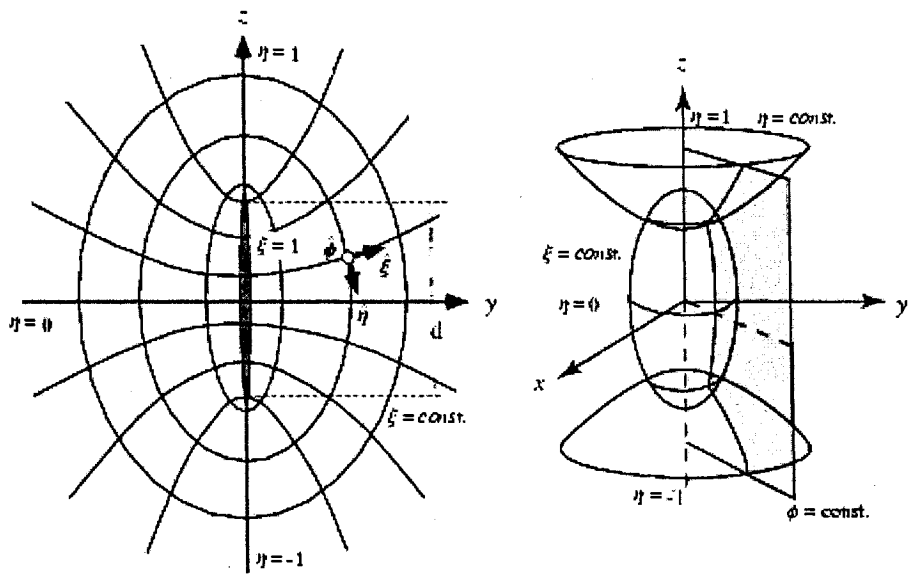

(b)

Fig. 2.1 (a) 3-D geometry of a prolate spheroid; (b) the prolate spheroidal coordinates (η, ξ, ϕ). Coordinate surfaces are prolate spheroids (ξ = constant), hyperboloids of revolution (η = constant), and half-planes (ϕ = constant).

2.3 Wave equation and its solution in prolate spheroidal coordinates

In a curvilinear orthogonal coordinate system, the scalar Helmoholtz wave equation

$$(\nabla^2 + k^2)\psi = 0 \tag{2.4}$$

can be written in a prolate spheroidal coordinate system as

$$\begin{aligned}&[\frac{\partial}{\partial\eta}(1-\eta^2)\frac{\partial}{\partial\eta}+\frac{\partial}{\partial\xi}(\xi^2-1)\frac{\partial}{\partial\xi}+\frac{\xi^2-\eta^2}{(\xi^2-1)(1-\eta^2)}\frac{\partial^2}{\partial\phi^2}]\psi \\ &+c^2(\xi^2-\eta^2)\psi=0\end{aligned} \tag{2.5}$$

where $c=\frac{1}{2}kd$, k is the propagation constant, and d is the interfocal distance.

By the usual procedure of the separation of variables, solution of equation (2.5) can be obtained in the form of the Lame product,

$$\psi_{mn} = S_{mn}(c,\eta)R_{mn}(c,\xi)\begin{matrix}\cos\\ \sin\end{matrix} m\varphi \ . \tag{2.6}$$

Substituting (2.6) into (2.5) and separating the equation, can obtain the second-order differential equations for the angular function $S_{mn}(c, \eta)$ and the radial function $R_{mn}(c, \xi)$ as

$$\frac{d}{d\eta}[(1-\eta 2)\frac{d}{d\eta}S_{mn}(c,\eta)]+[\lambda_{mn}-c^2\eta^2-\frac{m^2}{1-\eta^2}]S_{mn}(c,\eta)=0 \qquad (2.7)$$

$$\frac{d}{d\xi}[(\xi^2-1)\frac{d}{d\xi}R_{mn}(c,\xi)]-[\lambda_{mn}-c^2\xi^2+\frac{m^2}{\xi^2-1}]R_{mn}(c,\xi)=0 \qquad (2.8)$$

In these two equations, m and λ_{mn} are separation constants and, known as eigenvalues. Their values will be determined in the following sections. $S_{mn}(c, \eta)$ and $R_{mn}(c, \xi)$ are called, respectively, the angular and radial prolate spheroidal wave functions.

2.4 Angular and radial prolate spheroidal scalar wave functions

2.4.1 Angular wave functions

There are two linearly independent solutions, or two angular wave functions, that satisfy equation (2.7). They are the angular prolate spheroidal wave functions of the first and second kind given by

$$S_{mn}^{(1)}(c,\eta)=\sum_{k=0,1}^{\infty}{}'d_k^{mn}(c)P_{m+k}^m(\eta) \qquad (2.9)$$

$$S_{mn}^{(2)}(c,\eta)=\sum_{k=-\infty}^{\infty}{}'d_k^{mn}(c)Q_{m+k}^m(\eta) \qquad (2.10)$$

where $d_k^{mn}(c)$ are the expansion coefficients to be determined later; $P_{m+k}^m(x)$ is the associated Legendre function of the first kind with $-1 \le x \le 1$, and $Q_{m+k}^m(x)$ is the associated Legendre function of the second kind with $|x| \ge 1$. The prime on the summation sign indicates that the summation is carried out for even k when *(n-m)* is even and for odd k when *(n-m)* is odd.

In most problems only the angular spheroidal functions of the first kind are required. The angular spheroidal functions of the second kind have not found much application in electromagnetic wave theory. However, it is very useful to calculate the spheroidal radial function of the second kind, which will be introduced in the following sections.

2.4.2 Radial wave functions

The radial prolate spheroidal wave functions, which satisfy equation (2.8), are defined by

$$R_{mn}^{(p)}(c,\xi) = [\sum_{k=0,1}^{\infty}{}' \frac{(2m+k)!}{k!} d_k^{mn}(c)]^{-1} (1-\frac{1}{\xi^2})^{m/2} \cdot \sum_{k=0,1}^{\infty}{}' i^{k+m-n} \frac{(2m+k)!}{k!} d_k^{mn}(c) Z_{m+k}^{(p)}(c\xi) \tag{2.11}$$

where $d_k^{mn}(c)$ are the same expansion coefficients in the expansion of the angular wave functions in equations (2.9) and (2.10). $Z_n^{(p)}(c\xi)$ represents the spherical Bessel functions given by

$$Z^{(1)}(z)=\sqrt{\frac{\pi}{2z}}J_{n+1/2}(z)=j_n(z) \tag{2.12a}$$

$$Z^{(2)}(z)=\sqrt{\frac{\pi}{2z}}Y_{n+1/2}(z)=y_n(z) \tag{2.12b}$$

$$Z^{(3)}(z)=j_n(z)+iy_n(z)=h_n^{(1)}(z) \tag{2.12c}$$

$$Z^{(4)}(z)=j_n(z)-iy_n(z)=h_n^{(2)}(z) \tag{2.12d}$$

with $j_n(z)$ and $y_n(z)$ being the spherical Bessel and Neumann functions, and $h_n^{(1)}(z)$ and $h_n^{(2)}(z)$ denoting the spherical Hankel functions of the first and second kinds. Accordingly, $R_{mn}^{(3)}(c,\xi)$ and $R_{mn}^{(4)}(c,\xi)$ are related to $R_{mn}^{(1)}(c,\xi)$ and $R_{mn}^{(2)}(c,\xi)$ by

$$R_{mn}^{(3)}(c,\xi)=R_{mn}^{(1)}(c,\xi)+iR_{mn}^{(2)}(c,\xi) \tag{2.13a}$$

$$R_{mn}^{(4)}(c,\xi)=R_{mn}^{(1)}(c,\xi)-iR_{mn}^{(2)}(c,\xi) \tag{2.13b}$$

The radial prolate spheroidal wave functions satisfy the Wronskian relation

$$R_{mn}^{(1)}(c,\xi)\frac{d}{d\xi}R_{mn}^{(2)}(c,\xi)-R_{mn}^{(2)}(c,\xi)\frac{d}{d\xi}R_{mn}^{(1)}=\frac{1}{c(\xi^2-1)} \tag{2.14}$$

Equation (2.14) is a very useful relation of $R_{mn}^{(1)}(c,\xi)$ and $R_{mn}^{(2)}(c,\xi)$. It can be used to check the analytical or numerical solutions of $R_{mn}^{(1)}(c,\xi)$ and $R_{mn}^{(2)}(c,\xi)$.

2.4.3 Relation of spheroidal angular and radial wave functions

The angular wave function $S_{mn}(c, \eta)$ and radial wave function $R_{mn}(c, \xi)$ are related by

$$S_{mn}^{(1)}(c,z) = k_{mn}^{(1)}(c) R_{mn}^{(1)}(c,z) \tag{2.15}$$

$$S_{mn}^{(2)}(c,z) = k_{mn}^{(2)}(c) R_{mn}^{(2)}(c,z) \tag{2.16}$$

where $k_{mn}^{(1)}(c)$ and $k_{mn}^{(2)}(c)$ are called the jointing factors given by

$$k_{mn}^{(1)}(c) = \begin{cases} \dfrac{(2m+1)(n+m)! \sum_{k=0}^{\infty}{}' d_k^{mn}(c)(2m+k)!/k!}{2^{n+m} d_0^m(c) c^m m! (\frac{n-m}{2})! (\frac{n+m}{2})!} \\ (n-m = even) \\ \dfrac{(2m+3)(n+m+1)! \sum_{k=1}^{\infty}{}' d_k^{mn}(c)(2m+k)!/k!}{2^{n+m} d_1^m(c) c^{m+1} m! (\frac{n-m-1}{2})! (\frac{n+m+1}{2})!} \\ (n-m = odd) \end{cases} \tag{2.17}$$

and

$$k_{mn}^{(2)}(c) = \begin{cases} \dfrac{2^{n-m}(2m)! (\frac{n-m}{2})! (\frac{n+m}{2})! d_{-2m}^{mn}(c)}{(2m-1)m!(n+m)! c^{m-1}} \sum_{k=0}^{\infty}{}' d_k^{mn}(c)(2m+k)!/k! \\ (n-m = even) \\ \dfrac{2^{n-m}(2m)! (\frac{n-m-1}{2})! (\frac{n+m+1}{2})! d_{-2m+1}^{mn}(c)}{(2m-3)(2m-1)m!(n+m+1)! c^{m-2}} \sum_{k=1}^{\infty}{}' \dfrac{(2m+k)!}{k!} d_k^{mn}(c) \\ (n-m = odd) \end{cases} \tag{2.18}$$

Therefore, the radial wave function of the first kind and the second kind can also be obtained from equation (2.9) and equation (2.10) respectively as

$$R_{mn}^{(1)}(c,\xi)=\frac{1}{k_{mn}^{(1)}(c)}\sum_{k=0,1}^{\infty}{}'d_k^{mn}(c)P_{m+k}^{m}(\xi) \tag{2.19}$$

$$R_{mn}^{(2)}(c,\xi)=\frac{1}{k_{mn}^{(2)}}\sum_{k=-\infty}^{\infty}{}'d_k^{mn}(c)Q_{m+k}^{m}(\xi) \tag{2.20}$$

2.5 Eigenvalues λ_{mn} and expansion coefficients d_k^{mn}

The λ_{mn} in equations (2.7) and (2.8) are the eigenvalues of the prolate spheroidal angular and radial functions. To evaluate the prolate spheroidal wave functions, we have to determine the eigenvalues and the expansion coefficients.

2.5.1 Determination of expansion coefficients $d_k^{mn}(c)$

We substitute equation (2.9) into (2.7), to get

$$\sum_{k=0,1}^{\infty}{}'d_k^{mn}(c)\{\frac{d}{d\eta}[(1-\eta^2)\frac{d}{d\eta}P_{m+k}^{m}(\eta)]$$
$$+[\lambda_{mn}(c)-c^2\eta^2-\frac{m^2}{1-\eta^2}]P_{m+k}^{m}(\eta)\}=0\ . \tag{2.21}$$

Since the associated Legendre functions satisfy the differential equation

$$\frac{d}{d\eta}[(1-\eta^2)\frac{d}{d\eta}P^m_{m+k}(\eta)] + [(m+k)(m+k+1)-\frac{m^2}{1-\eta^2}]P^m_{m+k}(\eta)=0 \tag{2.22}$$

and the recurrence relation

$$(2n+1)\eta P^m_n(\eta)=(n+m)P^m_{n-1}(\eta)+(n-m+1)P^m_{n+1}(\eta) \tag{2.23}$$

we can write (2.21) as

$$\begin{aligned}\sum_{k=0,1}^{\infty}{}' d^{mn}_k(c)\{&\frac{(2m+k)(2m+k-1)}{(2m+2k+1)(2m+k-1)}c^2P^m_{m+k-2}(\eta)\\ &+[(m+k)(m+k+1)-\lambda_{mn}(c)\\ &+\frac{2(m+k)(m+k+1)-2m^2-1}{(2m+2k-1)(2m+2k+3)}c^2]P^m_{m+k}(\eta)\\ &+\frac{(k+1)(k+2)}{(2m+2k+1)(2m+2k+3)}c^2P^m_{m+k+2}(\eta)\}=0\end{aligned} \tag{2.24}$$

Setting the coefficient of the $P^m_{m+k}(\eta)$ equal to zero, we obtain

$$\begin{aligned}&\frac{(2m+k+2)(2m+k+1)}{(2m+2k+5)(2m+2k+3)}c^2d^{mn}_{k+2}(c)+[(m+k)(m+k+1)\\ &-\lambda_{mn}(c)+\frac{2(m+k)(m+k+1)-2m^2-1}{(2m+2k-1)(2m+2k+3)}c^2]d^{mn}_k(c)\\ &+\frac{k(k-1)}{(2m+2k-3)(2m+2k-1)}c^2d^{mn}_{k-2}(c)=0\end{aligned} \tag{2.25a}$$

which provides a recurrence relation for the expansion coefficients $d^{mn}_k(c)$. Let

$$\alpha_k = \frac{(2m+k+2)(2m+k+1)}{(2m+2k+5)(2m+2k+3)}c^2 \tag{2.25b}$$

$$\beta_k = (m+k)(m+k+1) + \frac{2(m+k)(m+k+1) - 2m^2 - 1}{(2m+2k-1)(2m+2k+3)}c^2 \tag{2.25c}$$

$$\gamma_k = \frac{k(k-1)}{(2m+2k-3)(2m+2k-1)}c^2 \tag{2.25d}$$

We rewrite (2.24) in a more compact form as

$$\alpha_0 d_2^{mn}(c) + [\beta_0 - \lambda_{mn}(c)] d_0^{mn}(c) = 0 \tag{2.26a}$$

$$\alpha_1 d_3^{mn}(c) + [\beta_1 - \lambda_{mn}(c)] d_1^{mn}(c) = 0 \tag{2.26b}$$

$$\alpha_k d_{k+2}^{mn}(c) + [\beta_k - \lambda_{mn}(c)] d_k^{mn}(c) + \gamma_k d_{k-2}^{mn}(c) = 0\,. \tag{2.26c}$$

Equations (2.26a)-(2.26c) represent a set of homogeneous equations, from which we can only determine the ratio of the expansion coefficients, that is, $d_k^{mn}(c)/d_{k-2}^{mn}(c)$. If we let $\eta = 0$, the angular wave functions $S_{mn}(c, \eta)$ reduce to the associated Legendre functions. Carrying out the normalization at $\eta = 0$, we require that

$$S_{mn}^{(1)}(c,0) = P_n^m(0) = \frac{(-1)^{(n-m)/2}(n+m)!}{2^n (\frac{n-m}{2})!(\frac{n+m}{2})!} \qquad (n-m = even) \tag{2.27a}$$

and

$$S'^{(1)}_{mn}(c,0) = P'^{m}_{n}(0) = \frac{(-1)^{(n-m-1)/2}(n+m+1)!}{2^n(\frac{n-m-1}{2})!(\frac{n+m+1}{2})!} \quad . \qquad (2.27b)$$
$$(n-m = odd)$$

We thus obtain the normalizing relations:

$$\sum_{k=0}^{\infty}{}' \frac{(-1)^{\frac{k}{2}}(k+2m)!}{2^k(\frac{k}{2})!(\frac{k+2m}{2})!} d_k^{mn}(c)$$
$$= \frac{(-1)^{\frac{n-m}{2}}(n+m)!}{2^{n-m}(\frac{n-m}{2})!(\frac{n+m}{2})!}, \qquad (n - m = even) \qquad (2.28a)$$

and

$$\sum_{k=1}^{\infty}{}' \frac{(-1)^{\frac{k-1}{2}}(k+2m+1)!}{2^k(\frac{k-1}{2})!(\frac{k+2m+1}{2})!} d_k^{mn}(c)$$
$$= \frac{(-1)^{\frac{n-m-1}{2}}(n+m+1)!}{2^{n-m}(\frac{n-m-1}{2})!(\frac{n+m+1}{2})!}, \quad (n - m = odd) \qquad (2.28b)$$

The expansion coefficients $d_k^{mn}(c)$ are thereby uniquely determined.

2.5.2 Determination of eigenvalues $\lambda_{mn}(c)$

It can be seen from equations (2.26a)-(2.26c) that in order to determine the expansion coefficients, we have to find the eigenvalues $\lambda_{mn}(c)$ first. Equations (2.26a)-(2.26c) define a set of homogeneous equations for $d_k^{mn}(c)$. To have a nontrivial solution, the

determinant must be zero, from which we can determine the eigenvalues $\lambda_{mn}(c)$. This is equivalent to solving the tridiagonal eigenvalue problem given by

$$\begin{bmatrix} \beta_0 & \alpha_0 & & & & \\ \gamma_2 & \beta_2 & \alpha_2 & & & \\ & \ddots & \ddots & \ddots & & \\ & & \gamma_{2k} & \beta_{2k} & \alpha_{2k} & \\ & & & \ddots & \ddots & \ddots \end{bmatrix} \begin{bmatrix} d_0^{mn}(c) \\ d_2^{mn}(c) \\ \vdots \\ d_{2k}^{mn}(c) \\ \vdots \end{bmatrix} = \lambda_{mn}(c) \begin{bmatrix} d_0^{mn}(c) \\ d_2^{mn}(c) \\ \vdots \\ d_{2k}^{mn}(c) \\ \vdots \end{bmatrix} \qquad (2.29a)$$

$$(n-m = even)$$

$$\begin{bmatrix} \beta_1 & \alpha_1 & & & & \\ \gamma_3 & \beta_3 & \alpha_3 & & & \\ & \ddots & \ddots & \ddots & & \\ & & \gamma_{2k+1} & \beta_{2k+1} & \alpha_{2k+1} & \\ & & & \ddots & \ddots & \ddots \end{bmatrix} \begin{bmatrix} d_1^{mn}(c) \\ d_3^{mn}(c) \\ \vdots \\ d_{2k+1}^{mn}(c) \\ \vdots \end{bmatrix} = \lambda_{mn}(c) \begin{bmatrix} d_1^{mn}(c) \\ d_3^{mn}(c) \\ \vdots \\ d_{2k+1}^{mn}(c) \\ \vdots \end{bmatrix} . \qquad (2.29b)$$

$$(n-m = odd)$$

The solution of equation (2.29) produces a sequence of eigenvalues $\lambda_{mn}(c)$ $(n = m, m+1, \ldots)$ for a given m and c.

2.6 Computation of prolate radial wave functions of the second kind

Once the expansion coefficients are determined, the prolate spheroidal wave functions can be computed using equations (2.9), (2.10), (2.11), (2.19) and (2.20) except for the radial wave function of the second kind when $c\xi$ is small. When the $c\xi$ is small, the rate of the decrease in $d_k^{mn}(c)$ is about the same as, or even slower than at the beginning, the rate of increase in $y_{m+k}(c\xi)$, thus making the summation converge very slowly. It is very difficult to obtain the accurate value of the prolate radial function of the second kind by simply adding more terms in the summation. In this case, the following method can be employed to calculate $R_{mn}^{(2)}(c,\xi)$ accurately.

In this method, we calculate $R_{mn}^{(2)}(c,\xi)$ from the angular function of the second kind using equation (2.16), let write (2.16) here as

$$R_{mn}^{(2)}(c,\xi) = [k_{mn}^{(2)}(c)]^{-1} S_{mn}^{(2)}(c,\xi) \tag{2.30}$$

where

$$\begin{aligned} S_{mn}^{(2)}(c,\xi) &= \sum_{k=-\infty}^{\infty}{}' d_k^{mn}(c) Q_{m+k}^m(\xi) \\ &= \sum_{k=0,1}^{\infty}{}' d_k^{mn}(c) Q_{m+k}^m(\xi) + \sum_{k=-1,-2}^{-2m \text{ or } -2m+1}{}' d_k^{mn}(c) Q_{m+k}^m(\xi) \cdot \\ &\quad + \sum_{\substack{k=2m+1 \\ 2m+2}}^{\infty}{}' d_{-k}^{mn}(c) Q_{m-k}^m(\xi) \end{aligned} \tag{2.31}$$

In the first summation, where $k \geq 0$, $d_k^{mn}(c)$ can be determined by equations (2.26) and (2.27). In the second summation, where $0 \geq k \geq -2m$, $d_k^{mn}(c)$ can be determined by equation (2.26) using the following procedure. Let us rewrite equation (2.26) as

$$A_{k+2}^m d_{k+2}^{mn}(c) + B_k^m d_k^{mn}(c) + C_{k-2}^m d_{k-2}^{mn}(c) = 0 \tag{2.32}$$

where

$$A_k^m = \alpha_{k-2} \qquad B_k^m = \beta_k - \lambda_{mn}(c) \qquad C_k^m = \gamma_{k+2}. \tag{2.33}$$

Dividing (2.32) by $d_k^{mn}(c)$ and letting $k = -k$ yields

$$\frac{d_{-k}^{mn}(c)}{d_{-k+2}^{mn}} = \frac{-A_{-k+2}^m}{B_{-k}^m + C_{-k-2}^m \dfrac{d_{-k-2}^m(c)}{d_{-k}^{mn}(c)}}. \tag{2.34}$$

Letting $k = k + 2$ and substituting into equation (2.34), we obtain, after a series of such substitutions, a continued fraction

$$\frac{d_{-k}^{mn}(c)}{d_{-k+2}^{mn}(c)} = -\frac{A_{-k+2}^m}{B_{-k}^m -} \frac{C_{-k-2}^m A_{-k}^m}{B_{-k-2}^m -} \frac{C_{-k-4}^m A_{-k-2}^m}{B_{-k-4}^m -} \cdots . \tag{2.35}$$

From equation (2.33) we know that $A_k^m = 0$ when $k = -2m$ or $k = -2m + 1$. Thus, equation (2.35) is a finite continued fraction when $0 > k \geq -2m$, from which we can calculate

$$\frac{d^{mn}_{-2m}(c)}{d^{mn}_{-2m+2}(c)}, \frac{d^{mn}_{-2m+2}(c)}{d^{mn}_{-2m+4}(c)}, \ldots, \frac{d^{mn}_{-2}(c)}{d^{mn}_{0}(c)} \qquad (n - m = even)$$

or

$$\frac{d^{mn}_{-(2m-1)}(c)}{d^{mn}_{-(2m-3)}(c)}, \frac{d^{mn}_{-(2m-3)}(c)}{d^{mn}_{-(2m-5)}(c)}, \ldots, \frac{d^{mn}_{-1}(c)}{d^{mn}_{1}(c)} \qquad (n - m = odd).$$

Since $d^{mn}_{0}(c)$ for $(n - m = even)$ or $d^{mn}_{1}(c)$ for $(n - m = odd)$ is already calculated, $d^{mn}_{-k}(c)$ can be determined for $0 > k \geq -2m$.

In the third summation in equation (2.31), when $d^{mn}_{-k}(c) \to 0$, $Q^{mn}_{m-k}(\xi) \to 0$. However, their product $d^{mn}_{-k}(c)Q^{m}_{m-k} \to$ *finite*. It was shown that

$$Q^{m}_{-(n+1)}(z) = Q^{m}_{n}(z) + \lim_{\rho \to 0} \frac{1}{\rho} P^{m}_{n-\rho}(z). \tag{2.36}$$

From equation (2.36) we can get

$$d^{mn}_{-k}(c)Q^{m}_{m-k}(\xi) = d^{mn}_{\rho|k}(c)P^{m}_{k-m-1}(\xi) \qquad (k > 2m) \tag{2.37}$$

where

$$d^{mn}_{\rho|k}(c) = \lim_{\rho \to 0} \frac{d^{mn}_{-k+\rho}(c)}{\rho}. \tag{2.38}$$

To calculate $d_{\rho|k}^{mn}(c)$, we first use (2.35) to calculate

$$\frac{d_{\rho|2m+2}^{mn}(c)}{d_{-2m}^{mn}(c)} = -\frac{[A_{-2m+\rho}^{m}/\rho]_{\rho\to 0}}{B_{-(2m+2)}^{m}-}\frac{C_{-(2m+4)}^{m}A_{-(2m+2)}^{m}}{B_{-(2m+4)}^{m}-}\frac{C_{-(2m+6)}^{m}A_{-(2m+4)}^{m}}{B_{-(2m+6)}^{m}-}\cdots \qquad (2.39a)$$

(n - m = even)

or

$$\frac{d_{\rho|2m+1}^{mn}(c)}{d_{-(2m-1)}^{mn}(c)} = -\frac{[A_{-(2m-1)+\rho}^{m}/\rho]_{\rho\to 0}}{B_{-(2m+1)}^{m}-}\frac{C_{-(2m+3)}^{m}A_{-(2m+1)}^{m}}{B_{-(2m+3)}^{m}-}\frac{C_{-(2m+5)}^{m}A_{-(2m+3)}^{m}}{B_{-(2m+5)}^{m}-}\cdots \qquad (2.39b)$$

(n - m = odd)

where

$$\left[A_{-2m+\rho}^{m}/\rho\right]_{\rho\to 0} = -\frac{c^2}{(2m-1)(2m+1)} \qquad (2.40a)$$

$$\left[A_{-(2m-1)+\rho}^{m}/\rho\right]_{\rho\to 0} = \frac{c^2}{(2m-1)(2m-1)}\ . \qquad (2.40b)$$

Then, we can calculate

$$\frac{d_{\rho|2m+4}^{mn}(c)}{d_{\rho|2m+2}^{mn}(c)}, \frac{d_{\rho|2m+6}^{mn}(c)}{d_{\rho|2m+4}^{mn}(c)}, \frac{d_{\rho|2m+8}^{mn}(c)}{d_{\rho|2m+6}^{mn}(c)}, \cdots \qquad (n-m = even) \qquad (2.41a)$$

or

$$\frac{d^{mn}_{\rho|2m+3}(c)}{d^{mn}_{\rho|2m+1}(c)}, \frac{d^{mn}_{\rho|2m+5}(c)}{d^{mn}_{\rho|2m+3}(c)}, \frac{d^{mn}_{\rho|2m+7}(c)}{d^{mn}_{\rho|2m+5}(c)}, \cdots \qquad (n-m = odd). \tag{2.41b}$$

Since we have already calculated $d^{mn}_{-2m}(c)$ (for n - m = *even*) or $d^{mn}_{-(2m-1)}(c)$ (for n - m = *odd*), $d^{mn}_{\rho|k}(c)$ can be readily determined for $k = 2m + 2$, $k = 2m + 4$,... (for $n - m$ = *even*) or $k = 2m + 1$, $k = 2m + 3$, ... (for $n - m = odd$).

Finally, substituting equations (2.31) and (2.37) into equation (2.30), we obtain

$$\begin{aligned} R^{(2)}_{mn}(c,\xi) = [k^{(2)}_{mn}(c)]^{-1} [& \sum_{k=0,1}^{\infty}{}' d^{mn}_{k}(c) Q^{m}_{m+k}(\xi) \\ & + \sum_{k=-1,-2}^{\substack{-2m \\ -2m+1}}{}' d^{mn}_{k}(c) Q^{m}_{m+k}(\xi) + \sum_{\substack{k=2m+1 \\ 2m+2}}^{\infty}{}' d^{mn}_{\rho|k}(c) P^{m}_{k-m-1}(\xi)] \end{aligned} \tag{2.42}$$

2.7 Derivatives of spheroidal wave functions

The first-order derivatives of the spheroidal angular functions can be obtained directly by taking the first-order derivatives of the associated Legendre functions. The first-order derivatives of the spheroidal radial functions can be obtained by taking the first-order derivatives of the spherical Bessel functions multiplied by $(1-\frac{1}{\xi^2})^{\frac{m}{2}}$.

2.8 Numerical calculation of spheroidal functions

Expressions for evaluating the angular and radial prolate spheroidal functions and their eigenvalues are computed. An efficient algorithm is developed using Matlab. The numerical results calculated are compared with results in the literature [35-38]. It is found that that the current algorithm is very efficient and accurate. The equations that are finally chosen in my Matlab code are as follows:

- Expansion Coefficients $d_k^{mn}(c)$ using equation (2.21)
- Eigenvalues $\lambda_{mn}(c)$ using equations (2.26a)-(2.26c) and (2.28)
- Prolate spheroidal angular function of the first kind and their first-order derivatives using equation (2.15)
- Prolate spheroidal angular function of the second kind and their first-order derivatives using equation (2.16)
- Prolate spheroidal radial function of the first kind and their first-order derivatives using equation (2.11)
- Prolate spheroidal radial function of the second kind and their first-order derivatives using equations (2.11) and (2.30).

The spheroidal angular and radial functions can be reduced to spherical Legendre and Bessel functions, respectively, when $c \to 0$. Plots of some prolate spheroidal functions are shown in figures 2.2-2.10. Some numerical results computed in this work and others from literatures [35]-[38] are shown in Tables d.1 to d.7 in Appendix

D. All the numerical results have been checked using the Wronskian relation in this work. In Table 2.1, some selected values of the Wronskian computed by this work and other researchers are compared with theoretical values. It can be seen that the algorithm developed here for calculating the prolate spheroidal functions has a better accuracy than other results in the literature.

Table 2.1 Comparison of selected values of the Wronskian computed by Flammer, Li-Wei Li, this work with theoretical values.

c	(m,n)	ξ	Flammer [35]	Li-Wei li [36]	This work	Theoretical values
1.0	(0,0)	1.005	99.75	99.7506	99.7506	99.7506
	(0,1)		99.75	99.7506	99.7506	99.7506
	(0,2)		99.75	99.7506	99.7506	99.7506
	(1,1)		99.75	99.7506	99.7506	99.7506
	(1,2)		99.75	99.7506	99.7506	99.7506
	(2,2)		99.75	99.7506	99.7506	99.7506
	(0,0)	1.077	6.253	6.2528	6.2528	6.2528
	(0,1)		6.253	6.2528	6.2528	6.2528
	(0,2)		6.253	6.2528	6.2528	6.2528
	(1,1)		6.253	6.2528	6.2528	6.2528
	(1,2)		6.253	6.2528	6.2528	6.2528
	(2,2)		6.253	6.2528	6.2528	6.2528
5.0	(0,0)	1.005	19.95	19.9501	19.9501	19.9501
	(0,1)		19.95	19.9501	19.9501	19.9501
	(0,2)		20.77	19.9503	19.9501	19.9501
	(1,1)		19.95	19.9501	19.9501	19.9501
	(1,2)		19.95	19.9501	19.9501	19.9501
	(2,2)		19.95	19.9501	19.9501	19.9501
	(0,0)	1.077	1.2506	1.2506	1.2506	1.2506
	(0,1)		1.2506	1.2506	1.2506	1.2506
	(0,2)		1.2503	1.2509	1.2506	1.2506
	(1,1)		1.2506	1.2506	1.2506	1.2506
	(1,2)		1.2506	1.2506	1.2506	1.2506
	(2,2)		1.2506	1.2506	1.2506	1.2506

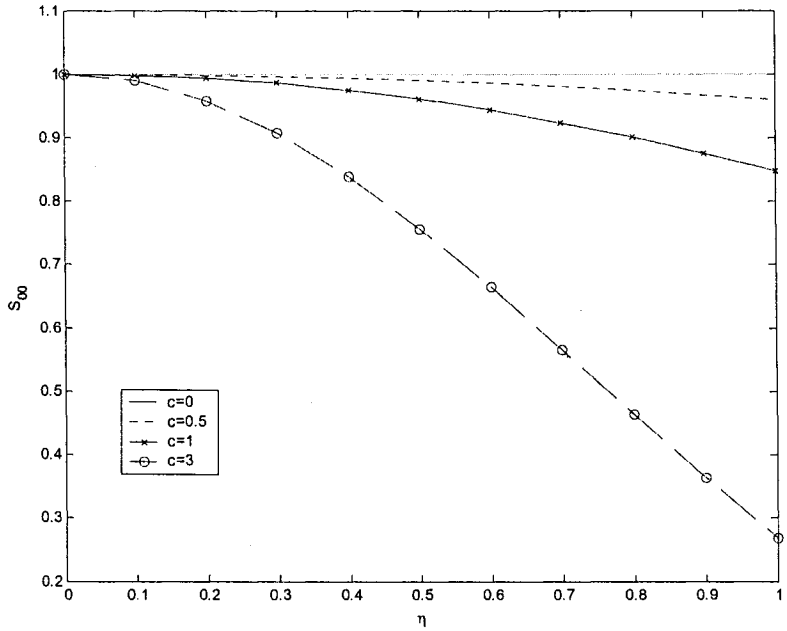

Fig. 2.2 $S_{00}(c,\eta)$ **versus** η **for different values of** c

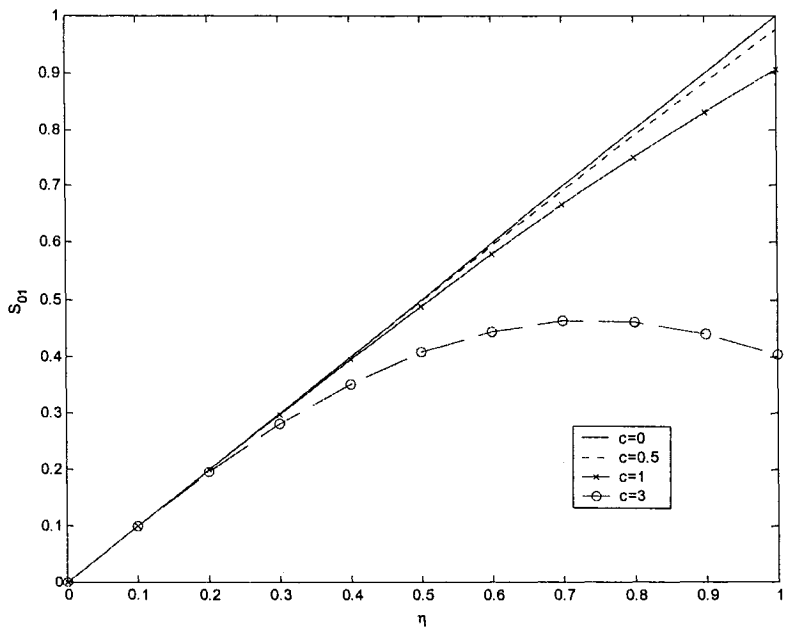

Fig. 2.3 $S_{01}(c,\eta)$ **versus** η **for different values of** c

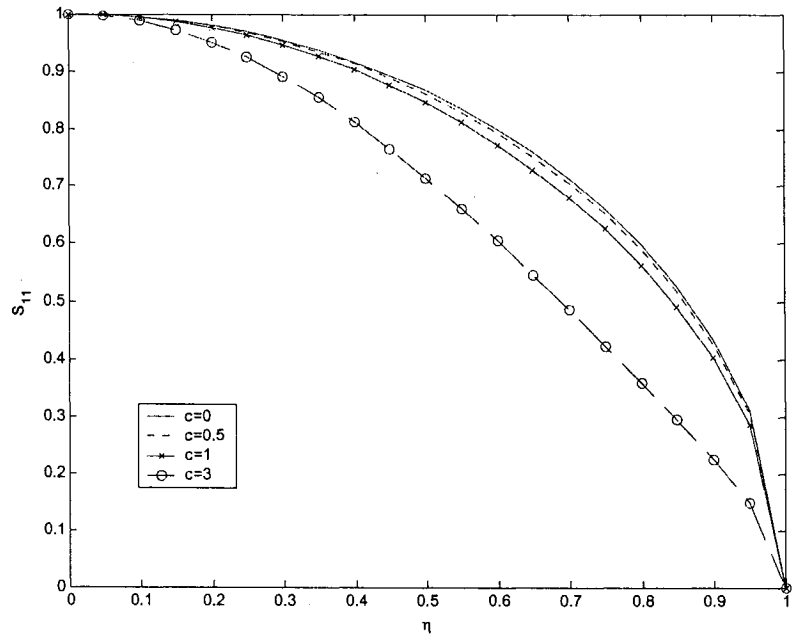

Fig. 2.4 $S_{11}(c,\eta)$ **versus** η **for different values of** c

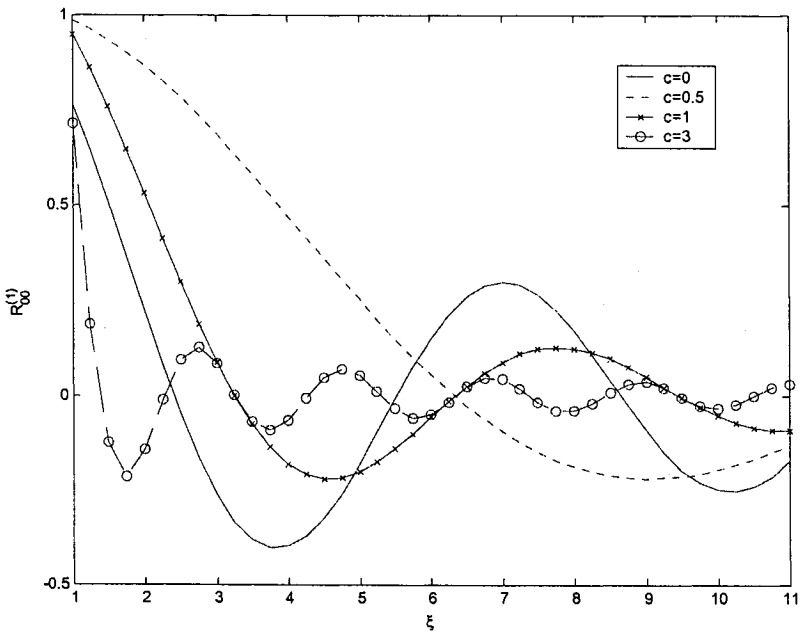

Fig. 2.5 $R_{00}^{(1)}(c,\xi)$ **versus** ξ **for different values of** c

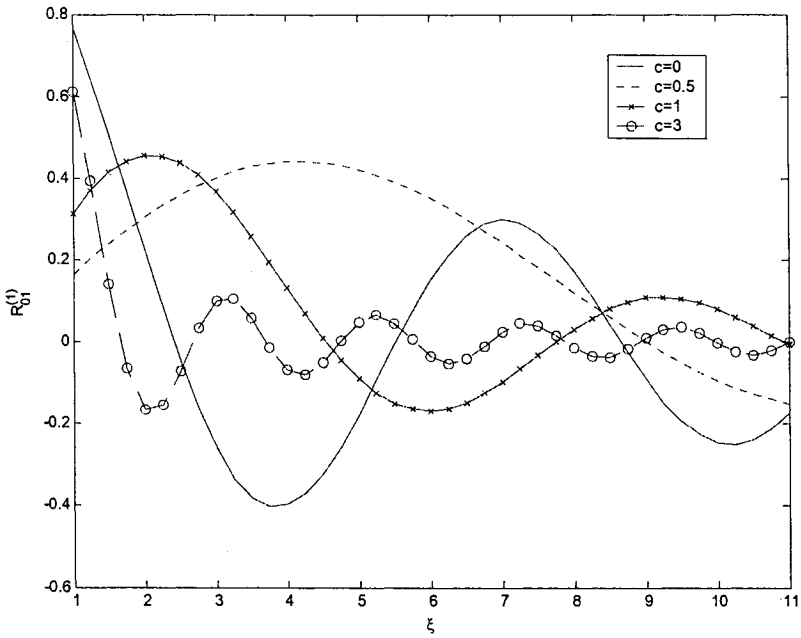

Fig. 2.6 $R_{01}^{(1)}(c,\xi)$ **versus** ξ **for different values of** c

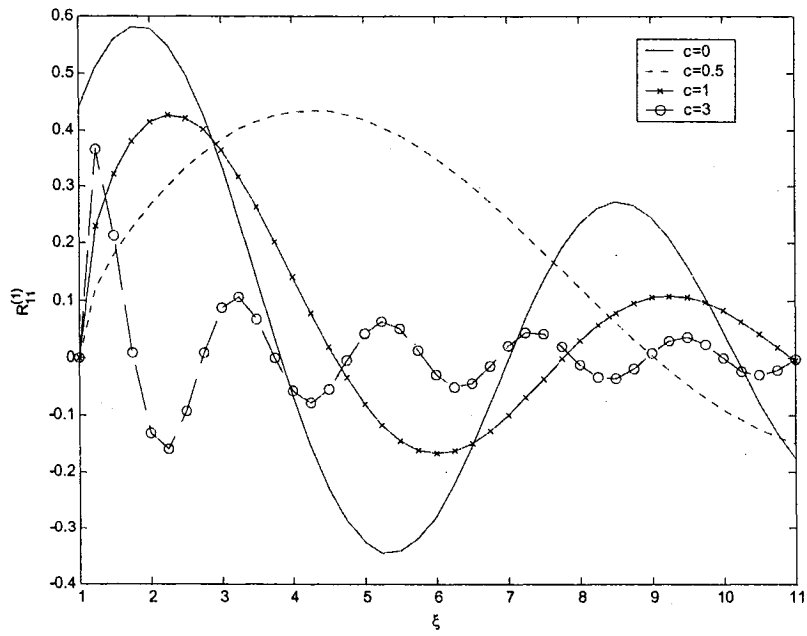

Fig. 2.7 $R_{11}^{(1)}(c,\xi)$ **versus** ξ **for different values of** c

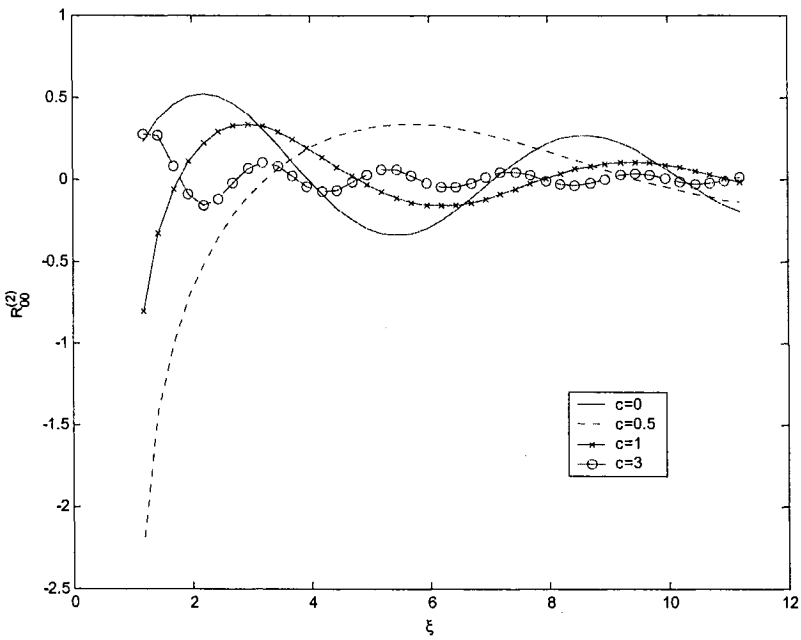

Fig. 2.8 $R_{00}^{(2)}(c,\xi)$ **versus** ξ **for different values of** c

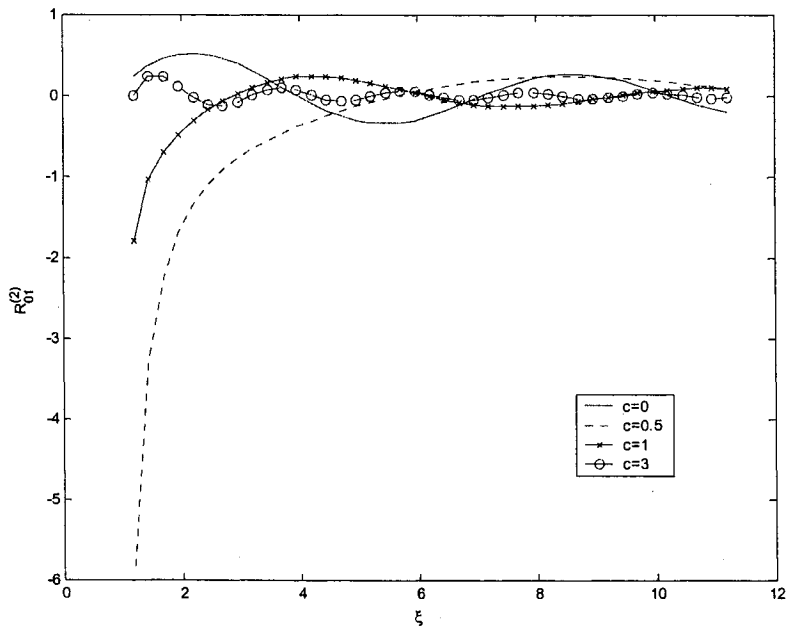

Fig. 2.9 $R_{01}^{(2)}(c,\xi)$ **versus** ξ **for different values of** c

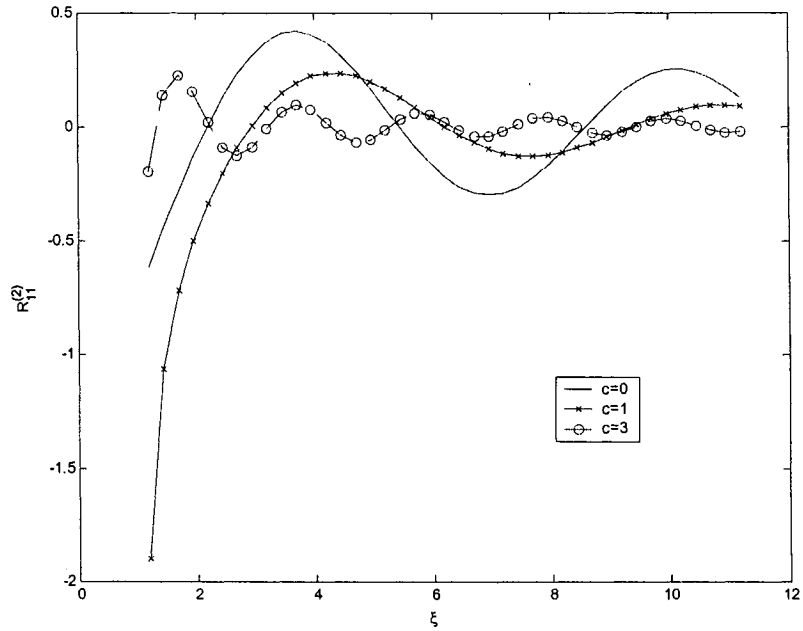

Fig. 2.10 $R_{11}^{(2)}(c,\xi)$ **versus** ξ **for different values of** c

2.9 Prolate spheroidal vector wave functions

A vector wave function, by definition, is an eigenfunction that is a solution of homogeneous vector wave equation. The vector wave functions are the building blocks of the eigenfunction expansions of various kinds of dyadic Green's functions. These functions were first introduced by Hansen [39]-[41] in formulating certain electromagnetic problems. The effectiveness of these functions was recognized by Stratton [42] who, for example, reformulated Mie's theory of diffraction of a plane electromagnetic wave by a sphere using the spherical vector wave function. In his

original work Hansen introduced three kinds of vector wave functions, denoted by $\boldsymbol{L}$, $\boldsymbol{M}$, and $\boldsymbol{N}$, which are solution of the homogeneous vector Helmholtz equation

$$(\nabla^2 + k^2)\boldsymbol{A} = 0. \tag{2.43}$$

Since it operates on vectors, by ∇^2 we mean here the operator

$$\nabla^2 = \nabla\nabla\cdot - \nabla\times\nabla\times\cdot \tag{2.44}$$

Since the gradient operator commutes with the Laplacian, one can obtain immediately an irrotational solution $\boldsymbol{L}$ of the vector wave equation from a solution ψ of the scalar wave equation, simply by taking the gradient of ψ. Thus

$$\boldsymbol{L} = \nabla\psi \tag{2.45}$$

is an irrotational vector wave function. We do not use $\boldsymbol{L}$ in this project.

Of more importance, however, are the solenoidal vector wave functions, which satisfy the equation

$$\nabla\times\nabla\times\boldsymbol{A} - k^2\boldsymbol{A} = 0 \tag{2.46}$$

The divergenceless nature of the functions is ensured by writing them in the form

$$A = \nabla \times \hat{a}\psi \tag{2.47}$$

where ψ is a scalar wave function, and $\hat{a}$ is a constant vector or the position vector. A can be expressed in the form

$$A = \nabla\psi \times \hat{a}, \qquad \hat{a} = \hat{e} \; or \; \hat{r} \tag{2.48}$$

where $\hat{e}$ denotes a constant unit vector such as $(\hat{x}, \hat{y}, \hat{z})$ and $\hat{r}$ is the position vector. If A is a solution of equation (2.46), a further solution is obviously $\nabla \times A$.

Spheroidal vector wave functions are obtained by expressing the quantities in equation (2.48) in spheroidal coordinates. The transformation between the unit vectors in the Cartesian and spheroidal coordinate systems is

$$\hat{x} = -\eta\left(\frac{\xi^2 - 1}{\xi^2 - \eta^2}\right)^{\frac{1}{2}} \cos\phi\hat{\eta} + \xi\left(\frac{1 - \eta^2}{\xi^2 - \eta^2}\right)^{\frac{1}{2}} \cos\phi\hat{\xi} - \sin\phi\hat{\phi}, \tag{2.49a}$$

$$\hat{y} = -\eta\left(\frac{\xi^2 - 1}{\xi^2 - \eta^2}\right)^{\frac{1}{2}} \sin\phi\hat{\eta} + \xi\left(\frac{1 - \eta^2}{\xi^2 - \eta^2}\right)^{\frac{1}{2}} \sin\phi\hat{\xi} + \cos\phi\hat{\phi}, \tag{2.49b}$$

$$\hat{z} = \xi\left(\frac{1 - \eta^2}{\xi^2 - \eta^2}\right)^{\frac{1}{2}} \hat{\eta} + \eta\left(\frac{\xi^2 - 1}{\xi^2 - \eta^2}\right)^{\frac{1}{2}} \hat{\xi}. \tag{2.49c}$$

The position vector $\hat{r}$ becomes, in spheroidal coordinates,

$$\hat{r} = \frac{1}{2} d\eta \left(\frac{1-\eta^2}{\xi^2-\eta^2}\right)^{\frac{1}{2}} \hat{\eta} + \frac{1}{2} d\xi \left(\frac{\xi^2-1}{\xi^2-\eta^2}\right)^{\frac{1}{2}} \hat{\xi}. \tag{2.50}$$

The spheroidal scalar wave functions are denoted in equation (2.6), they are

$$\psi^{(i)}{}_{mn} = S_{mn}(c,\eta) R^{(i)}_{mn}(c,\xi) \begin{matrix} cos \\ sin \end{matrix} m\phi \ . \tag{2.51}$$

We define now the following spheroidal vector wave functions:

$$\boldsymbol{M}^{a(i)}_{\substack{e_{mn} \\ o}}(c;\eta,\xi,\phi) = \nabla \times \left[\psi^{(i)}_{\substack{e_{mn} \\ o}} \hat{a} \right] \tag{2.52}$$

$$\boldsymbol{N}^{a(i)}_{\substack{e_{mn} \\ o}}(c;\eta,\xi,\phi) = \frac{1}{k} \nabla \times \nabla \times \left[\psi^{(i)}_{\substack{e_{mn} \\ o}} \hat{a} \right] \tag{2.53}$$

where $\hat{a} = \hat{x}$, $\hat{y}$, $\hat{z}$; or $\hat{r}$.

The explicit expression of the vector wave functions defined above is given in Appendix B. The vector wave functions of any one set are, unfortunately, neither orthogonal among themselves, nor orthogonal to those of the other sets. The appropriate spheroidal vector wave functions in terms of eigenfunction expansions are discussed in Chapter 3. Expansions of electromagnetic field in dyadic Green's function are also discussed in Chapter 3. It is worth noting that in the limit when the focal distance d becomes zero or the radial coordinate approach infinity (η = constant), $S_{mn}(c,\eta)$ reduces to the associated Legendre functions, $R^{(i)}_{mn}(c,\xi)$ reduces

to the spherical Bessel function and the spheroidal vector wave functions above reduce to vector wave functions in spherical coordinate system.

Chapter 3
Dyadic Green's Functions in Prolate Spheroidal System

3.1 Introduction

To analyze the electromagnetic radiation from an arbitrary current distribution located in a layered homogeneous medium, the dyadic Green's function technique is usually adopted. If the geometry is spheroidal, the representation of the dyadic Green's function (DGF) under the spheroidal coordinate system should be the most convenient. If the source current distribution is known, the electromagnetic fields can be integrated directly from DGF, which plays an important role as the response function of multilayered dielectric media. If the source is an unknown current distribution, the method of moments, which expands the current distribution into a series basis functions with unknown coefficients, can be employed. In this case, the DGF is considered as a kernel of the integral equation; and the unknown coefficients of the basis functions can be obtained by enforcing the boundary conditions.

In this work, it is required to get the dyadic Green's functions pertaining to a slot-aperture source inside a dielectric prolate hemi-spheroid, figure 1.1, of $\xi = \xi_0$ (region 2), characterized by permittivity ε_2 and permeability μ_2, and located in an unbounded medium (region 1), characterized by permittivity ε_1 and permeability μ_1. Image

theory shown in figure 3.1 permits the removal of the ground plane by placing a virtual image source of the other side of the ground plane. The ground plane in figure 1.1 is assumed infinite. Image theory can be used to remove the ground plane to obtain an equivalent problem of a full dielectric prolate spheroid excited by a magnetic current source. By applying image theory, the equivalent problem of figure 1.1 is shown in figure 3.2. The dyadic Green's functions $\overline{G}_{e_{m^2}}(r,r')$ pertaining to a magnetic-current source are called the electric and magnetic dyadic Green's function of the second kind according to Tai [43]. The EM fields inside and outside the spheroid are expressed in terms of the spheroidal dyadic Green's functions and an arbitrary current source distribution.

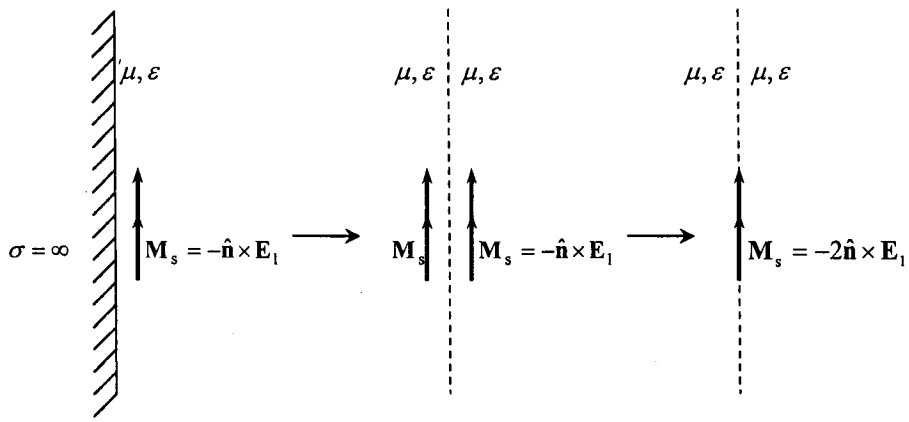

Fig. 3.1 Equivalent models for magnetic source radiation near a perfect electric conductor.

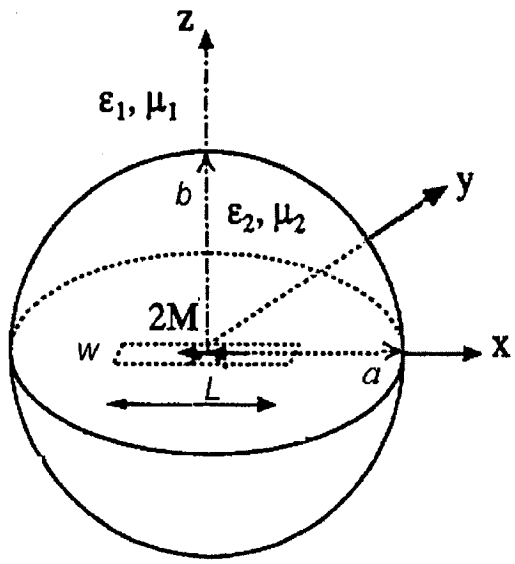

Fig. 3.2 Equivalent problems for the hemispheroidal dielectric resonator antenna in figure 1.1, excited by a slot aperture, after using image theory.

By using the principle of scattering superposition [36], the dyadic Green's functions can be considered as the sum of the unbounded dyadic Green's function and scattering dyadic Green's functions. The unbounded solution represents the source radiating in the unbounded dielectric medium, while the scattering solution accounts for the presence of the dielectric discontinuity. The unbounded dyadic Green's functions under prolate spheroidal coordinates are formulated in terms of prolate spheroidal vector wave functions $\boldsymbol{M}_{\substack{e_{mn} \\ o}}^{a(i)}$ and $\boldsymbol{N}_{\substack{e_{mn} \\ o}}^{a(i)}$ ($a = x, y, z$; and $i = 1, 2, 3$). The scattering dyadic Green's functions are formulated using the method originally developed by Tai [43] and later by Li *et al.* [36]. Scattering coefficients of each of the scattering dyadic Green's functions are coupled with one another. The coupled system of linear equations satisfied by these coefficients is constructed under the

requirements of the boundary conditions, and these unknown coefficients can be solved numerically. The dyadic Green's functions of the first kind $\overline{\overline{G}}_{em^1}(\boldsymbol{r},\boldsymbol{r}')$ pertain to an electric-current source, and the dyadic Green's functions of the second kind $\overline{\overline{G}}_{em^2}(\boldsymbol{r},\boldsymbol{r}')$ pertain to a magnetic-current source. Here, only the dyadic Green's functions of the second kind $\overline{\overline{G}}_{em^2}(\boldsymbol{r},\boldsymbol{r}')$ are presented because the dyadic Green's functions of the first kind $\overline{\overline{G}}_{em^1}(\boldsymbol{r},\boldsymbol{r}')$ can be obtained from the second kind $\overline{\overline{G}}_{em^2}(\boldsymbol{r},\boldsymbol{r}')$ by applying the duality principle $\boldsymbol{M} \to \boldsymbol{H}$, $\boldsymbol{H} \to -\boldsymbol{E}$, $\boldsymbol{J} \to \boldsymbol{M}$, $\boldsymbol{M} \to -\boldsymbol{J}$, $\mu \to \varepsilon$, and $\varepsilon \to -\mu$.

3.2 General formulation

The EM radiation fields $\boldsymbol{E}_f$ and $\boldsymbol{H}_f$ in the fth region (f = 1 and 2), due to magnetic current source $\boldsymbol{M}$ located in region 2 are expressed by

$$\nabla \times \nabla \times \boldsymbol{E}_f - k_f^2 \boldsymbol{E}_f = (-\nabla \times \boldsymbol{M})\delta_{f2} \tag{3.1a}$$

$$\nabla \times \nabla \times \boldsymbol{H}_f - k_f^2 \boldsymbol{H}_f = (j\omega\varepsilon_f \boldsymbol{M})\delta_{f2} \tag{3.1b}$$

where δ_{f2} is the Kronecker delta ($\delta_{f2} = 1$ for $f = 2$ and 0 for $f \neq 2$), $k_f = \omega\sqrt{\mu_f \varepsilon_f}$ is the propagation constant in the fth layer of the multilayered medium. A time dependence $e^{-i\omega t}$ is assumed throughout this project.

The EM field excited by a magnetic current source $\boldsymbol{M}$, which is in region 2, can be expressed in term of integrals containing dyadic Green's functions as

$$\boldsymbol{E}_f(\boldsymbol{r}) = -\iiint_v \overline{\boldsymbol{G}}_{m2}^{(f)}(\boldsymbol{r},\boldsymbol{r}') \cdot \boldsymbol{M}(\boldsymbol{r}')dv' \tag{3.2a}$$

$$\boldsymbol{H}_f(\boldsymbol{r}) = i\omega\varepsilon_f \iiint_v \overline{\boldsymbol{G}}_{e2}^{(f)}(\boldsymbol{r},\boldsymbol{r}') \cdot \boldsymbol{M}(\boldsymbol{r}')dv' \tag{3.2b}$$

where $\boldsymbol{r}$ denotes the coordinates (ξ,η,ϕ) at the field point; $\boldsymbol{r}'$ denotes the coordinates (ξ',η',ϕ') of the magnetic current source $\boldsymbol{M}$; v denotes the volume occupied by the source in region 2; $\overline{\boldsymbol{G}}_{m2}^{(f)}(\boldsymbol{r},\boldsymbol{r}')$ denotes the magnetic dyadic Green's function of the second kind; $\overline{\boldsymbol{G}}_{e2}^{(f)}(\boldsymbol{r},\boldsymbol{r}')$ denotes the electric dyadic Green's function of the second kind. The superscript (f) denotes the dyadic Green's function in region 1 or region 2.

Substituting (3.2a) and (3.2b) into (3.1a) and (3.1b), respectively, we obtain

$$\nabla\times\nabla\times\overline{\boldsymbol{G}}_{e2}^{(f)}(\boldsymbol{r},\boldsymbol{r}') - k_f^2\overline{\boldsymbol{G}}_{e2}^{(f)}(\boldsymbol{r},\boldsymbol{r}') = \bar{\boldsymbol{I}}\delta(\boldsymbol{r}-\boldsymbol{r}')\delta_{f2} \tag{3.3a}$$

$$\nabla\times\nabla\times\overline{\boldsymbol{G}}_{m2}^{(f)}(\boldsymbol{r},\boldsymbol{r}') - k_f^2\overline{\boldsymbol{G}}_{m2}^{(f)}(\boldsymbol{r},\boldsymbol{r}') = \nabla\times\bar{\boldsymbol{I}}\delta(\boldsymbol{r}-\boldsymbol{r}')\delta_{f2} \tag{3.3b}$$

where $\bar{\boldsymbol{I}}$ is the unit dyad and $\delta(\boldsymbol{r}-\boldsymbol{r}')$ is the three-dimensional Dirac delta function. $\overline{\boldsymbol{G}}_{m2}^{(f)}(\boldsymbol{r},\boldsymbol{r}')$ and $\overline{\boldsymbol{G}}_{e2}^{(f)}(\boldsymbol{r},\boldsymbol{r}')$ are related as

$$\nabla\times\overline{\boldsymbol{G}}_{e2}^{(f)}(\boldsymbol{r},\boldsymbol{r}') = \overline{\boldsymbol{G}}_{m2}^{(f)}(\boldsymbol{r},\boldsymbol{r}') \tag{3.3c}$$

$$\nabla \times \overline{G}_{m2}^{(f)}(r,r') = k_f^2 \overline{G}_{e2}^{(f)}(r,r') + \bar{I}\delta(r-r') \tag{3.3d}$$

By solving equations (3.3a) and (3.3b), we can obtain the Dyadic Green's functions of the second kind, which are $\overline{G}_{m2}^{(f)}(r,r')$ and $\overline{G}_{e2}^{(f)}(r,r')$.

Since the electric dyadic Green's functions can be obtained simply from the magnetic dyadic Green's functions using equation (3.3a) or equation (3.3b), we need to solve one of them first. Let's solve the magnetic dyadic Green's function of the second kind $\overline{G}_{m2}^{(f)}(r,r')$. The magnetic dyadic Green's function of the second kind $\overline{G}_{m2}^{(f)}(r,r')$ satisfies the following boundary conditions at the spheroid interface ($\xi = \xi_0$):

$$\hat{\xi} \times \overline{G}_{m2}^{(1)} = \hat{\xi} \times \overline{G}_{m2}^{(2)} \tag{3.4a}$$

$$\frac{1}{\varepsilon_1} \hat{\xi} \times \nabla \times \overline{G}_{m2}^{(1)} = \frac{1}{\varepsilon_2} \hat{\xi} \times \nabla \times \overline{G}_{m2}^{(2)}. \tag{3.4b}$$

To construct the EM dyadic Green's functions in the layered media, two methods are usually employed. One of them is to apply the coordinate tensors to represent the dyadic Green's functions while the other is to use the vector wave functions to formulate the dyadic Green's functions. Here, we will use the latter method to construct the dyadic Green's functions. First, we construct the unbounded dyadic Green's function, and then construct scattering dyadic Green's functions. By using the principle of scattering superposition, the dyadic Green's functions can be considered

as the sum of the unbounded dyadic Green's function and scattering dyadic Green's functions. The unknown scattering and transmission coefficients can be solved by using the following EM boundary conditions at the prolate spheroidal interface, i.e., continuity of the tangential component of both electric and magnetic fields.

$$\hat{\xi} \times \boldsymbol{E}_1 = \hat{\xi} \times \boldsymbol{E}_2 \tag{3.4c}$$

$$\frac{1}{\mu_1} \hat{\xi} \times \nabla \times \boldsymbol{E}_1 = \frac{1}{\mu_2} \hat{\xi} \times \nabla \times \boldsymbol{E}_2 \tag{3.4d}$$

Substituting equations (3.2a) and (3.2b) into equations (3.4c) and (3.4d), we get

$$\hat{\xi} \times \iiint_v \overline{\boldsymbol{G}}_{m2}^{(1)}(\boldsymbol{r},\boldsymbol{r}')\boldsymbol{M}(\boldsymbol{r}')dv' = \hat{\xi} \times \iiint_v \overline{\boldsymbol{G}}_{m2}^{(2)}(\boldsymbol{r},\boldsymbol{r}') \cdot \boldsymbol{M}(\boldsymbol{r}')dv' \tag{3.4e}$$

$$\frac{1}{\mu_1} \hat{\xi} \times \nabla \times \iiint_v \overline{\boldsymbol{G}}_{m2}^{(1)}(\boldsymbol{r},\boldsymbol{r}')\boldsymbol{M}(\boldsymbol{r}')dv' = \frac{1}{\mu_2} \hat{\xi} \times \nabla \times \iiint_v \overline{\boldsymbol{G}}_{m2}^{(2)}(\boldsymbol{r},\boldsymbol{r}')\boldsymbol{M}(\boldsymbol{r}')dv' \tag{3.4f}$$

3.3 Unbounded dyadic Green's functions

According to Tai [43], the unbounded magnetic dyadic Green's functions of the second kind can be expressed in terms of the scalar Green's function $G(\boldsymbol{r},\boldsymbol{r}')$ as

$$\overline{\boldsymbol{G}}_{m0}(\boldsymbol{r},\boldsymbol{r}') = \nabla \times [\bar{I}G(\boldsymbol{r},\boldsymbol{r}')] = \nabla G(\boldsymbol{r},\boldsymbol{r}') \times \bar{I} \tag{3.5}$$

The scalar Green's function $G(\boldsymbol{r},\boldsymbol{r}')$ of the scalar wave equation is, by definition, the function which gives the solution at the point $\boldsymbol{r}$ when there is a unit source at the point $\boldsymbol{r}'$. $G(\boldsymbol{r},\boldsymbol{r}')$ satisfies the inhomogeneous equation

$$(\nabla^2 + k^2)G(\boldsymbol{r},\boldsymbol{r}') = -\delta(\boldsymbol{r}-\boldsymbol{r}') \tag{3.6a}$$

where $\delta(\boldsymbol{r}-\boldsymbol{r}')$ is the three-dimensional Dirac delta function. In spheroidal coordinates $\delta(\boldsymbol{r}-\boldsymbol{r}')$ is

$$\delta(\boldsymbol{r}-\boldsymbol{r}') = h_\eta^{-1}h_\xi^{-1}h_\phi^{-1}\delta(\eta-\eta')\delta(\xi-\xi')\delta(\phi-\phi') \tag{3.6b}$$

When there are no boundaries, the well-known solution of equation (3.6a) which satisfies the radiation condition at infinity, i.e., represents diverging wave at large distance, is

$$G(\boldsymbol{r},\boldsymbol{r}') = \frac{e^{ik|\boldsymbol{r}-\boldsymbol{r}'|}}{4\pi|\boldsymbol{r}-\boldsymbol{r}'|}\,. \tag{3.7}$$

We expand this scalar Green's function in terms of the spheroidal wave functions. According to Flammer [35], we get

$$\begin{aligned} G(\boldsymbol{r},\boldsymbol{r}') &= \frac{e^{ik|\boldsymbol{r}-\boldsymbol{r}'|}}{4\pi|\boldsymbol{r}-\boldsymbol{r}'|} \\ &= \frac{ik}{2\pi}\sum_{n=0}^{\infty}\sum_{m=0}^{n}\frac{2-\delta_{m0}}{N_{mn}}S_{mn}(c,\eta)S_{mn}(c,\eta')^{cos}_{sin}[m(\phi-\phi')] \\ &\quad\times\begin{cases} R_{mn}^{(1)}(c,\xi)R_{mn}^{(3)}(c,\xi'), & \xi<\xi' \\ R_{mn}^{(1)}(c,\xi')R_{mn}^{(3)}(c,\xi), & \xi>\xi' \end{cases} \end{aligned} \tag{3.8}$$

where δ_{m0} is the Kronecker delta and $N_{mn} = 2\sum_{k=0,1}^{\infty}{}' \frac{(k+2m)!(d_k^{mn})^2}{(2k+2m+1)k!}$ is the normalization factor of the angular function of the first kind.

To develop the dyadic Green's functions for a prolate spheroid, a very convenient and compact method is to employ the spheroidal vector wave functions for construction. Several kinds of vector wave functions have been proposed, and almost all of them have been used in the study of plane wave scattering by a single spheroid, a system of two spheroids, and a layered spheroid. However, not all of these vector wave functions can be used conveniently to construct dyadic Green's functions for electromagnetic radiation problems. Although it is possible to use these vector wave functions with piloting vectors $\hat{\eta}, \hat{\xi}$, and $\hat{\phi}$, they are still inconvenient spheroidal vector wave functions. Since $\nabla \times (\hat{\eta}, \hat{\xi}, \hat{\phi}) \neq 0$ in spheroidal coordinates,

$$\nabla \times \underset{o}{\boldsymbol{N}}^{a(i)}_{e_{mn}} \neq k \underset{o}{\boldsymbol{M}}^{a(i)}_{e_{mn}} \tag{3.9}$$

where $a = \eta, \xi$, or ϕ.

Thus, the most appropriate spheroidal vector wave functions for the construction of dyadic Green's functions are defined in terms of the scalar eigenfunctions are

$$\underset{o}{\boldsymbol{M}}^{a(i)}_{e_{mn}}(c;\eta,\xi,\phi) = \nabla \times \left[\underset{o}{\psi}^{(i)}_{e_{mn}} \hat{a} \right] \tag{3.10a}$$

$$\boldsymbol{N}_{\substack{e_{mn}\\o}}^{a(i)}(c;\eta,\xi,\phi)=\frac{1}{k}\nabla\times\nabla\times\left[\psi_{\substack{e_{mn}\\o}}^{(i)}\hat{a}\right] \tag{3.10b}$$

where $\hat{a}=\hat{x}$, $\hat{y}$, $\hat{z}$.

These vector eigenfunctions are obtained by using the scalar eigenfunctions ψ shown in Chapter 2 as the generating function and the coordinate vector $\hat{x}$, $\hat{y}$, or $\hat{z}$ as piloting vector. The explicit expression of the vector wave functions defined above is given in Appendix B. The vector wave functions of any one set are, unfortunately, neither orthogonal among themselves, nor, in general, orthogonal to those of the other sets. Thus, it is inconvenient to employ them to construct dyadic Green's functions by the conventional method described by Tai [43]. A combined method, developed from the two methods above, is thereby presented for spheroid.

In terms of the above-defined spheroidal vector wave functions, the magnetic dyadic Green's function given in (3.5) can be obtained by substituting equation (3.8) into (3.5). We get

$$\begin{aligned}\overline{\boldsymbol{G}}_{m0}(\boldsymbol{r},\boldsymbol{r}')=\frac{ik_2}{2\pi}\sum_{n=0}^{\infty}\sum_{m=0}^{n}\frac{2-\delta_{m0}}{N_{mn}}\cdot\begin{cases}\psi_{\substack{e_{mn}\\o}}^{(1)}(c_2,\boldsymbol{r}')\\ \psi_{\substack{e_{mn}\\o}}^{(3)}(c_2,\boldsymbol{r}')\end{cases}\\ \cdot\begin{cases}(\boldsymbol{M}_{\substack{e_{mn}\\o}}^{x(3)}(c_2,\boldsymbol{r})\hat{x}+\boldsymbol{M}_{\substack{e_{mn}\\o}}^{y(3)}(c_2,\boldsymbol{r})\hat{y}+\boldsymbol{M}_{\substack{e_{mn}\\o}}^{z(3)}(c_2,\boldsymbol{r})\hat{z}) & (\xi>\xi')\\ (\boldsymbol{M}_{\substack{e_{mn}\\o}}^{x(1)}(c_2,\boldsymbol{r})\hat{x}+\boldsymbol{M}_{\substack{e_{mn}\\o}}^{y(1)}(c_2,\boldsymbol{r})\hat{y}+\boldsymbol{M}_{\substack{e_{mn}\\o}}^{z(1)}(c_2,\boldsymbol{r})\hat{z}) & (\xi<\xi')\end{cases}\end{aligned} \tag{3.11}$$

where $c_2 = \frac{1}{2}k_2 d$, k_2 is propagation constant in region 2, and d is the interfocal distance of the prolate spheroid. $\boldsymbol{r}$ denotes (η,ξ,ϕ) and $\boldsymbol{r}'$ denotes (η',ξ',ϕ').

3.4 Scattering dyadic Green's functions

By using the principle of scattering superposition, the dyadic Green's function can be considered as the sum of the unbounded Green's dyadic in equation (3.11) and the scattering dyadic Green's functions to be determined. The dyadic Green's functions are therefore given by

$$\overline{\boldsymbol{G}}_{m2}^{(1)}(\boldsymbol{r},\boldsymbol{r}') = \overline{\boldsymbol{G}}_{ms}^{(1)}(\boldsymbol{r},\boldsymbol{r}') \tag{3.12a}$$

$$\overline{\boldsymbol{G}}_{m2}^{(2)}(\boldsymbol{r},\boldsymbol{r}') = \overline{\boldsymbol{G}}_{m0}(\boldsymbol{r},\boldsymbol{r}') + \overline{\boldsymbol{G}}_{ms}^{(2)}(\boldsymbol{r},\boldsymbol{r}') \tag{3.12b}$$

where the scattering dyadic Green's function $\overline{\boldsymbol{G}}_{ms}^{(f)}(\boldsymbol{r},\boldsymbol{r}')$ represents the scattered-wave portion of the field due to the discontinuity of the boundary while the unbounded dyadic Green's function, $\overline{\boldsymbol{G}}_{m0}(\boldsymbol{r},\boldsymbol{r}')$, given by equation (3.11) represents the contribution of the direct waves from radiation sources in an unbounded medium. The subscript *(s)* denotes the scattering dyadic Green's functions. For the sake of simplicity, only $\overline{\boldsymbol{G}}_{ms}^{(f)}(\boldsymbol{r},\boldsymbol{r}')$ will be considered since $\overline{\boldsymbol{G}}_{es}^{(f)}(\boldsymbol{r},\boldsymbol{r}')$ can be obtained directly from $\overline{\boldsymbol{G}}_{ms}^{(f)}(\boldsymbol{r},\boldsymbol{r}')$ using equation (3.3c) or equation (3.3d).

The scattering dyadic Green's functions must be of a form similar to that of the unbounded dyadic Green's functions. To satisfy the boundary conditions, however, the additional spheroidal vector wave functions $\underset{e}{\overset{a(3)}{M}}_{o_{mn}}$ and $\underset{e}{\overset{a(3)}{N}}_{o_{mn}}$ *(a = x, y, or z)* should be included to account for the effects of multiple transmissions and reflections and satisfy the boundary conditions. Such an inclusion can be found in the cylindrical case in Tai [43]. The dyadic Green's functions for each region can be expressed as

$$
\begin{aligned}
\overline{G}_{ms}^{(1)}(\mathbf{r},\mathbf{r}') = {} & \frac{ik_2}{4\pi}\sum_{n=0}^{\infty}\sum_{m=0}^{n}\frac{2-\delta_{m0}}{N_{mn}}\underset{o}{\overset{(1)}{\psi}}_{e_{mn}}(c_2,\mathbf{r}')\cdot \\
& \{[A^{+xM}_{o_{emn}}((\underset{o}{\overset{x(3)}{M}}_{e_{mn}}(c_1,\mathbf{r}) \mp \underset{e}{\overset{y(3)}{M}}_{o_{mn}}(c_1,\mathbf{r})) + A^{+xN}_{e_{omn}}((\underset{e}{\overset{x(3)}{N}}_{o_{mn}}(c_1,\mathbf{r}) \pm \underset{o}{\overset{y(3)}{N}}_{e_{mn}}(c_1,\mathbf{r})) \\
& + A^{-xM}_{o_{emn}}((\underset{o}{\overset{x(3)}{M}}_{e_{mn}}(c_1,\mathbf{r}) \pm \underset{e}{\overset{y(3)}{M}}_{o_{mn}}(c_1,\mathbf{r})) + A^{-xN}_{e_{omn}}((\underset{e}{\overset{x(3)}{N}}_{o_{mn}}(c_1,\mathbf{r}) \mp \underset{o}{\overset{y(3)}{N}}_{e_{mn}}(c_1,\mathbf{r}))]\hat{x} \\
& + [A^{+yM}_{e_{omn}}((\underset{e}{\overset{x(3)}{M}}_{o_{mn}}(c_1,\mathbf{r}) \pm \underset{o}{\overset{y(3)}{M}}_{e_{mn}}(c_1,\mathbf{r})) + A^{+yN}_{o_{emn}}((\underset{o}{\overset{x(3)}{N}}_{e_{mn}}(c_1,\mathbf{r}) \mp \underset{e}{\overset{y(3)}{N}}_{o_{mn}}(c_1,\mathbf{r})) \\
& + A^{-yM}_{e_{omn}}((\underset{e}{\overset{x(3)}{M}}_{o_{mn}}(c_1,\mathbf{r}) \mp \underset{o}{\overset{y(3)}{M}}_{e_{mn}}(c_1,\mathbf{r})) + A^{-yN}_{o_{emn}}((\underset{o}{\overset{x(3)}{N}}_{e_{mn}}(c_1,\mathbf{r}) \pm \underset{e}{\overset{y(3)}{N}}_{o_{mn}}(c_1,\mathbf{r}))]\hat{y} \\
& + 2\cdot[A^{zM}_{o_{emn}}\underset{o}{\overset{z(3)}{M}}_{e_{mn}}(c_1,\mathbf{r}) + A^{zN}_{e_{omn}}\underset{e}{\overset{z(3)}{N}}_{o_{mn}}(c_1,\mathbf{r})]\hat{z}\}
\end{aligned}
\tag{3.13}
$$

$$
\begin{aligned}
\overline{G}_{ms}^{(2)}(\mathbf{r},\mathbf{r}') = {} & \frac{ik_2}{4\pi}\sum_{n=0}^{\infty}\sum_{m=0}^{n}\frac{2-\delta_{m0}}{N_{mn}}\underset{o}{\overset{(1)}{\psi}}_{e_{mn}}(c_2,\mathbf{r}')\cdot \\
& \{[B^{+xM}_{o_{emn}}((\underset{o}{\overset{x(1)}{M}}_{e_{mn}}(c_2,\mathbf{r}) \mp \underset{e}{\overset{y(1)}{M}}_{o_{mn}}(c_2,\mathbf{r})) + B^{+xN}_{e_{omn}}((\underset{e}{\overset{x(1)}{N}}_{o_{mn}}(c_2,\mathbf{r}) \pm \underset{o}{\overset{y(1)}{N}}_{e_{mn}}(c_2,\mathbf{r})) \\
& + B^{-xM}_{o_{emn}}((\underset{o}{\overset{x(1)}{M}}_{e_{mn}}(c_2,\mathbf{r}) \pm \underset{e}{\overset{y(1)}{M}}_{o_{mn}}(c_2,\mathbf{r})) + B^{-xN}_{e_{omn}}((\underset{e}{\overset{x(1)}{N}}_{o_{mn}}(c_2,\mathbf{r}) \mp \underset{o}{\overset{y(1)}{N}}_{e_{mn}}(c_2,\mathbf{r}))]\hat{x} \\
& + [B^{+yM}_{e_{omn}}((\underset{e}{\overset{x(1)}{M}}_{o_{mn}}(c_2,\mathbf{r}) \pm \underset{o}{\overset{y(1)}{M}}_{e_{mn}}(c_2,\mathbf{r})) + B^{+yN}_{o_{emn}}((\underset{o}{\overset{x(1)}{N}}_{e_{mn}}(c_2,\mathbf{r}) \mp \underset{e}{\overset{y(1)}{N}}_{o_{mn}}(c_2,\mathbf{r})) \\
& + B^{-yM}_{e_{omn}}((\underset{e}{\overset{x(1)}{M}}_{o_{mn}}(c_2,\mathbf{r}) \mp \underset{o}{\overset{y(1)}{M}}_{e_{mn}}(c_2,\mathbf{r})) + B^{-yN}_{o_{emn}}((\underset{o}{\overset{x(1)}{N}}_{e_{mn}}(c_2,\mathbf{r}) \pm \underset{e}{\overset{y(1)}{N}}_{o_{mn}}(c_2,\mathbf{r}))]\hat{y} \\
& + 2\cdot[B^{zM}_{o_{emn}}\underset{o}{\overset{z(1)}{M}}_{e_{mn}}(c_2,\mathbf{r}) + B^{zN}_{e_{omn}}\underset{e}{\overset{z(1)}{N}}_{o_{mn}}(c_2,\mathbf{r})]\hat{z}\}
\end{aligned}
\tag{3.14}
$$

where δ_{m0} is the Kronecker delta function. $c_i = \frac{1}{2}k_i d$ *(i = 1 or 2).* $A^{(\pm x,\pm y,z),(M,N)}_{e_{mn}}$ and $B^{(\pm x,\pm y,z),(M,N)}_{e_{mn}}$ are unknown scattering coefficients to be determined from the EM field boundary conditions at the interface $\xi = \xi_0$. The above vector wave functions denoted

by the superscripts *(1)* and *(3)* are chosen so that the functions $R_{mn}^{(1)}(c,\xi)$ and $R_{mn}^{(3)}(c,\xi)$, in spheroidal coordinates, represent waves which remain finite at $\xi = 0$ and $\xi \to \infty$, respectively.

So far, the dyadic Green's functions are obtained. The unknown scattering coefficients of the dyadic Green's functions will be determined in Chapter 4.

Chapter 4
Application to Prolate Hemispheroidal DRA

4.1 Introduction

In this chapter, the solution to the problem of radiation by a hemispheroidal dielectric resonator antenna, in figure 1.1, excited by a slot aperture is presented. The equivalent problem of a full dielectric spheroid is shown in figure 3.2 by using image theory. The early studies have proven that the DRA can be excited efficiently with different excitation mechanisms, such as a coaxial probe [14], microstrip-transmission line [48], an aperture-coupled microstrip-transmission line [47], [5], and a coplanar waveguide [49]. A coaxial probe feed may be difficult to fabricate for high-frequency array applications. In microstrip-transmission line feed and the coplanar-waveguide feed excitation methods, the DRA is on the same side of the feed network and is not isolated from active circuitry. This causes spurious radiation and coupling between the DRA and active circuitry. These problems are avoided in the aperture-coupling by virtue of the ground-plane isolation.

The radiation fields are expanded in terms of dyadic Green's functions. In this analysis, the slot field distribution is assumed to be known and of a sinusoidal form. The unknown scattering coefficients are determined by a system of equations derived

from the boundary conditions. According to equations 3.2a and 3.2b, the general expressions of electromagnetic fields are obtained. For the electromagnetic far field, we can simplify the formulation according to the asymptotic form of spheroidal radial function when $c\xi \to \infty$. The electromagnetic far fields are then expressed analytically in a very compact form.

4.2 Determination of scattering coefficients

In equations (3.12a), (3.12b), (3.13) and (3.14), the dyadic Green's functions in terms of appropriate prolate spheroidal vector wave functions using the principle of scattering superposition are formulated. Because of the lack of general orthogonalty of the spheroidal vector wave functions, the dyadic Green's functions are expressed in a different way, where the coordinate unit vectors also combined in the construction. The unknown scattering coefficients can be determined from the EM field boundary conditions on the spheroidal interface ($\xi = \xi_0$). The boundary conditions are expressed in equations (3.4). As regards the boundary conditions, it is only demanded that the tangential components of $\overline{\boldsymbol{G}}_{m2}^{(1)}$ and $\overline{\boldsymbol{G}}_{m2}^{(2)}$, which pertaining to the tangential components of $\boldsymbol{E}$ and $\boldsymbol{H}$, be continuous across the surface of the spheroid [36]. The condition that the normal components be continuous across the surface follows from the above conditions and from Maxwell's equations. Substituting equations (3.12a) and (3.12b) into equation (3.4), the coupled unknown coefficients in the equations (3.13) and (3.14) can be solved uniquely.

In Chapter 2, it has been shown that the angular functions depend not only on the angular component but also on the characteristics of the medium c. In spherical coordinate systems, however, the angular functions reduced to $P_n^m(\eta)$, which are not dependent on c. Only one of the three independent functions is dependent on c in spherical coordinate systems, so that the determination of the scattering coefficients is only associated with this independent function that has a particular value at the interface. In the spheroidal coordinates, however, two functions, i.e. the radial and the angular functions, are related to the propagation constant. Therefore, the equations used to determine the unknown coefficients constitute an infinite system of coupled linear equations with complex coefficients.

The following is the procedure for obtaining a system of linear equations for the unknown coefficients from application of boundary conditions. By solving this system of linear equations, we can obtain the unknown coefficients of the scattering dyadic Green's functions.

First the dyadic Green's functions equations (3.12a) and (3.12b) are substituted into the boundary conditions (3.4e) and (3.4f), respectively. After some lengthy manipulations, the boundary conditions can be expressed as

$$
\begin{aligned}
\hat{\xi}\times\sum_{n=0}^{\infty}\sum_{m=0}^{n}\Bigg\{&\{[\,A_{\substack{e_{mn}\\o}}^{+xM}((\boldsymbol{M}_{\substack{e_{mn}\\o}}^{x(3)}(c_1,\boldsymbol{r})\mp\boldsymbol{M}_{\substack{o_{mn}\\e}}^{y(3)}(c_1,\boldsymbol{r}))+A_{\substack{o_{mn}\\e}}^{+xN}((\boldsymbol{N}_{\substack{o_{mn}\\e}}^{x(3)}(c_1,\boldsymbol{r})\pm\boldsymbol{N}_{\substack{e_{mn}\\o}}^{y(3)}(c_1,\boldsymbol{r}))\\
&+A_{\substack{e_{mn}\\o}}^{-xM}((\boldsymbol{M}_{\substack{e_{mn}\\o}}^{x(3)}(c_1,\boldsymbol{r})\pm\boldsymbol{M}_{\substack{o_{mn}\\e}}^{y(3)}(c_1,\boldsymbol{r}))+A_{\substack{o_{mn}\\e}}^{-xN}((\boldsymbol{N}_{\substack{o_{mn}\\e}}^{x(3)}(c_1,\boldsymbol{r})\mp\boldsymbol{N}_{\substack{e_{mn}\\o}}^{y(3)}(c_1,\boldsymbol{r}))]\,\hat{x}\\
&+[\,A_{\substack{o_{mn}\\e}}^{+yM}((\boldsymbol{M}_{\substack{o_{mn}\\e}}^{x(3)}(c_1,\boldsymbol{r})\pm\boldsymbol{M}_{\substack{e_{mn}\\o}}^{y(3)}(c_1,\boldsymbol{r}))+A_{\substack{e_{mn}\\o}}^{+yN}((\boldsymbol{N}_{\substack{e_{mn}\\o}}^{x(3)}(c_1,\boldsymbol{r})\mp\boldsymbol{N}_{\substack{o_{mn}\\e}}^{y(3)}(c_1,\boldsymbol{r}))\\
&+A_{\substack{o_{mn}\\e}}^{-yM}((\boldsymbol{M}_{\substack{o_{mn}\\e}}^{x(3)}(c_1,\boldsymbol{r})\mp\boldsymbol{M}_{\substack{e_{mn}\\o}}^{y(3)}(c_1,\boldsymbol{r}))+A_{\substack{e_{mn}\\o}}^{-yN}((\boldsymbol{N}_{\substack{e_{mn}\\o}}^{x(3)}(c_1,\boldsymbol{r})\pm\boldsymbol{N}_{\substack{o_{mn}\\e}}^{y(3)}(c_1,\boldsymbol{r}))]\,\hat{y}\\
&+2\cdot[\,A_{\substack{e_{mn}\\o}}^{zM}\boldsymbol{M}_{\substack{e_{mn}\\o}}^{z(3)}(c_1,\boldsymbol{r})+A_{\substack{o_{mn}\\e}}^{zN}\boldsymbol{N}_{\substack{o_{mn}\\e}}^{z(3)}(c_1,\boldsymbol{r})]\,\hat{z}\}\\
&\cdot\iiint_{v}\frac{2-\delta_{m0}}{N_{mn}}\psi_{\substack{e_{mn}\\o}}^{(1)}(c_2,\boldsymbol{r}')\boldsymbol{M}_s(\boldsymbol{r}')dv'\Bigg\}\\
=\hat{\xi}\times\sum_{n=0}^{\infty}\sum_{m=0}^{n}\Bigg\{&\{[\,B_{\substack{e_{mn}\\o}}^{+xM}((\boldsymbol{M}_{\substack{e_{mn}\\o}}^{x(1)}(c_2,\boldsymbol{r})\mp\boldsymbol{M}_{\substack{o_{mn}\\e}}^{y(1)}(c_2,\boldsymbol{r}))+B_{\substack{o_{mn}\\e}}^{+xN}((\boldsymbol{N}_{\substack{o_{mn}\\e}}^{x(1)}(c_2,\boldsymbol{r})\pm\boldsymbol{N}_{\substack{e_{mn}\\o}}^{y(1)}(c_2,\boldsymbol{r}))\\
&+B_{\substack{e_{mn}\\o}}^{-xM}((\boldsymbol{M}_{\substack{e_{mn}\\o}}^{x(1)}(c_2,\boldsymbol{r})\pm\boldsymbol{M}_{\substack{o_{mn}\\e}}^{y(1)}(c_2,\boldsymbol{r}))+B_{\substack{o_{mn}\\e}}^{-xN}((\boldsymbol{N}_{\substack{o_{mn}\\e}}^{x(1)}(c_2,\boldsymbol{r})\mp\boldsymbol{N}_{\substack{e_{mn}\\o}}^{y(1)}(c_2,\boldsymbol{r}))]\,\hat{x}\\
&+[\,B_{\substack{o_{mn}\\e}}^{+yM}((\boldsymbol{M}_{\substack{o_{mn}\\e}}^{x(1)}(c_2,\boldsymbol{r})\pm\boldsymbol{M}_{\substack{e_{mn}\\o}}^{y(1)}(c_2,\boldsymbol{r}))+B_{\substack{e_{mn}\\o}}^{+yN}((\boldsymbol{N}_{\substack{e_{mn}\\o}}^{x(1)}(c_2,\boldsymbol{r})\mp\boldsymbol{N}_{\substack{o_{mn}\\e}}^{y(1)}(c_2,\boldsymbol{r}))\\
&+B_{\substack{o_{mn}\\e}}^{-yM}((\boldsymbol{M}_{\substack{o_{mn}\\e}}^{x(1)}(c_2,\boldsymbol{r})\mp\boldsymbol{M}_{\substack{e_{mn}\\o}}^{y(1)}(c_2,\boldsymbol{r}))+B_{\substack{e_{mn}\\o}}^{-yN}((\boldsymbol{N}_{\substack{e_{mn}\\o}}^{x(1)}(c_2,\boldsymbol{r})\pm\boldsymbol{N}_{\substack{o_{mn}\\e}}^{y(1)}(c_2,\boldsymbol{r}))]\,\hat{y}\\
&+2\cdot[\,B_{\substack{e_{mn}\\o}}^{zM}\boldsymbol{M}_{\substack{e_{mn}\\o}}^{z(1)}(c_2,\boldsymbol{r})+B_{\substack{o_{mn}\\e}}^{zN}\boldsymbol{N}_{\substack{o_{mn}\\e}}^{z(1)}(c_2,\boldsymbol{r})]\,\hat{z}\}\\
&\cdot\iiint_{v}\frac{2-\delta_{m0}}{N_{mn}}\psi_{\substack{e_{mn}\\o}}^{(1)}(c_2,\boldsymbol{r}')\boldsymbol{M}_s(\boldsymbol{r}')dv'\Bigg\}
\end{aligned}
\qquad (4.1a)
$$

and

$$\hat{\xi}\times\frac{1}{\sqrt{\varepsilon_{r1}}}\sum_{n=0}^{\infty}\sum_{m=0}^{n}\Big\{\{[A_{e_{mn}}^{+xM}((N_{e_{mn}}^{x(3)}(c_1,r)\mp N_{o_{mn}}^{y(3)}(c_1,r))+A_{o_{mn}}^{+xN}((M_{o_{mn}}^{x(3)}(c_1,r)\pm M_{e_{mn}}^{y(3)}(c_1,r))$$
$$+A_{o_{mn}}^{-xM}((N_{o_{mn}}^{x(3)}(c_1,r)\pm N_{e_{mn}}^{y(3)}(c_1,r))+A_{e_{mn}}^{-xN}((M_{e_{mn}}^{x(3)}(c_1,r)\mp M_{o_{mn}}^{y(3)}(c_1,r))]\hat{x}$$
$$+[A_{o_{mn}}^{+yM}((N_{o_{mn}}^{x(3)}(c_1,r)\pm N_{e_{mn}}^{y(3)}(c_1,r))+A_{e_{mn}}^{+yN}((M_{e_{mn}}^{x(3)}(c_1,r)\mp M_{o_{mn}}^{y(3)}(c_1,r))$$
$$+A_{o_{mn}}^{-yM}((N_{o_{mn}}^{x(3)}(c_1,r)\mp N_{e_{mn}}^{y(3)}(c_1,r))+A_{e_{mn}}^{-yN}((M_{e_{mn}}^{x(3)}(c_1,r)\pm M_{o_{mn}}^{y(3)}(c_1,r))]\hat{y}$$
$$+2\cdot[A_{e_{mn}}^{zM}N_{e_{mn}}^{z(3)}(c_1,r)+A_{o_{mn}}^{zN}M_{o_{mn}}^{z(3)}(c_1,r)]\hat{z}\}$$
$$\cdot\iiint_{v}\frac{2-\delta_{m0}}{N_{mn}}\psi_{e_{mn}}^{(1)}(c_2,r')M_s(r')dv'\Big\}$$
$$=\hat{\xi}\times\frac{1}{\sqrt{\varepsilon_{r2}}}\sum_{n=0}^{\infty}\sum_{m=0}^{n}\Big\{\{[B_{e_{mn}}^{+xM}((N_{e_{mn}}^{x(1)}(c_2,r)\mp N_{o_{mn}}^{y(1)}(c_2,r))+B_{o_{mn}}^{+xN}((M_{o_{mn}}^{x(1)}(c_2,r)\pm M_{e_{mn}}^{y(1)}(c_2,r))$$
$$+B_{e_{mn}}^{-xM}((N_{e_{mn}}^{x(1)}(c_2,r)\pm N_{o_{mn}}^{y(1)}(c_2,r))+B_{o_{mn}}^{-xN}((M_{o_{mn}}^{x(1)}(c_2,r)\mp M_{e_{mn}}^{y(1)}(c_2,r))$$
$$+2N_{e_{mn}}^{x(3)}(c_2,r)]\hat{x}$$
$$+[B_{o_{mn}}^{+yM}((N_{o_{mn}}^{x(1)}(c_2,r)\pm N_{e_{mn}}^{y(1)}(c_2,r))+B_{e_{mn}}^{+yN}((M_{e_{mn}}^{x(1)}(c_2,r)\mp M_{o_{mn}}^{y(1)}(c_2,r))$$
$$+B_{o_{mn}}^{-yM}((N_{o_{mn}}^{x(1)}(c_2,r)\mp N_{e_{mn}}^{y(1)}(c_2,r))+B_{e_{mn}}^{-yN}((M_{e_{mn}}^{x(1)}(c_2,r)\pm M_{o_{mn}}^{y(1)}(c_2,r))$$
$$+2N_{e_{mn}}^{y(3)}(c_2,r)]\hat{y}$$
$$+2\cdot[B_{e_{mn}}^{zM}N_{e_{mn}}^{z(1)}(c_2,r)+B_{o_{mn}}^{zN}M_{o_{mn}}^{z(1)}(c_2,r)+N_{e_{mn}}^{z(3)}(c_2,r)]\hat{z}\}$$
$$\cdot\iiint_{v}\frac{2-\delta_{m0}}{N_{mn}}\psi_{e_{mn}}^{(1)}(c_2,r')M_s(r')dv'\Big\} \qquad (4.1b)$$

In equation (4.1a), we now consider the $\hat{x}$ component, $\hat{y}$ component and $\hat{z}$ component, respectively. We employ $K_{e_{o_{mn}}}=\iiint_{v}\frac{2-\delta_{m0}}{N_{mn}}\psi_{e_{mn}}^{(1)}(c_2,r')M_s(r')dv'$ in the following expressions. Split equation (4.1a) into three equations as follows:

- From the $\hat{x}$ component of equation (4.1a), we get

$$\begin{aligned}
&\hat{\xi}\times\sum_{n=0}^{\infty}\sum_{m=0}^{n}\mathrm{K}_{\substack{e\\o}mn}\\
&\cdot[A^{+xM}_{\substack{e_{mn}\\o}}((\boldsymbol{M}^{x(3)}_{\substack{e_{mn}\\o}}(c_1,\boldsymbol{r})\mp\boldsymbol{M}^{y(3)}_{\substack{o_{mn}\\e}}(c_1,\boldsymbol{r}))+A^{+xN}_{\substack{o_{mn}\\e}}((\boldsymbol{N}^{x(3)}_{\substack{o_{mn}\\e}}(c_1,\boldsymbol{r})\pm\boldsymbol{N}^{y(3)}_{\substack{e_{mn}\\o}}(c_1,\boldsymbol{r}))\\
&+A^{-xM}_{\substack{e_{mn}\\o}}((\boldsymbol{M}^{x(3)}_{\substack{e_{mn}\\o}}(c_1,\boldsymbol{r})\pm\boldsymbol{M}^{y(3)}_{\substack{o_{mn}\\e}}(c_1,\boldsymbol{r}))+A^{-xN}_{\substack{o_{mn}\\e}}((\boldsymbol{N}^{x(3)}_{\substack{o_{mn}\\e}}(c_1,\boldsymbol{r})\mp\boldsymbol{N}^{y(3)}_{\substack{e_{mn}\\o}}(c_1,\boldsymbol{r}))]\\
&=\hat{\xi}\times\sum_{n=0}^{\infty}\sum_{m=0}^{n}\mathrm{K}_{\substack{e\\o}mn}\\
&\cdot[B^{+xM}_{\substack{e_{mn}\\o}}((\boldsymbol{M}^{x(1)}_{\substack{e_{mn}\\o}}(c_2,\boldsymbol{r})\mp\boldsymbol{M}^{y(1)}_{\substack{o_{mn}\\e}}(c_2,\boldsymbol{r}))+B^{+xN}_{\substack{o_{mn}\\e}}((\boldsymbol{N}^{x(1)}_{\substack{o_{mn}\\e}}(c_2,\boldsymbol{r})\pm\boldsymbol{N}^{y(1)}_{\substack{e_{mn}\\o}}(c_2,\boldsymbol{r}))\\
&+B^{-xM}_{\substack{e_{mn}\\o}}((\boldsymbol{M}^{x(1)}_{\substack{e_{mn}\\o}}(c_2,\boldsymbol{r})\pm\boldsymbol{M}^{y(1)}_{\substack{o_{mn}\\e}}(c_2,\boldsymbol{r}))+B^{-xN}_{\substack{o_{mn}\\e}}((\boldsymbol{N}^{x(1)}_{\substack{o_{mn}\\e}}(c_2,\boldsymbol{r})\mp\boldsymbol{N}^{y(1)}_{\substack{e_{mn}\\o}}(c_2,\boldsymbol{r}))\\
&+2\boldsymbol{M}^{x(3)}_{\substack{e_{mn}\\o}}(c_2,\boldsymbol{r})]
\end{aligned}\tag{4.2a}$$

- From the $\hat{y}$ component of equation (4.1a), we get

$$\begin{aligned}
&\hat{\xi}\times\sum_{n=0}^{\infty}\sum_{m=0}^{n}\mathrm{K}_{\substack{e\\o}mn}\\
&\cdot[A^{+yM}_{\substack{o_{mn}\\e}}((\boldsymbol{M}^{x(3)}_{\substack{o_{mn}\\e}}(c_1,\boldsymbol{r})\pm\boldsymbol{M}^{y(3)}_{\substack{e_{mn}\\o}}(c_1,\boldsymbol{r}))+A^{+yN}_{\substack{e_{mn}\\o}}((\boldsymbol{N}^{x(3)}_{\substack{e_{mn}\\o}}(c_1,\boldsymbol{r})\mp\boldsymbol{N}^{y(3)}_{\substack{o_{mn}\\e}}(c_1,\boldsymbol{r}))\\
&+A^{-yM}_{\substack{o_{mn}\\e}}((\boldsymbol{M}^{x(3)}_{\substack{o_{mn}\\e}}(c_1,\boldsymbol{r})\mp\boldsymbol{M}^{y(3)}_{\substack{e_{mn}\\o}}(c_1,\boldsymbol{r}))+A^{-yN}_{\substack{e_{mn}\\o}}((\boldsymbol{N}^{x(3)}_{\substack{e_{mn}\\o}}(c_1,\boldsymbol{r})\pm\boldsymbol{N}^{y(3)}_{\substack{o_{mn}\\e}}(c_1,\boldsymbol{r}))]\\
&=\hat{\xi}\times\sum_{n=0}^{\infty}\sum_{m=0}^{n}\mathrm{K}_{\substack{e\\o}mn}\\
&\cdot[B^{+yM}_{\substack{o_{mn}\\e}}((\boldsymbol{M}^{x(1)}_{\substack{o_{mn}\\e}}(c_2,\boldsymbol{r})\pm\boldsymbol{M}^{y(1)}_{\substack{e_{mn}\\o}}(c_2,\boldsymbol{r}))+B^{+yN}_{\substack{e_{mn}\\o}}((\boldsymbol{N}^{x(1)}_{\substack{e_{mn}\\o}}(c_2,\boldsymbol{r})\mp\boldsymbol{N}^{y(1)}_{\substack{o_{mn}\\e}}(c_2,\boldsymbol{r}))\\
&+B^{-yM}_{\substack{o_{mn}\\e}}((\boldsymbol{M}^{x(1)}_{\substack{o_{mn}\\e}}(c_2,\boldsymbol{r})\mp\boldsymbol{M}^{y(1)}_{\substack{e_{mn}\\o}}(c_2,\boldsymbol{r}))+B^{-yN}_{\substack{e_{mn}\\o}}((\boldsymbol{N}^{x(1)}_{\substack{e_{mn}\\o}}(c_2,\boldsymbol{r})\pm\boldsymbol{N}^{y(1)}_{\substack{o_{mn}\\e}}(c_2,\boldsymbol{r}))\\
&+2\boldsymbol{M}^{y(3)}_{\substack{e_{mn}\\o}}(c_2,\boldsymbol{r})]
\end{aligned}\tag{4.2b}$$

- From the $\hat{z}$ component of equation (4.1a), we get

$$\begin{aligned}
&\hat{\xi}\times\sum_{n=0}^{\infty}\sum_{m=0}^{n}\frac{2-\delta_{m0}}{N_{mn}}\mathrm{K}_{\substack{e\\o}mn}\\
&\cdot[A_{\substack{e_{mn}\\o}}^{zM}\boldsymbol{M}_{\substack{e_{mn}\\o}}^{z(3)}(c_1,\boldsymbol{r})+A_{\substack{o_{mn}\\e}}^{zN}\boldsymbol{N}_{\substack{o_{mn}\\e}}^{z(3)}(c_1,\boldsymbol{r})]\\
&=\hat{\xi}\times\sum_{n=0}^{\infty}\sum_{m=0}^{n}\mathrm{K}_{\substack{e\\o}mn}\\
&\cdot[B_{\substack{e_{mn}\\o}}^{zM}\boldsymbol{M}_{\substack{e_{mn}\\o}}^{z(1)}(c_2,\boldsymbol{r})+B_{\substack{o_{mn}\\e}}^{zN}\boldsymbol{N}_{\substack{o_{mn}\\e}}^{z(1)}(c_2,\boldsymbol{r})]
\end{aligned}\tag{4.2c}$$

In equation (4.1b), similarly, we consider the $\hat{x}$ component, $\hat{y}$ component and $\hat{z}$ component, respectively. Split equation (4.1b) into three equations as follows:

- From the $\hat{x}$ component of equation (4.1b) , we get

$$\begin{aligned}
&\hat{\xi}\times\frac{1}{\sqrt{\varepsilon_{r1}}}\sum_{n=0}^{\infty}\sum_{m=0}^{n}\mathrm{K}_{\substack{e\\o}mn}\\
&\cdot[A_{\substack{e_{mn}\\o}}^{+xM}((N_{\substack{e_{mn}\\o}}^{x(3)}(c_1,\boldsymbol{r})\mp N_{\substack{o_{mn}\\e}}^{y(3)}(c_1,\boldsymbol{r}))+A_{\substack{o_{mn}\\e}}^{+xN}((\boldsymbol{M}_{\substack{o_{mn}\\e}}^{x(3)}(c_1,\boldsymbol{r})\pm\boldsymbol{M}_{\substack{e_{mn}\\o}}^{y(3)}(c_1,\boldsymbol{r}))\\
&+A_{\substack{e_{mn}\\o}}^{-xM}((N_{\substack{e_{mn}\\o}}^{x(3)}(c_1,\boldsymbol{r})\pm N_{\substack{o_{mn}\\e}}^{y(3)}(c_1,\boldsymbol{r}))+A_{\substack{o_{mn}\\e}}^{-xN}((\boldsymbol{M}_{\substack{o_{mn}\\e}}^{x(3)}(c_1,\boldsymbol{r})\mp\boldsymbol{M}_{\substack{e_{mn}\\o}}^{y(3)}(c_1,\boldsymbol{r}))]\\
&=\hat{\xi}\times\frac{1}{\sqrt{\varepsilon_{r2}}}\sum_{n=0}^{\infty}\sum_{m=0}^{n}\mathrm{K}_{\substack{e\\o}mn}\\
&\cdot[B_{\substack{e_{mn}\\o}}^{+xM}((N_{\substack{e_{mn}\\o}}^{x(1)}(c_2,\boldsymbol{r})\mp N_{\substack{o_{mn}\\e}}^{y(1)}(c_2,\boldsymbol{r}))+B_{\substack{o_{mn}\\e}}^{+xN}((\boldsymbol{M}_{\substack{o_{mn}\\e}}^{x(1)}(c_2,\boldsymbol{r})\pm\boldsymbol{M}_{\substack{e_{mn}\\o}}^{y(1)}(c_2,\boldsymbol{r}))\\
&+B_{\substack{e_{mn}\\o}}^{-xM}((N_{\substack{e_{mn}\\o}}^{x(1)}(c_2,\boldsymbol{r})\pm N_{\substack{o_{mn}\\e}}^{y(1)}(c_2,\boldsymbol{r}))+B_{\substack{o_{mn}\\e}}^{-xN}((\boldsymbol{M}_{\substack{o_{mn}\\e}}^{x(1)}(c_2,\boldsymbol{r})\mp\boldsymbol{M}_{\substack{e_{mn}\\o}}^{y(1)}(c_2,\boldsymbol{r}))\\
&+2\boldsymbol{N}_{\substack{e_{mn}\\o}}^{x(3)}(c_2,\boldsymbol{r})]
\end{aligned}\tag{4.3a}$$

- From the $\hat{y}$ component of equation (4.1b), we get

$$\begin{aligned}
&\hat{\xi}\times\frac{1}{\sqrt{\varepsilon_{r1}}}\sum_{n=0}^{\infty}\sum_{m=0}^{n}\mathrm{K}_{\substack{e\\o}mn}\\
&\cdot[A^{+yM}_{\substack{o\\e}mn}((N^{x(3)}_{\substack{o\\e}mn}(c_1,\boldsymbol{r})\pm N^{y(3)}_{\substack{e\\o}mn}(c_1,\boldsymbol{r}))+A^{+yN}_{\substack{e\\o}mn}((\boldsymbol{M}^{x(3)}_{\substack{e\\o}mn}(c_1,\boldsymbol{r})\mp \boldsymbol{M}^{y(3)}_{\substack{o\\e}mn}(c_1,\boldsymbol{r}))\\
&+A^{-yM}_{\substack{o\\e}mn}((N^{x(3)}_{\substack{o\\e}mn}(c_1,\boldsymbol{r})\mp N^{y(3)}_{\substack{e\\o}mn}(c_1,\boldsymbol{r}))+A^{-yN}_{\substack{e\\o}mn}((\boldsymbol{M}^{x(3)}_{\substack{e\\o}mn}(c_1,\boldsymbol{r})\pm \boldsymbol{M}^{y(3)}_{\substack{o\\e}mn}(c_1,\boldsymbol{r}))]\\
&=\hat{\xi}\times\frac{1}{\sqrt{\varepsilon_{r2}}}\sum_{n=0}^{\infty}\sum_{m=0}^{n}\mathrm{K}_{\substack{e\\o}mn}\\
&\cdot[B^{+yM}_{\substack{o\\e}mn}((N^{x(1)}_{\substack{o\\e}mn}(c_2,\boldsymbol{r})\pm N^{y(1)}_{\substack{e\\o}mn}(c_2,\boldsymbol{r}))+B^{+yN}_{\substack{e\\o}mn}((\boldsymbol{M}^{x(1)}_{\substack{e\\o}mn}(c_2,\boldsymbol{r})\mp \boldsymbol{M}^{y(1)}_{\substack{o\\e}mn}(c_2,\boldsymbol{r}))\\
&+B^{-yM}_{\substack{o\\e}mn}((N^{x(1)}_{\substack{o\\e}mn}(c_2,\boldsymbol{r})\mp N^{y(1)}_{\substack{e\\o}mn}(c_2,\boldsymbol{r}))+B^{-yN}_{\substack{e\\o}mn}((\boldsymbol{M}^{x(1)}_{\substack{e\\o}mn}(c_2,\boldsymbol{r})\pm \boldsymbol{M}^{y(1)}_{\substack{o\\e}mn}(c_2,\boldsymbol{r}))\\
&+2N^{y(3)}_{\substack{e\\o}mn}(c_2,\boldsymbol{r})]
\end{aligned}\tag{4.3b}$$

- From the $\hat{z}$ component of equation (4.1b), we get

$$\begin{aligned}
&\hat{\xi}\times\frac{1}{\sqrt{\varepsilon_{r1}}}\sum_{n=0}^{\infty}\sum_{m=0}^{n}\mathrm{K}_{\substack{e\\o}mn}\\
&\cdot[A^{zM}_{\substack{e\\o}mn}\boldsymbol{N}^{z(3)}_{\substack{e\\o}mn}(c_1,\boldsymbol{r})+A^{zN}_{\substack{o\\e}mn}\boldsymbol{M}^{z(3)}_{\substack{o\\e}mn}(c_1,\boldsymbol{r})]\\
&=\hat{\xi}\times\frac{1}{\sqrt{\varepsilon_{r2}}}\sum_{n=0}^{\infty}\sum_{m=0}^{n}\mathrm{K}_{\substack{e\\o}mn}\\
&\cdot[B^{zM}_{\substack{o\\e}mn}\boldsymbol{N}^{z(1)}_{\substack{o\\e}mn}(c_2,\boldsymbol{r})+\boldsymbol{N}^{z(3)}_{\substack{e\\o}mn}(c_2,\boldsymbol{r})+B^{zN}_{\substack{e\\o}mn}\boldsymbol{M}^{z(1)}_{\substack{o\\e}mn}(c_2,\boldsymbol{r})]
\end{aligned}\tag{4.3c}$$

Because of the orthogonality of the trigonometric functions $\cos(m\phi)$ and $\sin(m\phi)$, in each expansion, the coefficients of the same ϕ-dependent trigonometric function must be equal, component by component. The equalities must hold for each corresponding term in the summation over m. So we can eliminate the summation with respect to m.

For the summation over n, however, the individual terms in the series cannot be matched term by term. This is the cause of difficulty in determining the unknown coefficients in spheroidal coordinates because of the dependence of the angular function on the electrical properties of the medium.

At the interface ($\xi = \xi_0$), as mentioned above, the tangential components of fields are continuous, *i.e.*, the $\hat{\eta}$-component and $\hat{\phi}$-component of fields are continuous. Therefore, the boundary conditions can be expressed more specifically as follows. Rewriting equations (4.2a), (4.2b), (4.2c) and equations (4.3a), (4.3b), (4.3c), respectively, we obtain

$$\begin{aligned}
&\sum_{n=m}^{\infty} \mathrm{K}_{\substack{e \\ o}}{}^{mn} \Big[A_{\substack{e_{mn} \\ o}}^{+xM} \big(\boldsymbol{M}_{\substack{e_{mnu} \\ o}}^{x(3)}(c_1,\boldsymbol{r}) \mp \boldsymbol{M}_{\substack{o_{mnu} \\ e}}^{y(3)}(c_1,\boldsymbol{r}) \big) + A_{\substack{o_{mn} \\ e}}^{+xN} \big(\boldsymbol{N}_{\substack{o_{mnu} \\ e}}^{x(3)}(c_1,\boldsymbol{r}) \pm \boldsymbol{N}_{\substack{e_{mnu} \\ o}}^{y(3)}(c_1,\boldsymbol{r}) \big) \\
&\quad + A_{\substack{e_{mn} \\ o}}^{-xM} \big(\boldsymbol{M}_{\substack{e_{mnu} \\ o}}^{x(3)}(c_1,\boldsymbol{r}) \pm \boldsymbol{M}_{\substack{o_{mnu} \\ e}}^{y(3)}(c_1,\boldsymbol{r}) \big) + A_{\substack{o_{mn} \\ e}}^{-xN} \big(\boldsymbol{N}_{\substack{o_{mnu} \\ e}}^{x(3)}(c_1,\boldsymbol{r}) \mp \boldsymbol{N}_{\substack{e_{mnu} \\ o}}^{y(3)}(c_1,\boldsymbol{r}) \big) \Big] \\
&= \sum_{n=m}^{\infty} \mathrm{K}_{\substack{e \\ o}}{}^{mn} \Big[B_{\substack{e_{mn} \\ o}}^{+xM} \big(\boldsymbol{M}_{\substack{e_{mnu} \\ o}}^{x(1)}(c_2,\boldsymbol{r}) \mp \boldsymbol{M}_{\substack{o_{mnu} \\ e}}^{y(1)}(c_2,\boldsymbol{r}) \big) + B_{\substack{o_{mn} \\ e}}^{+xN} \big(\boldsymbol{N}_{\substack{o_{mnu} \\ e}}^{x(1)}(c_2,\boldsymbol{r}) \pm \boldsymbol{N}_{\substack{e_{mnu} \\ o}}^{y(1)}(c_2,\boldsymbol{r}) \big) \\
&\quad + B_{\substack{e_{mn} \\ o}}^{-xM} \big(\boldsymbol{M}_{\substack{e_{mnu} \\ o}}^{x(1)}(c_2,\boldsymbol{r}) \pm \boldsymbol{M}_{\substack{o_{mnu} \\ e}}^{y(1)}(c_2,\boldsymbol{r}) \big) + B_{\substack{o_{mn} \\ e}}^{-xN} \big(\boldsymbol{N}_{\substack{o_{mnu} \\ e}}^{x(1)}(c_2,\boldsymbol{r}) \mp \boldsymbol{N}_{\substack{e_{mnu} \\ o}}^{y(1)}(c_2,\boldsymbol{r}) \big) \\
&\quad + 2\boldsymbol{M}_{\substack{e_{mnu} \\ o}}^{x(3)}(c_2,\boldsymbol{r}) \Big]
\end{aligned} \tag{4.5a}$$

$$\sum_{n=m}^{\infty} \mathrm{K}_{\substack{e \\ o}}{}^{mn} [A_{\substack{e_{mn} \\ o}}^{+yM} (\boldsymbol{M}_{\substack{o_{mnu} \\ e}}^{x(3)}(c_1,\boldsymbol{r}) \pm \boldsymbol{M}_{\substack{e_{mnu} \\ o}}^{y(3)}(c_1,\boldsymbol{r})) + A_{\substack{e_{mn} \\ o}}^{+yN} (\boldsymbol{N}_{\substack{o_{mnu} \\ o}}^{x(3)}(c_1,\boldsymbol{r}) \mp \boldsymbol{N}_{\substack{o_{mnu} \\ e}}^{y(3)}(c_1,\boldsymbol{r}))$$
$$+ A_{\substack{o_{mn} \\ e}}^{-yM} (\boldsymbol{M}_{\substack{o_{mnu} \\ e}}^{x(3)}(c_1,\boldsymbol{r}) \mp \boldsymbol{M}_{\substack{e_{mnu} \\ o}}^{y(3)}(c_1,\boldsymbol{r})) + A_{\substack{e_{mn} \\ o}}^{-yN} (\boldsymbol{N}_{\substack{o_{mnu} \\ o}}^{x(3)}(c_1,\boldsymbol{r}) \pm \boldsymbol{N}_{\substack{o_{mnu} \\ e}}^{y(3)}(c_1,\boldsymbol{r}))]$$
$$= \sum_{n=m}^{\infty} \mathrm{K}_{\substack{e \\ o}}{}^{mn} [B_{\substack{o_{mn} \\ e}}^{+yM} (\boldsymbol{M}_{\substack{o_{mnu} \\ e}}^{x(1)}(c_2,\boldsymbol{r}) \pm \boldsymbol{M}_{\substack{e_{mnu} \\ o}}^{y(1)}(c_2,\boldsymbol{r})) + B_{\substack{e_{mn} \\ o}}^{+yN} (\boldsymbol{N}_{\substack{o_{mnu} \\ o}}^{x(1)}(c_2,\boldsymbol{r}) \mp \boldsymbol{N}_{\substack{o_{mnu} \\ e}}^{y(1)}(c_2,\boldsymbol{r}))$$
$$+ B_{\substack{o_{mn} \\ e}}^{-yM} (\boldsymbol{M}_{\substack{o_{mnu} \\ e}}^{x(1)}(c_2,\boldsymbol{r}) \mp \boldsymbol{M}_{\substack{e_{mnu} \\ o}}^{y(1)}(c_2,\boldsymbol{r})) + B_{\substack{e_{mn} \\ o}}^{-yN} (\boldsymbol{N}_{\substack{o_{mnu} \\ o}}^{x(1)}(c_2,\boldsymbol{r}) \pm \boldsymbol{N}_{\substack{o_{mnu} \\ e}}^{y(1)}(c_2,\boldsymbol{r}))$$
$$+ 2\boldsymbol{M}_{\substack{e_{mnu} \\ o}}^{y(3)}(c_2,\boldsymbol{r})] \tag{4.5b}$$

$$\sum_{n=m}^{\infty} \mathrm{K}_{\substack{e \\ o}}{}^{mn} [A_{\substack{e_{mn} \\ o}}^{zM} \boldsymbol{M}_{\substack{e_{mnu} \\ o}}^{z(3)}(c_1,\boldsymbol{r}) + A_{\substack{o_{mn} \\ e}}^{zN} \boldsymbol{N}_{\substack{o_{mnu} \\ e}}^{z(3)}(c_1,\boldsymbol{r})]$$
$$= \sum_{n=m}^{\infty} \mathrm{K}_{\substack{e \\ o}}{}^{mn} [B_{\substack{e_{mn} \\ o}}^{zM} \boldsymbol{M}_{\substack{e_{mnu} \\ o}}^{z(1)}(c_2,\boldsymbol{r}) + \boldsymbol{M}_{\substack{e_{mnu} \\ o}}^{z(3)}(c_2,\boldsymbol{r}) + B_{\substack{o_{mn} \\ e}}^{zN} \boldsymbol{N}_{\substack{o_{mnu} \\ e}}^{z(1)}(c_2,\boldsymbol{r})] \tag{4.5c}$$

$$\sum_{n=m}^{\infty} \mathrm{K}_{\substack{e \\ o}}{}^{mn} [A_{\substack{e_{mn} \\ o}}^{+xM} (\boldsymbol{N}_{\substack{o_{mnu} \\ o}}^{x(3)}(c_1,\boldsymbol{r}) \mp \boldsymbol{N}_{\substack{o_{mnu} \\ e}}^{y(3)}(c_1,\boldsymbol{r})) + A_{\substack{o_{mn} \\ e}}^{+xN} (\boldsymbol{M}_{\substack{o_{mnu} \\ e}}^{x(3)}(c_1,\boldsymbol{r}) \pm \boldsymbol{M}_{\substack{e_{mnu} \\ o}}^{y(3)}(c_1,\boldsymbol{r}))$$
$$+ A_{\substack{e_{mn} \\ o}}^{-xM} (\boldsymbol{N}_{\substack{e_{mnu} \\ o}}^{x(3)}(c_1,\boldsymbol{r}) \pm \boldsymbol{N}_{\substack{o_{mnu} \\ e}}^{y(3)}(c_1,\boldsymbol{r})) + A_{\substack{o_{mn} \\ e}}^{-xN} (\boldsymbol{M}_{\substack{e_{mnu} \\ e}}^{x(3)}(c_1,\boldsymbol{r}) \mp \boldsymbol{M}_{\substack{e_{mnu} \\ o}}^{y(3)}(c_1,\boldsymbol{r}))]$$
$$= \sqrt{\frac{\varepsilon_{r1}}{\varepsilon_{r2}}} \sum_{n=m}^{\infty} \mathrm{K}_{\substack{e \\ o}}{}^{mn} [B_{\substack{e_{mn} \\ o}}^{+xM} (\boldsymbol{N}_{\substack{o_{mnu} \\ o}}^{x(1)}(c_2,\boldsymbol{r}) \mp \boldsymbol{N}_{\substack{o_{mnu} \\ e}}^{y(1)}(c_2,\boldsymbol{r})) + B_{\substack{o_{mn} \\ e}}^{+xN} (\boldsymbol{M}_{\substack{o_{mnu} \\ e}}^{x(1)}(c_2,\boldsymbol{r}) \pm \boldsymbol{M}_{\substack{e_{mnu} \\ o}}^{y(1)}(c_2,\boldsymbol{r}))$$
$$+ B_{\substack{e_{mn} \\ o}}^{-xM} (\boldsymbol{N}_{\substack{e_{mnu} \\ o}}^{x(1)}(c_2,\boldsymbol{r}) \pm \boldsymbol{N}_{\substack{o_{mnu} \\ e}}^{y(1)}(c_2,\boldsymbol{r})) + B_{\substack{o_{mn} \\ e}}^{-xN} (\boldsymbol{M}_{\substack{e_{mnu} \\ e}}^{x(1)}(c_2,\boldsymbol{r}) \mp \boldsymbol{M}_{\substack{e_{mnu} \\ o}}^{y(1)}(c_2,\boldsymbol{r}))$$
$$+ 2\boldsymbol{N}_{\substack{e_{mnu} \\ o}}^{x(3)}(c_2,\boldsymbol{r})] \tag{4.6a}$$

$$\sum_{n=m}^{\infty} \mathrm{K}_{\substack{e \\ o}^{mn}} [A_{\substack{o \\ e}^{mn}}^{+yM} (N_{\substack{o \\ e}^{mn\eta}}^{x(3)}(c_1,\boldsymbol{r}) \pm N_{\substack{e \\ o}^{mnu}}^{y(3)}(c_1,\boldsymbol{r})) + A_{\substack{e \\ o}^{mn}}^{+yN} (\boldsymbol{M}_{\substack{e \\ o}^{mnu}}^{x(3)}(c_1,\boldsymbol{r}) \mp \boldsymbol{M}_{\substack{o \\ e}^{mnu}}^{y(3)}(c_1,\boldsymbol{r}))$$
$$+ A_{\substack{o \\ e}^{mn}}^{-yM} (N_{\substack{o \\ e}^{mnu}}^{x(3)}(c_1,\boldsymbol{r}) \mp N_{\substack{e \\ o}^{mnu}}^{y(3)}(c_1,\boldsymbol{r})) + A_{\substack{e \\ o}^{mn}}^{-yN} (\boldsymbol{M}_{\substack{e \\ o}^{mnu}}^{x(3)}(c_1,\boldsymbol{r}) \pm \boldsymbol{M}_{\substack{o \\ e}^{mnu}}^{y(3)}(c_1,\boldsymbol{r}))]$$
$$= \sum_{n=m}^{\infty} \mathrm{K}_{\substack{e \\ o}^{mn}} [B_{\substack{o \\ e}^{mn}}^{+yM} (N_{\substack{o \\ e}^{mnu}}^{x(1)}(c_2,\boldsymbol{r}) \pm N_{\substack{e \\ o}^{mnu}}^{y(1)}(c_2,\boldsymbol{r})) + B_{\substack{e \\ o}^{mn}}^{+yN} (\boldsymbol{M}_{\substack{e \\ o}^{mnu}}^{x(1)}(c_2,\boldsymbol{r}) \mp \boldsymbol{M}_{\substack{o \\ e}^{mnu}}^{y(1)}(c_2,\boldsymbol{r}))$$
$$+ B_{\substack{o \\ e}^{mn}}^{-yM} (N_{\substack{o \\ e}^{mnu}}^{x(1)}(c_2,\boldsymbol{r}) \mp N_{\substack{e \\ o}^{mnu}}^{y(1)}(c_2,\boldsymbol{r})) + B_{\substack{e \\ o}^{mn}}^{-yN} (\boldsymbol{M}_{\substack{e \\ o}^{mnu}}^{x(1)}(c_2,\boldsymbol{r}) \pm \boldsymbol{M}_{\substack{o \\ e}^{mnu}}^{y(1)}(c_2,\boldsymbol{r}))$$
$$+ 2N_{\substack{e \\ o}^{mnu}}^{y(3)}(c_2,\boldsymbol{r})] \tag{4.6b}$$

$$\sum_{n=m}^{\infty} \mathrm{K}_{\substack{e \\ o}^{mn}} [A_{\substack{e \\ o}^{mn}}^{zM} \boldsymbol{N}_{\substack{e \\ o}^{mnu}}^{z(3)}(c_1,\boldsymbol{r}) + A_{\substack{o \\ e}^{mn}}^{zN} \boldsymbol{M}_{\substack{o \\ e}^{mnu}}^{z(3)}(c_1,\boldsymbol{r})]$$
$$= \sum_{n=m}^{\infty} \mathrm{K}_{\substack{e \\ o}^{mn}} [B_{\substack{e \\ o}^{mn}}^{zM} \boldsymbol{N}_{\substack{e \\ o}^{mnu}}^{z(1)}(c_2,\boldsymbol{r}) + \boldsymbol{N}_{\substack{e \\ o}^{mnu}}^{z(3)}(c_2,\boldsymbol{r}) + B_{\substack{o \\ e}^{mn}}^{zN} \boldsymbol{M}_{\substack{o \\ e}^{mnu}}^{z(1)}(c_2,\boldsymbol{r})] \tag{4.6c}$$

where u denotes $\hat{\eta}$- or $\hat{\phi}$-component, and $\mathrm{K}_{\substack{e \\ o}^{mn}} = \iiint_{v} \frac{2-\delta_{m0}}{N_{mn}} \psi_{\substack{e \\ o}^{mn}}^{(1)}(c_2,\boldsymbol{r}')\boldsymbol{M}_s(\boldsymbol{r}')dv'$.

The method used to solve equations (4.5a), (4.5b), (4.6a) and (4.6b) is as follows: the equations that stand for the continuity of $\hat{\eta}$- components are multiplied by

$$(\xi_0^2-\eta^2)^{2/5}\sqrt{(1-\eta^2)/(\xi_0^2-1)} = [(\xi_0^2-1)+(1-\eta^2)]^{2/5}\sqrt{(1-\eta^2)/(\xi_0^2-1)} \tag{4.7a}$$

and the equations that stand for the continuity of $\hat{\phi}$-components are multiplied by

$$(\xi_0^2-\eta^2)\sqrt{(1-\eta^2)} = [(\xi_0^2-1)+(1-\eta^2)]\sqrt{(1-\eta^2)}\,. \tag{4.7b}$$

The method used to solve equations (4.5c) and (4.6c) is as follows: the equations that stand for the continuity of $\hat{\eta}$ - components are multiplied by

$$\frac{d}{2}(\xi_0^2-\eta^2)^{2/5}=\frac{d}{2}[(\xi_0^2-1)+(1-\eta^2)]^{2/5} \tag{4.7c}$$

and the equations that stand for the continuity of $\hat{\phi}$ -components are multiplied by

$$(\xi_0^2-\eta^2)(1-\eta^2)/(\xi_0^2-1)^{1/2}=[(\xi_0^2-1)+(1-\eta^2)]/(\xi_0^2-1)^{1/2}. \tag{4.7d}$$

These multipliers are positive in the full range of η. Replace all the factors that are functions of η by the series of the associated Legendre functions of the first kind, which are orthogonal functions in the interval $-1\le\eta\le1$. The functions of η can be expanded in term of $P_{m-1+t}^{m-1}(\eta)$ as follows [25], [44]:

$$(1-\eta^2)^{-1/2}S_{mn}(c,\eta)=\sum_{t=0}^{\infty}I_{t,0}^{mn}(c)\cdot P_{m-1+t}^{m-1}(\eta) \tag{4.8a}$$

$$(1-\eta^2)^{1/2}S_{mn}(c,\eta)=\sum_{t=0}^{\infty}I_{t,1}^{mn}(c)\cdot P_{m-1+t}^{m-1}(\eta) \tag{4.8b}$$

$$(1-\eta^2)^{3/2}S_{mn}(c,\eta)=\sum_{t=0}^{\infty}I_{t,2}^{mn}(c)\cdot P_{m-1+t}^{m-1}(\eta) \tag{4.8c}$$

$$(1-\eta^2)^{5/2}S_{mn}(c,\eta)=\sum_{t=0}^{\infty}I_{t,3}^{mn}(c)\cdot P_{m-1+t}^{m-1}(\eta) \tag{4.8d}$$

$$\eta(1-\eta^2)^{-1/2} S_{mn}(c,\eta) = \sum_{t=0}^{\infty} I_{t,4}^{mn}(c) \cdot P_{m-1+t}^{m-1}(\eta) \tag{4.8e}$$

$$\eta(1-\eta^2)^{1/2} S_{mn}(c,\eta) = \sum_{t=0}^{\infty} I_{t,5}^{mn}(c) \cdot P_{m-1+t}^{m-1}(\eta) \tag{4.8f}$$

$$\eta(1-\eta^2)^{3/2} S_{mn}(c,\eta) = \sum_{t=0}^{\infty} I_{t,6}^{mn}(c) \cdot P_{m-1+t}^{m-1}(\eta) \tag{4.8g}$$

$$(1-\eta^2)^{1/2} \frac{dS_{mn}(c,\eta)}{d\eta} = \sum_{t=0}^{\infty} I_{t,7}^{mn}(c) \cdot P_{m-1+t}^{m-1}(\eta) \tag{4.8h}$$

$$(1-\eta^2)^{3/2} \frac{dS_{mn}(c,\eta)}{d\eta} = \sum_{t=0}^{\infty} I_{t,8}^{mn}(c) \cdot P_{m-1+t}^{m-1}(\eta) \tag{4.8i}$$

$$(1-\eta^2)^{5/2} \frac{dS_{mn}(c,\eta)}{d\eta} = \sum_{t=0}^{\infty} I_{t,9}^{mn}(c) \cdot P_{m-1+t}^{m-1}(\eta) \tag{4.8j}$$

$$(1-\eta^2)^{1/2} \frac{dS_{mn}(c,\eta)}{d\eta} = \sum_{t=0}^{\infty} I_{t,10}^{mn}(c) \cdot P_{m-1+t}^{m-1}(\eta) \tag{4.8k}$$

$$\eta(1-\eta^2)^{3/2} \frac{dS_{mn}(c,\eta)}{d\eta} = \sum_{t=0}^{\infty} I_{t,11}^{mn}(c) \cdot P_{m-1+t}^{m-1}(\eta) \tag{4.8l}$$

$$(1-\eta^2)^{1/2} S_{0n}(c,\eta) = \sum_{t=0}^{\infty} I_{t,1}^{0n}(c) \cdot P_{1+t}^{1}(\eta) \tag{4.8m}$$

$$(1-\eta^2)^{3/2} S_{0n}(c,\eta) = \sum_{t=0}^{\infty} I_{t,2}^{0n}(c) \cdot P_{1+t}^{1}(\eta) \tag{4.8n}$$

$$(1-\eta^2)^{5/2} S_{0n}(c,\eta) = \sum_{t=0}^{\infty} I_{t,3}^{0n}(c) \cdot P_{1+t}^{1}(\eta) \tag{4.8o}$$

$$\eta(1-\eta^2)^{-1/2} \frac{dS_{0n}(c,\eta)}{d\eta} = \sum_{t=0}^{\infty} I_{t,10}^{0n}(c) \cdot P_{1+t}^{1}(\eta) \tag{4.8p}$$

$$\eta(1-\eta^2)^{3/2} \frac{dS_{0n}(c,\eta)}{d\eta} = \sum_{t=0}^{\infty} I_{t,11}^{0n}(c) \cdot P_{1+t}^{1}(\eta) \ . \tag{4.8q}$$

The coefficients of these expansions are functions of c and can be evaluated by using equation (2.9) to express the angular function $S_{mn}(c,\eta)$ and its derivatives in terms of $P_{m+r}^{m}(\eta)$ and it derivatives. The closed form expressions of these intermediate coefficients $I_{t,k}^{mn}$ are given in Appendix B.

Inserting equations (4.8a)-(4.8q) into the equations representing the boundary conditions, and then considering the orthogonality of the associated Legendre functions of the first kind, it can be seen that the individual terms in the summation over t must be matched term by term.

For easier manipulation of the equations, we employ the following substitutions. They are defined by

$$\begin{aligned} u_{\substack{e_{mn\eta} \\ o}}^{\pm(i),t}(c) &= (\boldsymbol{M}_{\substack{e_{mn\eta} \\ o}}^{x(i)} \mp \boldsymbol{M}_{\substack{o_{mn\eta} \\ e}}^{y(i)}) \times \frac{d}{2}(\xi_0^2-\eta^2)^{2/5} \sqrt{(1-\eta^2)/(\xi_0^2-1)} \\ &= [\frac{dR_{mn}^{(i)}(c,\xi_0)}{d\xi_0} \mp \frac{m\xi_0}{\xi_0^{\ 2}-1} R_{mn}^{(i)}(c,\xi_0)] \\ &\quad \times [(\xi_0^{\ 2}-1)^2 I_{t,1}^{mn}(c) + 2(\xi_0^{\ 2}-1) I_{t,2}^{mn}(c) + I_{t,3}^{mn}(c)] \end{aligned} \tag{4.9a}$$

$$u_{o\,e_{mn\phi}}^{\pm(i),t}(c)=(\boldsymbol{M}_{o\,e_{mn\phi}}^{x(i)}\mp\boldsymbol{M}_{e\,o_{mn\phi}}^{y(i)})\times\frac{d}{2}(\xi_0^2-\eta^2)\sqrt{(1-\eta^2)}$$
$$=\frac{dR_{mn}^{(i)}(c,\xi_0)}{d\xi_0}I_{t,5}^{mn}(c)+\xi_0R_{mn}^{(i)}(c,\xi_0)I_{t,8}^{mn}(c) \qquad (4.9b)$$

$$v_{o\,e_{mn\eta}}^{\pm i,t}(c)=(\boldsymbol{N}_{o\,e_{mn\eta}}^{x(i)}\pm\boldsymbol{N}_{e\,o_{mn\eta}}^{y(i)})\times\frac{d}{2}(\xi_0^2-\eta^2)^{2/5}\sqrt{(1-\eta^2)/(\xi_0^2-1)}$$
$$=\frac{1}{c}(\{[(\xi_0{}^2-1)(\lambda_{mn}-c^2\xi^2+\frac{m^2}{\xi_0{}^2-1})-2m(m\pm1)]R_{mn}^{(i)}(c,\xi_0)$$
$$-\xi_0(\xi_0{}^2-1)\frac{dR_{mn}^{(i)}(c,\xi_0)}{d\xi_0}\}I_{t,5}^{mn}(c)\mp[(m\pm1)(\xi_0{}^2-1)$$
$$\cdot R_{mn}^{(i)}(c,\xi_0)I_{t,7}^{mn}(c)+[(\lambda_{mn}-c^2\xi^2\mp\frac{m}{\xi_0{}^2-1})R_{mn}^{(i)}(c,\xi_0)$$
$$+\xi_0\frac{dR_{mn}^{(i)}(c,\xi_0)}{d\xi_0}]I_{t,6}^{mn}(c)+[\xi_0(\xi_0{}^2-1)\frac{dR_{mn}^{(i)}(c,\xi_0)}{d\xi_0}$$
$$-(3\pm2m)R_{mn}^{(i)}(c,\xi_0)]I_{t,8}^{mn}(c)+[\xi_0\frac{dR_{mn}^{(i)}(c,\xi_0)}{d\xi_0}+(2\mp\frac{m}{\xi_0{}^2-1})$$
$$\cdot R_{mn}^{(i)}(c,\xi_0)]I_{t,9}^{mn}(c)-[m(m\pm1)(\xi_0{}^2-1)R_{mn}^{(i)}(c,\xi_0)]I_{t,4}^{mn}(c) \qquad (4.9c)$$

$$v_{o\,e_{mn\phi}}^{\pm(i),t}(c)=(\boldsymbol{N}_{o\,e_{mn\phi}}^{x(i)}\pm\boldsymbol{N}_{e\,o_{mn\phi}}^{y(i)})\times\frac{d}{2}(\xi_0^2-\eta^2)\sqrt{(1-\eta^2)}$$
$$=\frac{1}{c}\{[m(m\pm1)R_{mn}^{(i)}(c,\xi_0)]I_{t,0}^{mn}(c)+[(1\pm m)R_{mn}^{(i)}(c,\xi_0)]I_{t,10}^{mn}(c)$$
$$-[c^2R_{mn}^{(i)}(c,\xi_0)]I_{t,2}^{mn}(c)+[(-c^2(\xi_0^2-1)+\frac{m(m\pm1)}{\xi_0^2-1})R_{mn}^{(i)}(c,\xi_0)]$$
$$\cdot I_{t,1}^{mn}(c)-[(1\pm m)\xi_0\frac{dR_{mn}^{(i)}(c,\xi_0)}{d\xi_0}]I_{t,1}^{mn}(c)\} \qquad (4.9d)$$

$$u_{o\,e_{mn\eta}}^{z(i),t}(c)=\boldsymbol{M}_{o\,e_{mn\eta}}^{z(i)}\times\frac{d}{2}(\xi_0^2-\eta^2)^{2/5}$$
$$=mR_{mn}^{(i)}(c,\xi_0)[(\xi_0{}^2-1)^2I_{t,4}^{mn}(c)+2(\xi_0{}^2-1)I_{t,5}^{mn}(c)+I_{t,6}^{mn}(c)] \qquad (4.10a)$$

$$u^{z(i),t}_{o\,e_{mn\phi}}(c) = \boldsymbol{M}^{z(i)}_{o\,e_{mn\phi}} \times \frac{d}{2}(\xi_0^2-\eta^2)(1-\mu^2)(\xi_0^2-1)^{-\frac{1}{2}}$$

$$= R^{(i)}_{mn}(c,\xi_0) I^{mn}_{t,11}(c) - \xi_0 \frac{dR^{(i)}_{mn}(c,\xi_0)}{d\xi_0}] I^{mn}_{t,2}(c) \qquad (4.10b)$$

$$v^{\pm x(i),t}_{o\,e_{mn\eta}}(c) = \boldsymbol{N}^{z(i)}_{o\,e_{mn\eta}} \times \frac{d}{2}(\xi_0^2-\eta^2)^{2/5}$$

$$= \frac{1}{c}\{[(\xi_0^{\,2}-1)^2 \frac{dR^{(i)}_{mn}(c,\xi_0)}{d\xi_0}] I^{mn}_{t,10}(c)$$

$$+ [(\xi_0^{\,2}-1)\frac{dR^{(i)}_{mn}(c,\xi_0)}{d\xi_0} + 2\xi_0 R^{(i)}_{mn}(c,\xi_0)] I^{mn}_{t,11}(c)$$

$$-(\xi_0^{\,2}-1)[\xi_0(\lambda_{mn}-c^2\xi^2-\frac{m^2}{\xi_0^{\,2}-1})R^{(i)}_{mn}(c,\xi_0) - (\xi_0^{\,2}+1) \qquad (4.10c)$$

$$\cdot\frac{dR^{(i)}_{mn}(c,\xi_0)}{d\xi_0}] I^{mn}_{t,1}(c) - [\xi_0(\lambda_{mn}-c^2\xi^2)R^{(i)}_{mn}(c,\xi_0) + (\xi_0^{\,2}-1)$$

$$\cdot\frac{dR^{(i)}_{mn}(c,\xi_0)}{d\xi_0}] \times I^{mn}_{t,2}(c) + [m^2\xi_0(\xi_0^{\,2}-1)R^{(i)}_{mn}(c,\xi_0)] I^{mn}_{t,0}(c)\}$$

$$v^{z(i),t}_{o\,e_{mn\phi}}(c) = \boldsymbol{N}^{z(i)}_{o\,e_{mn\phi}} \times \frac{d}{2}(\xi_0^2-\eta^2)(1-\mu^2)(\xi_0^2-1)^{-\frac{1}{2}} \qquad (4.10d)$$

$$= \frac{m}{c}\{[\frac{\xi_0}{\xi_0^{\,2}-1} R^{(i)}_{mn}(c,\xi_0)] I^{mn}_{t,8}(c) + [\frac{dR^{(i)}_{mn}(c,\xi_0)}{d\xi_0}] I^{mn}_{t,5}(c)\}$$

where the intermediate coefficients $I^{mn}_{t,l}(c)$ *(t = 0, 1, 2, ... and l = 0, 1, 2, ... 11)* are provided in closed form in Appendix B.

With these parameters, the equations for determining the unknown coefficients in the prolate spheroidal system are now written for each value of *m*, in the following forms:

- From equations (4.5a) and (4.6a), the coefficients of the dyadic Green's functions associated with $\boldsymbol{M}\hat{x}$ and $\boldsymbol{N}\hat{x}$ in equations (3.13) and (3.14) can be calculated from equations (4.11) and (4.12) where $\rho = \sqrt{\varepsilon_{r1}/\varepsilon_{r2}}$ as

$$\sum_{n=m}^{\infty} \mathrm{K}_{\substack{e\\o}mn} \begin{pmatrix} \mp u^{+(3),t}_{\substack{e\\o}mn\eta}(c_1) & v^{+(3),t}_{\substack{o\\e}mn\eta}(c_1) & \pm u^{+(1),t}_{\substack{e\\o}mn\eta}(c_2) & -v^{+(1),t}_{\substack{o\\e}mn\eta}(c_2) \\ u^{+(3),t}_{\substack{e\\o}mn\varphi}(c_1) & \mp v^{+(3),t}_{\substack{o\\e}mn\varphi}(c_1) & -u^{+(1),t}_{\substack{e\\o}mn\varphi}(c_2) & \pm v^{+(1),t}_{\substack{o\\e}mn\varphi}(c_2) \\ v^{+(3),t}_{\substack{e\\o}mn\eta}(c_1) & \pm u^{+(3),t}_{\substack{o\\e}mn\eta}(c_1) & -\rho v^{+(1),t}_{\substack{e\\o}mn\eta}(c_2) & \mp \rho u^{+(1),t}_{\substack{o\\e}mn\eta}(c_2) \\ \pm v^{+(3),t}_{\substack{e\\o}mn\varphi}(c_1) & u^{+(3),t}_{\substack{o\\e}mn\varphi}(c_1) & \mp \rho v^{+(1),t}_{\substack{e\\o}mn\varphi}(c_2) & -\rho u^{+(1),t}_{\substack{o\\e}mn\varphi}(c_2) \end{pmatrix} \begin{pmatrix} A^{+xM}_{\substack{e\\o}mn} \\ A^{+xN}_{\substack{o\\e}mn} \\ B^{+xM}_{\substack{e\\o}mn} \\ B^{+xN}_{\substack{o\\e}mn} \end{pmatrix} = \sum_{n=m}^{\infty} \mathrm{K}_{\substack{e\\o}mn} \begin{pmatrix} \mp u^{+(3),t}_{\substack{e\\o}mn\eta}(c_2) \\ u^{+(3),t}_{\substack{e\\o}mn\varphi}(c_2) \\ \rho v^{+(3),t}_{\substack{e\\o}mn\eta}(c_2) \\ \pm \rho v^{+(3),t}_{\substack{e\\o}mn\varphi}(c_2) \end{pmatrix} \tag{4.11}$$

$$\sum_{n=m}^{\infty} \mathrm{K}_{\substack{e\\o}mn} \begin{pmatrix} \pm u^{-(3),t}_{\substack{e\\o}mn\eta}(c_1) & v^{-(3),t}_{\substack{o\\e}mn\eta}(c_1) & \mp u^{-(1),t}_{\substack{e\\o}mn\eta}(c_2) & -v^{-(1),t}_{\substack{o\\e}mn\eta}(c_2) \\ u^{-(3),t}_{\substack{e\\o}mn\varphi}(c_1) & \pm v^{-(3),t}_{\substack{o\\e}mn\varphi}(c_1) & -u^{-(1),t}_{\substack{e\\o}mn\varphi}(c_2) & \mp v^{-(1),t}_{\substack{o\\e}mn\varphi}(c_2) \\ v^{-(3),t}_{\substack{e\\o}mn\eta}(c_1) & \mp u^{-(3),t}_{\substack{o\\e}mn\eta}(c_1) & -\rho v^{-(1),t}_{\substack{e\\o}mn\eta}(c_2) & \pm \rho u^{-(1),t}_{\substack{o\\e}mn\eta}(c_2) \\ \mp v^{-(3),t}_{\substack{e\\o}mn\varphi}(c_1) & u^{-(3),t}_{\substack{o\\e}mn\varphi}(c_1) & \pm \rho v^{-(1),t}_{\substack{e\\o}mn\varphi}(c_2) & -\rho u^{-(1),t}_{\substack{o\\e}mn\varphi}(c_2) \end{pmatrix} \begin{pmatrix} A^{-xM}_{\substack{e\\o}mn} \\ A^{-xN}_{\substack{o\\e}mn} \\ B^{-xM}_{\substack{e\\o}mn} \\ B^{-xN}_{\substack{o\\e}mn} \end{pmatrix} = \sum_{n=m}^{\infty} \mathrm{K}_{\substack{e\\o}mn} \begin{pmatrix} \pm u^{-(3),t}_{\substack{e\\o}mn\eta}(c_2) \\ u^{-(3),t}_{\substack{e\\o}mn\varphi}(c_2) \\ \rho v^{-(3),t}_{\substack{e\\o}mn\eta}(c_2) \\ \mp \rho v^{-(3),t}_{\substack{e\\o}mn\varphi}(c_2) \end{pmatrix} \tag{4.12}$$

- From equations (4.5b) and (4.6b), the coefficients of the dyadic Green's functions associated with $M\hat{y}$ and $N\hat{y}$ in equations (3.13) and (3.14) can be calculated from equations (4.13) and (4.14) where $\rho = \sqrt{\varepsilon_{r1} / \varepsilon_{r2}}$ as

$$\sum_{n=m}^{\infty} \mathrm{K}_{\substack{e\\o}mn} \begin{pmatrix} \pm u^{+(3),t}_{\substack{e\\o}mn\eta}(c_1) & v^{+(3),t}_{\substack{o\\e}mn\eta}(c_1) & \mp u^{+(1),t}_{\substack{e\\o}mn\eta}(c_2) & -v^{+(1),t}_{\substack{o\\e}mn\eta}(c_2) \\ u^{+(3),t}_{\substack{e\\o}mn\varphi}(c_1) & \pm v^{+(3),t}_{\substack{o\\e}mn\varphi}(c_1) & -u^{+(1),t}_{\substack{e\\o}mn\varphi}(c_2) & \mp v^{+(1),t}_{\substack{o\\e}mn\varphi}(c_2) \\ v^{+(3),t}_{\substack{e\\o}mn\eta}(c_1) & \mp u^{+(3),t}_{\substack{o\\e}mn\eta}(c_1) & -\rho v^{+(1),t}_{\substack{e\\o}mn\eta}(c_2) & \pm \rho u^{+(1),t}_{\substack{o\\e}mn\eta}(c_2) \\ \mp v^{+(3),t}_{\substack{e\\o}mn\varphi}(c_1) & u^{+(3),t}_{\substack{o\\e}mn\varphi}(c_1) & \pm \rho v^{+(1),t}_{\substack{e\\o}mn\varphi}(c_2) & -\rho u^{+(1),t}_{\substack{o\\e}mn\varphi}(c_2) \end{pmatrix} \begin{pmatrix} A^{+yM}_{\substack{o\\e}mn} \\ A^{+yN}_{\substack{e\\o}mn} \\ B^{+yM}_{\substack{o\\e}mn} \\ B^{+yN}_{\substack{e\\o}mn} \end{pmatrix} = \sum_{n=m}^{\infty} \mathrm{K}_{\substack{e\\o}mn} \begin{pmatrix} +u^{+(3),t}_{\substack{e\\o}mn\eta}(c_2) \\ \pm u^{+(3),t}_{\substack{e\\o}mn\varphi}(c_2) \\ \pm \rho v^{+(3),t}_{\substack{e\\o}mn\eta}(c_2) \\ -\rho v^{+(3),t}_{\substack{e\\o}mn\varphi}(c_2) \end{pmatrix} \tag{4.13}$$

$$\sum_{n=m}^{\infty} \mathrm{K}_{\substack{e\\o}mn} \begin{pmatrix} \mp u^{-(3),t}_{\substack{e\\o}mn\eta}(c_1) & v^{-(3),t}_{\substack{o\\e}mn\eta}(c_1) & \pm u^{-(1),t}_{\substack{e\\o}mn\eta}(c_2) & -v^{-(1),t}_{\substack{o\\e}mn\eta}(c_2) \\ u^{-(3),t}_{\substack{e\\o}mn\varphi}(c_1) & \mp v^{-(3),t}_{\substack{o\\e}mn\varphi}(c_1) & -u^{-(1),t}_{\substack{e\\o}mn\varphi}(c_2) & \pm v^{-(1),t}_{\substack{o\\e}mn\varphi}(c_2) \\ v^{-(3),t}_{\substack{e\\o}mn\eta}(c_1) & \pm u^{-(3),t}_{\substack{o\\e}mn\eta}(c_1) & -\rho v^{-(1),t}_{\substack{e\\o}mn\eta}(c_2) & \pm \mp \rho u^{-(1),t}_{\substack{o\\e}mn\eta}(c_2) \\ \pm v^{-(3),t}_{\substack{e\\o}mn\varphi}(c_1) & u^{-(3),t}_{\substack{o\\e}mn\varphi}(c_1) & \mp \rho v^{-(1),t}_{\substack{e\\o}mn\varphi}(c_2) & -\rho u^{-(1),t}_{\substack{o\\e}mn\varphi}(c_2) \end{pmatrix} \begin{pmatrix} A^{-yM}_{\substack{o\\e}mn} \\ A^{-yN}_{\substack{e\\o}mn} \\ B^{-yM}_{\substack{o\\e}mn} \\ B^{-yN}_{\substack{e\\o}mn} \end{pmatrix} = \sum_{n=m}^{\infty} \mathrm{K}_{\substack{e\\o}mn} \begin{pmatrix} +u^{-(3),t}_{\substack{e\\o}mn\eta}(c_2) \\ \mp u^{-(3),t}_{\substack{e\\o}mn\varphi}(c_2) \\ \mp \rho v^{-(3),t}_{\substack{e\\o}mn\eta}(c_2) \\ -\rho v^{-(3),t}_{\substack{e\\o}mn\varphi}(c_2) \end{pmatrix} \tag{4.14}$$

- From equations (4.5c) and (4.6c), the coefficients of the dyadic Green's functions associated with $M\hat{z}$ and $N\hat{z}$ in equations (3.13) and (3.14) can be calculated from equation (4.15) where $\rho = \sqrt{\varepsilon_{r1} / \varepsilon_{r2}}$ as

$$\sum_{n=m}^{\infty} \mathrm{K}_{\substack{e \\ o}mn} \begin{pmatrix} \pm u^{z(3),t}_{\substack{e \\ o}mn\eta}(c_1) & v^{z(3),t}_{\substack{o \\ e}mn\eta}(c_1) & \mp u^{z(1),t}_{\substack{e \\ o}mn\eta}(c_2) & -v^{z(1),t}_{\substack{o \\ e}mn\eta}(c_2) \\ u^{z(3),t}_{\substack{e \\ o}mn\varphi}(c_1) & \pm v^{z(3),t}_{\substack{o \\ e}mn\varphi}(c_1) & -u^{z(1),t}_{\substack{e \\ o}mn\varphi}(c_2) & \mp v^{z(1),t}_{\substack{o \\ e}mn\varphi}(c_2) \\ v^{z(3),t}_{\substack{e \\ o}mn\eta}(c_1) & \mp u^{z(3),t}_{\substack{o \\ e}mn\eta}(c_1) & -\rho v^{z(1),t}_{\substack{e \\ o}mn\eta}(c_2) & \pm \rho u^{z(1),t}_{\substack{o \\ e}mn\eta}(c_2) \\ \mp v^{z(3),t}_{\substack{e \\ o}mn\varphi}(c_1) & u^{z(3),t}_{\substack{o \\ e}mn\varphi}(c_1) & \pm \rho v^{z(1),t}_{\substack{e \\ o}mn\varphi}(c_2) & -\rho u^{z(1),t}_{\substack{o \\ e}mn\varphi}(c_2) \end{pmatrix} \begin{pmatrix} A^{zM}_{\substack{e \\ o}mn} \\ A^{zN}_{\substack{o \\ e}mn} \\ B^{zM}_{\substack{e \\ o}mn} \\ B^{zN}_{\substack{o \\ e}mn} \end{pmatrix} = \sum_{n=m}^{\infty} \mathrm{K}_{\substack{e \\ o}mn} \begin{pmatrix} \pm u^{z(3),t}_{\substack{e \\ o}mn\eta}(c_2) \\ u^{z(3),t}_{\substack{e \\ o}mn\varphi}(c_2) \\ \rho v^{z(3),t}_{\substack{e \\ o}mn\eta}(c_2) \\ \mp \rho v^{z(3),t}_{\substack{o \\ e}mn\varphi}(c_2) \end{pmatrix} \tag{4.15}$$

Thus, we have obtained an infinite system of coupled linear equations with complex coefficients.

4.3 Convergence of the solution

Equations 4.11-4.15 are valid for each value of t, so that taking t sufficiently large an adequate number of relations between unknown coefficients is generated. The convergence of the infinite series is expected both physically and mathematically. Practically, the infinite system of equations is truncated to a finite number of equations. According to Sinha and MacPhie [26], this truncated number is taken as N_t = Integer $(|kb| + 4)$ (where k is the propagation constant in the media, b is the major semiaxial length of the spheroid). In other words, there exist $4 \times N_t$ scalar unknowns

for each of the above matrix systems. Assuming that the index t in the equations is taken as $0, 1, \ldots, N_t - 1$, we can obtain a $4N_t \times 4N_t$ matrix system, and determine these $4 \times N_t$ unknowns uniquely.

Because of the non-existence of orthogonality of spheroidal wave functions, the unknown scattering coefficients are coupled to each other. By using the method of functional expansion, the coupled unknowns are then determined explicitly from the matrix system of the linear equations. Although determination of these unknowns has been provided in closed form, it should be noted that the point source information is also included inside the coupled equations, and the unknowns cannot be obtained analytically from the equations without the integrals of the source current. This is different from the spherical case, where the transmitting and scattering coefficients are integrals of source currents and decoupled from each other. However, for a given source excitation in a spheroidal structure, the distribution is known and the source point does not appear after integration over the entire source region.

4.4 Far field expression

4.4.1 Slot-aperture excitation

Figure 1.1 shows the configuration of the prolate hemispheroidal DRA, excited by a narrow slot. The narrow rectangular slot with width w and length l, and is parallel to

the x-axis at the centre of the dielectric spheroid. At the opening, the field is approximated by the dominant TE_{10} mode [45]. The electric field, $\boldsymbol{E}_s$, in the slot along the x-axis is assumed to be y-directed, and must vanish at the ends of the slot. Also, the electric field is assumed not to vary across the width of the slot. Thus

$$\boldsymbol{E}_s = \hat{y}E_0 \cos(\frac{\pi}{l}x') \qquad \begin{cases} -l/2 \le x' \le l/2 \\ -w/2 \le y' \le w/2 \end{cases}. \tag{4.16}$$

As discussed in Chapter 3, image theory is used to remove the ground plane to obtain an equivalent problem of a full dielectric prolate spheroid, excited by $\boldsymbol{M}_s = 2\boldsymbol{M}$, as shown in figure 4.1. The equivalent magnetic current is x-directed and only varies in the x-direction. It is

$$\boldsymbol{M}_s = \begin{cases} -2\hat{z} \times \boldsymbol{E}_s = -2\hat{z} \times \hat{y}E_0 = \hat{x}2E_0 \cos(\frac{\pi}{l}x') & \begin{cases} -l/2 \le x' \le l/2 \\ -w/2 \le y' \le w/2. \end{cases} \\ 0 & \textit{elsewhere} \end{cases} \tag{4.17}$$

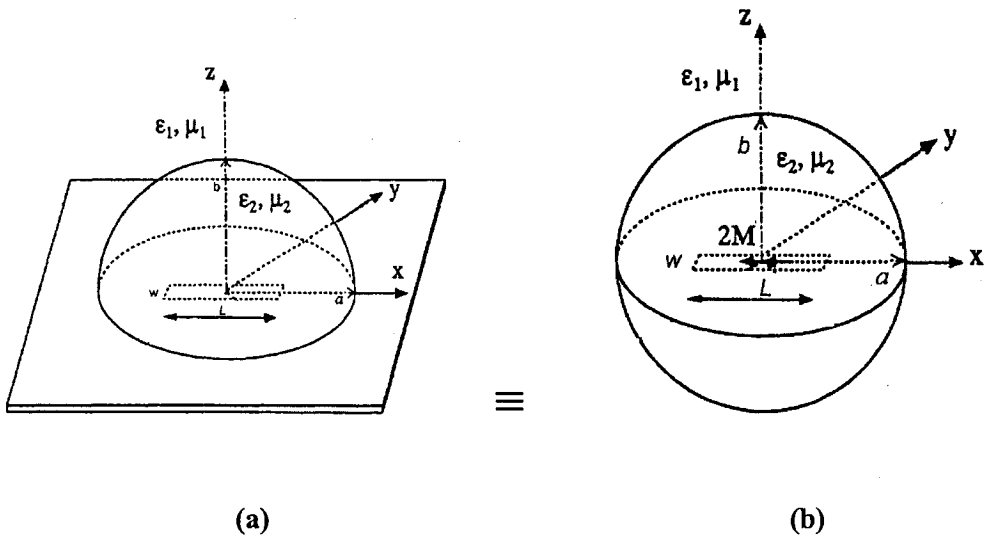

(a) (b)

Fig. 4.1 (a) The hemispheroidal dielectric resonator antenna excited by a slot aperture; (b) Equivalent problems for the hemispheroidal dielectric resonator antenna, excited by a slot aperture, after using image theory.

4.4.2 Formulation of far field

The general expressions of electromagnetic fields are expressed in terms of dyadic Green's functions pertaining to a magnetic-current source located in a dielectric spheroid in Chapter 3. We can use these general expressions of electromagnetic fields to calculate the electromagnetic field everywhere, such as far field, near field and the field inside the spheroid. In this work, the source current distribution only has an $\hat{x}$-component. Thus, only the $\hat{x}$-component of the dyadic Green's functions is needed. For the electromagnetic far field, we can simplify the formula according to the asymptotic form of spheroidal radial function when $c\xi \to \infty$ [35]. The far zone electric field can be expressed as

$$E_\eta = \frac{-ik_2}{\pi d c_1^2 \xi}\sum_{n=0}^{\infty}\sum_{m=0}^{n}\Big\{(c_1^2 S_{mn} + c_1 S_{mn} + 1)\cdot e^{i[c_1\xi - \frac{1}{2}(n+1)\pi]}$$
$$\cdot[A_e^{+xM}\cdot sin((m+1)\phi) - A_e^{-xM}\cdot sin((m-1)\phi) -$$
$$A_o^{+xN}\cdot sin((m+1)\phi)\cdot(\rho_1+\rho_2) + A_o^{-xN}\cdot sin((m-1)\phi)\cdot(\rho_1-\rho_2)] \tag{4.18}$$
$$\cdot \iiint_v \Gamma_{mn} M_x(\bar{r}')dv' \Big\}$$

$$E_\phi = \frac{-ik_2}{\pi d c_1^2 \xi}\sum_{n=0}^{\infty}\sum_{m=0}^{n}\Big\{(-c_1^2\eta S_{mn} + c_1\eta S_{mn} + 1)\cdot e^{i[c_1\xi - \frac{1}{2}(n+1)\pi]}$$
$$\cdot[A_e^{+xM}\cdot cos((m+1)\phi) + A_e^{-xM}\cdot cos((m-1)\phi) -$$
$$A_o^{+xN}\cdot cos((m+1)\phi)\cdot(\rho_3+\rho_4) + A_o^{-xN}\cdot cos((m-1)\phi)\cdot(\rho_3-\rho_4)] \tag{4.19}$$
$$\cdot \iiint_v \Gamma_{mn} M_x(\bar{r}')dv' \Big\}$$

$$E_\xi = \frac{-ik_2}{2\pi d c_1^2 \xi^2}\sum_{n=0}^{\infty}\sum_{m=0}^{n}\Big\{[-c_1(1-\eta^2)^{1/2} + 2c_1 - 2]\cdot e^{i[c_1\xi - \frac{1}{2}(n+1)\pi]}$$
$$\cdot[A_e^{+xM}\cdot sin((m+1)\phi)\cdot(\frac{dS_{mn}}{d\eta} + \frac{m\eta}{1-\eta^2}S_{mn})$$
$$- A_e^{-xM}\cdot sin((m-1)\phi)\cdot(\frac{dS_{mn}}{d\eta} - \frac{m\eta}{1-\eta^2}S_{mn}) \tag{4.20}$$
$$- A_o^{+xN}\cdot sin((m+1)\phi)\cdot(\rho_5-\rho_6) + A_o^{-xN}\cdot sin((m-1)\phi)\cdot(\rho_5+\rho_6)]$$
$$\cdot \iiint_v \Gamma_{mn} M_x(\bar{r}')dv' \Big\}$$

where the prime symbol denotes the source point location; M_x is the magnetic current distribution that is along x-axis. A_e^{+xM}, A_e^{-xM}, A_o^{+xN}, and A_o^{-xN} are scattering coefficients, which were already determined in section 4.2; Γ_{mn}, ρ_1, ρ_2, ρ_3, ρ_4, ρ_5, and ρ_6 are

$$\Gamma_{mn} = \frac{2-\delta_{m0}}{N_{mn}}\psi^{(1)}_{\substack{e_{mn}\\ o}}(c_2, \mathbf{r}') \tag{4.21}$$

$$\rho_1 = \frac{m}{\xi^2} \cdot \frac{dS_{mn}}{d\eta} + \frac{m\eta}{\xi^2(1-\eta^2)} S_{mn} \tag{4.22}$$

$$\rho_2 = (c_1 + 1)(1-\eta^2)\frac{dS_{mn}}{d\eta} + (c_1{}^2\eta^2 + \frac{m^2\eta}{\xi^2(1-\eta^2)} S_{mn} \tag{4.23}$$

$$\rho_3 = \frac{\eta}{\xi^2} \cdot \frac{dS_{mn}}{d\eta} + (c_1{}^2 + \frac{m^2}{\xi^2(1-\eta^2)}) S_{mn} \tag{4.24}$$

$$\rho_4 = \frac{m\eta}{\xi^2} \cdot \frac{dS_{mn}}{d\eta} + \frac{m\eta^2}{\xi^2(1-\eta^2)} S_{mn} \tag{4.25}$$

$$\rho_5 = -(c_1 + 1)\eta(1-\eta^2)^{\frac{1}{2}} \frac{dS_{mn}}{d\eta} + \frac{m^2(\xi-1) - (c_1+1)(1+\eta^2)\xi}{\xi^2(1-\eta^2)^{\frac{1}{2}}} S_{mn} \tag{4.26}$$

$$\rho_6 = \frac{m + m\xi(c_1+1)}{\xi(1-\eta^2)^{\frac{1}{2}}} S_{mn} . \tag{4.27}$$

From equations (4.18), (4.19) and (4.20), it can be seen that the $\hat{\eta}$- and $\hat{\phi}$-components of the electric field become dominant in the far field. The $\hat{\xi}$-component of electric field is very small because of the factor of $\frac{1}{\xi^2}$. The detailed derivation of the above far field expressions is presented in Appendix C.

Chapter 5
Results and Discussion

5.1 Introduction

In this chapter, radiation patterns and directivity of the hemispheroidal DRA as shown in figure 1.1, excited by slot aperture with different parameters are presented. To check the validity of the solution, the numerical results, when the axial ratio approaches one, are compared with published data [14] of the corresponding hemispherical DRA. Also, the validity of the solution is examined by comparing the numerical results with HFSS simulation results. In addition, the HFSS simulation results for input impedance are presented to show the effects of the slot length and the dielectric constant on the input impedance of the hemispheroidal DRA.

5.2 Radiation Pattern

The relative radiation patterns calculated for the hemispheroidal DRA in figure 1.1 are shown in figures 5.1-5.9b. As a test of the validity and accuracy of the solution, the radiation patterns for an extreme case, *i.e.* $b/a \approx 1$, are calculated and shown in figure 5.1. Also shown are the corresponding hemispherical DRA results calculated by Kishk *et al.* [14]. It can be noted that our results are in a good agreement with

Kishk's results. Another test of validity and accuracy of the solution is that the calculated radiation patterns are compared with HFSS simulation results (*b/a = 1.15).* The calculated radiation patterns and simulation results are shown in figure 5.2. It can be seen that our results are in very good agreement with HFSS simulation results.

To examine the effects of the axial ratio of *b/a* on the magnitude of the radiation field, H-plane and E-plane patterns for the prolate hemispheroidal DRA with different values of *b/a* are shown in figures 5.3a-5.3b. All the calculated patterns are normalized using same normalization factor. It can be noted that the beam width becomes wider when the ratio of *b/a* becomes bigger. Therefore, when the slot length *L* is fixed, increasing the ratio of *b/a* increases the radiated power.

To examine the effects of the slot length (*L*) on the magnitude of the radiation field, H-plane and E-plane patterns for the prolate hemispheroidal DRA with different values of *L* are illustrated in figures 5.4a-5.4b. Again, all the calculated patterns are normalized using same normalized factor. These figures show that when the axial ration *b/a* is fixed, decreasing the slot length *L* decreases the radiated power.

Radiation patterns of the hemispheroidal DRA are calculated at the resonant frequency (f_0) and other frequencies ($0.95f_0$ and $1.05f_0$). H-plane and E-plane patterns are shown in figures 5.5a-5.5b. It can be seen that the antenna radiates the most power at the resonant frequency.

To examine the effects of the dielectric constant (ε_r) on the magnitude of the radiated field, the calculated radiation patterns for the hemispheroidal DRA with different values of ε_r are shown in figure 5.6. It is found that when the slot length and the axial ratio *b/a* are fixed, increasing the value of ε_r increases the radiated power.

More patterns of the hemispheroidal DRA are calculated for big values of *b/a*. They are shown in figures 5.7-5.8. We can note that the bigger the ratio of *b/a* is, the wider the beam width becomes.

In figures 5.9a-5.9b, the radiation patterns of a hemispheroidal DRA are computed and compared with HFSS simulation results of a cylindrical DRA. The radius (*r*) of the cylindrical DRA is equal to the minor radius (*a*) of the prolate hemispheroidal DRA. The height (*h*) of the cylindrical DRA is equal to the major radius (*b*) of the prolate hemispheroidal DRA. These figures show that the patterns of the hemispheroidal DRA is more directive than those of the cylindrical DRA.

In addition, the directivities are calculated numerically for different values of *b/a* at resonant frequencies. The directivity of an antenna is the ratio of the radiated intensity in a given direction from the antenna to the radiation intensity averaged over all directions. The average radiation intensity is equal to the total power radiated by the

antenna divided by 4π. If the direction is not specified, the direction of the maximum radiation intensity is implied. In mathematical form, it can be written as

$$D_0 = \frac{4\pi U_{\max}}{P_{rad}} \qquad \text{(dimensionless)} \tag{5.1}$$

where $$P_{rad} = \int_0^{2\pi} \int_0^{\pi} U \sin\theta d\theta d\phi \tag{5.2}$$

$$U(\theta,\phi) \approx \frac{1}{2\eta_0}\left[|E_\theta(\theta,\phi)|^2 + |E_\phi(\theta,\phi)|^2 \right]. \tag{5.3}$$

The directivities of the prolate hemispheroidal DRA with different values of *b/a* are calculated and shown in table 5.1. It is noted that for a fixed slot length, increasing the ratio of *b/a* decreases the directivity.

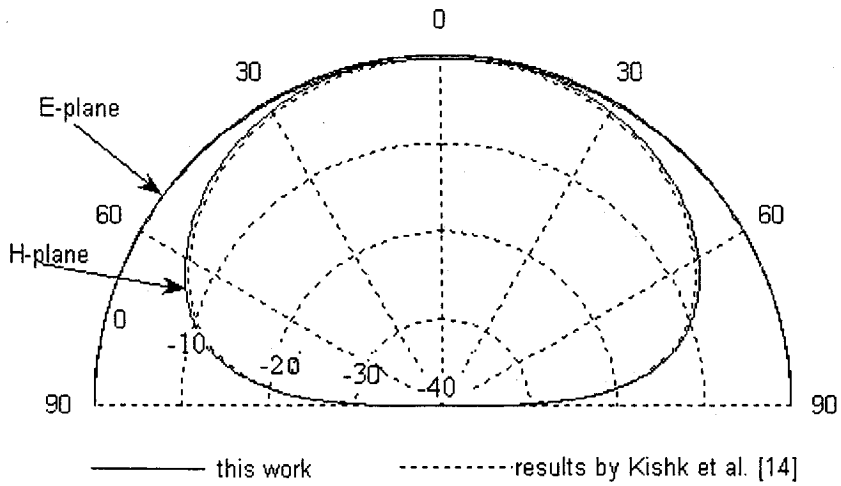

Fig. 5.1 **Radiation patterns (in dB) of DRAs with a = 2.975 cm, L = 5.0 cm, W = 0.06 cm, ε_r = 6.49, and f = 1.375 GHz. Solid line denotes patterns of a hemispheroidal DRA (b/a=1.001) of this work, and dash line denotes patterns of a hemispherical DRA [14].**

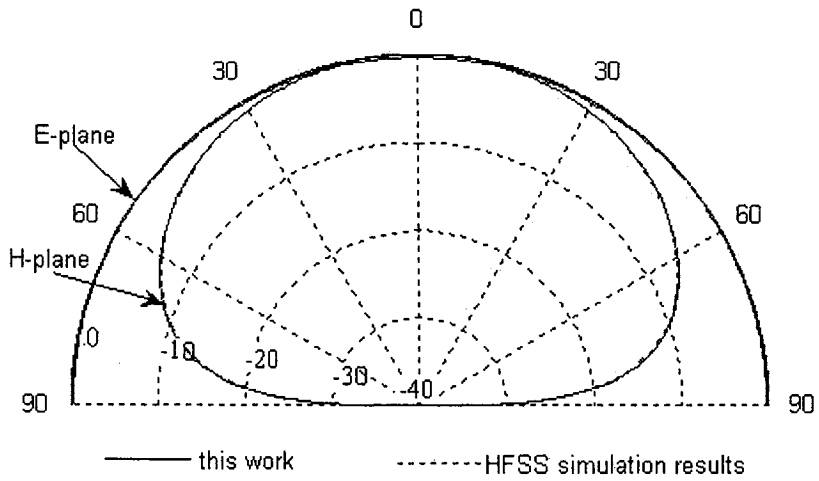

Fig. 5.2 **Radiation patterns (in dB) of a hemispheroidal DRA excited by a slot aperture, with a = 2.975 cm, b/a = 1.15, L= 5.0 cm, W = 0.06 cm, ε_r = 6.49, and f = 1.375 GHz. Solid line denotes results of hemispheroidal DRA of this work, and dash line denotes HFSS simulation results.**

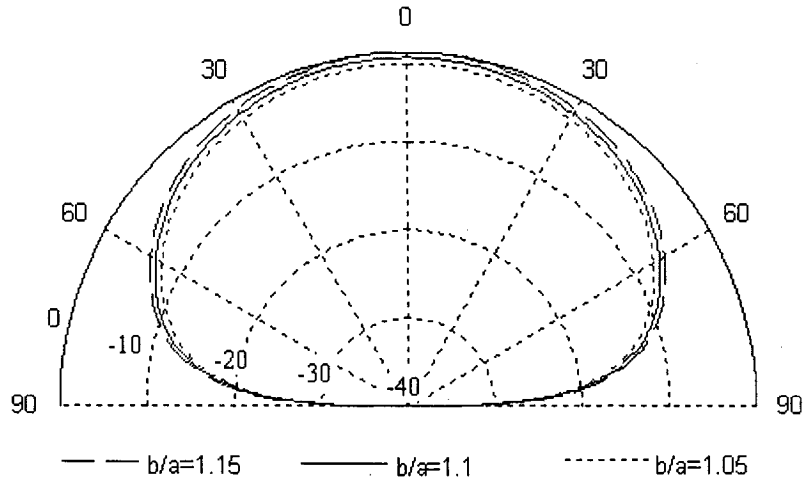

Fig. 5.3a **Calculated radiation patterns (H-plane in dB) of a hemispheroidal DRA excited by a slot aperture, with a = 2.975 cm, L= 5.0 cm, W = 0.06 cm, ε_r = 6.49, f = 1.375 GHz and different values of b/a.**

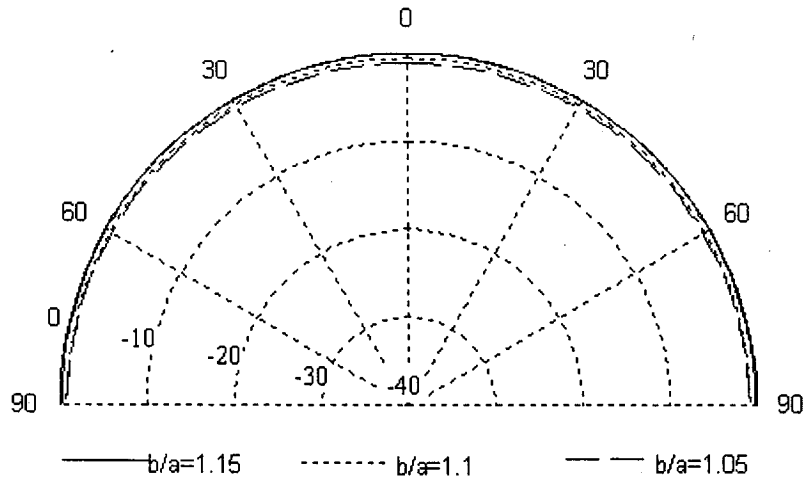

Fig. 5.3b **Calculated radiation patterns (E-plane in dB) of a hemispheroidal DRA excited by a slot aperture, with a = 2.975 cm, L= 5.0 cm, W = 0.06 cm, ε_r = 6.49, f = 1.375 GHz and different values of b/a.**

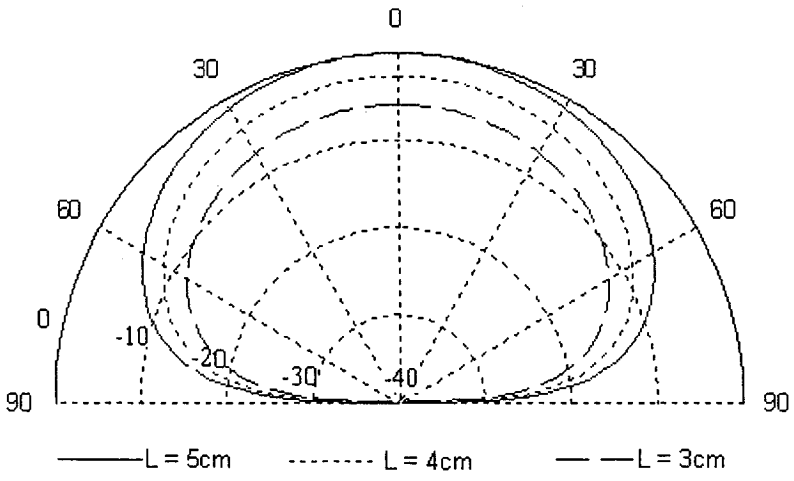

Fig. 5.4a **Calculated radiation patterns (H-plane in dB) of a hemispheroidal DRA excited by a slot aperture, with a = 2.975 cm, b/a = 1.15, W = 0.06 cm, ε_r = 6.49, f = 1.375 GHz and different values of L.**

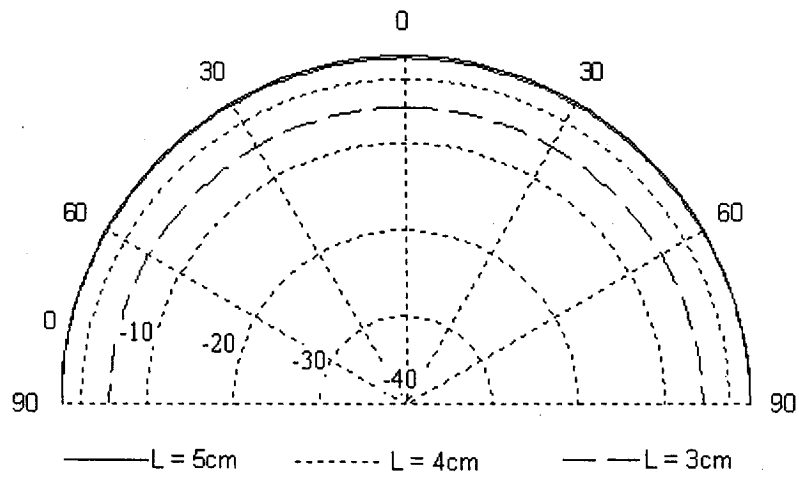

Fig. 5.4b **Calculated radiation patterns (E-plane in dB) of a hemispheroidal DRA excited by a slot aperture, with a = 2.975 cm, b/a = 1.15, W = 0.06 cm, ε_r = 6.49, f = 1.375 GHz and different values of L.**

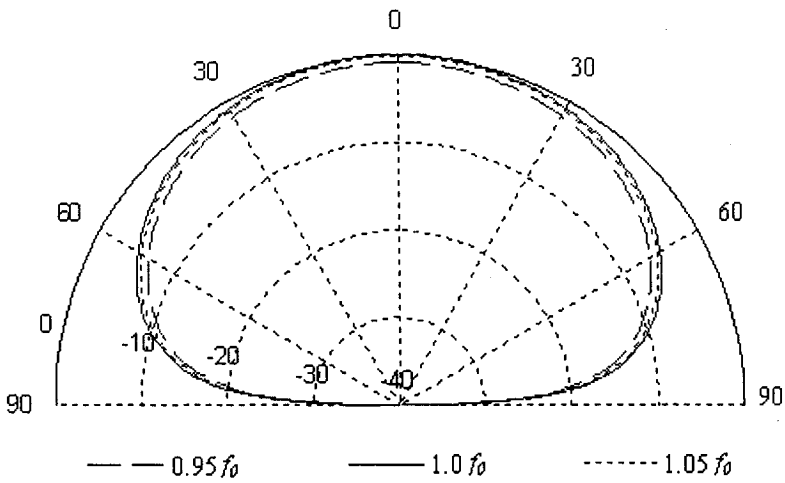

Fig. 5.5a **Calculated radiation patterns (H-plane in dB) of a hemispheroidal DRA excited by a slot aperture, with a = 2.975 cm, b/a = 1.5, W = 0.06 cm, ε_r = 6.49, L = 5 cm and different frequencies (f_0 is the resonant frequency).**

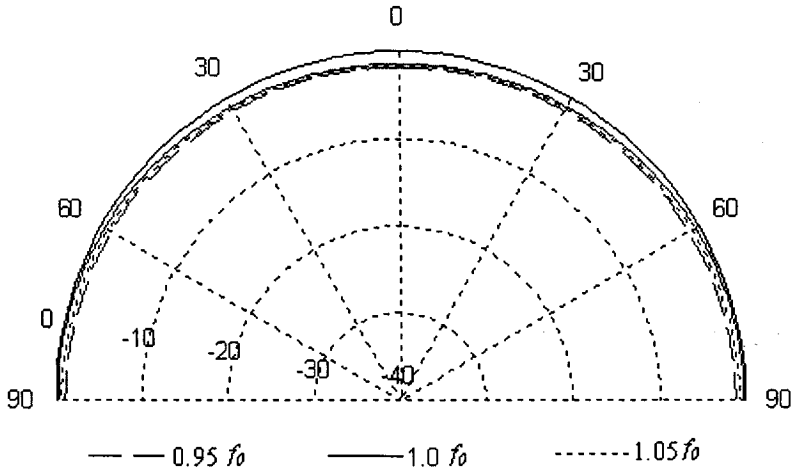

Fig. 5.5b **Calculated radiation patterns (E-plane in dB) of a hemispheroidal DRA excited by a slot aperture, with a = 2.975 cm, b/a = 1.5, W = 0.06 cm, ε_r = 6.49, L = 5 cm and different frequencies (f_0 is the resonant frequency).**

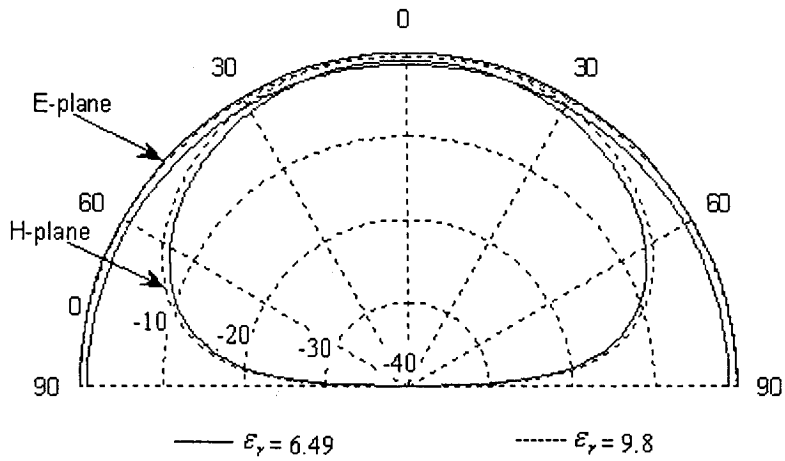

Fig. 5.6 **Calculated radiation patterns (in dB) of a hemispheroidal DRA excited by a slot aperture, with a = 2.975 cm, b/a = 1.2, L= 5.0 cm, W = 0.06 cm, f = 1.375 GHz and different values of ε_r.**

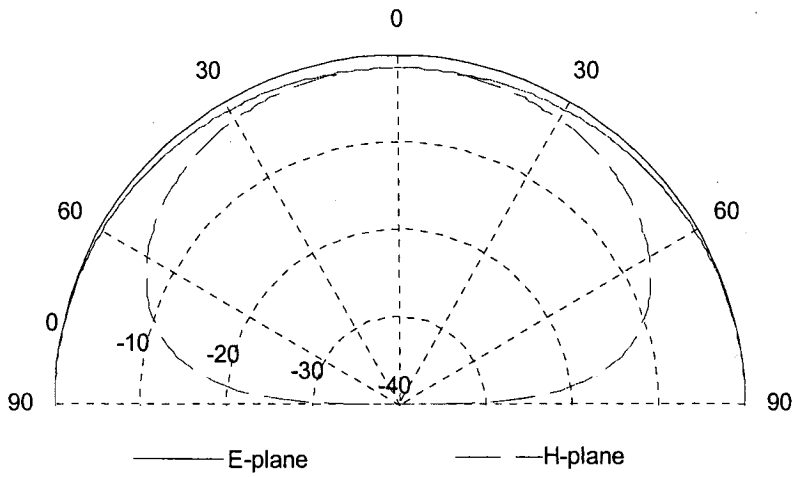

Fig. 5.7 **Calculated radiation patterns (in dB) of a hemispheroidal DRA excited by a slot aperture, with a = 2.975 cm, b/a = 2, L= 5.0 cm, W = 0.06 cm, ε_r = 6.49 and resonant frequency f_0 = 1.15 GHz.**

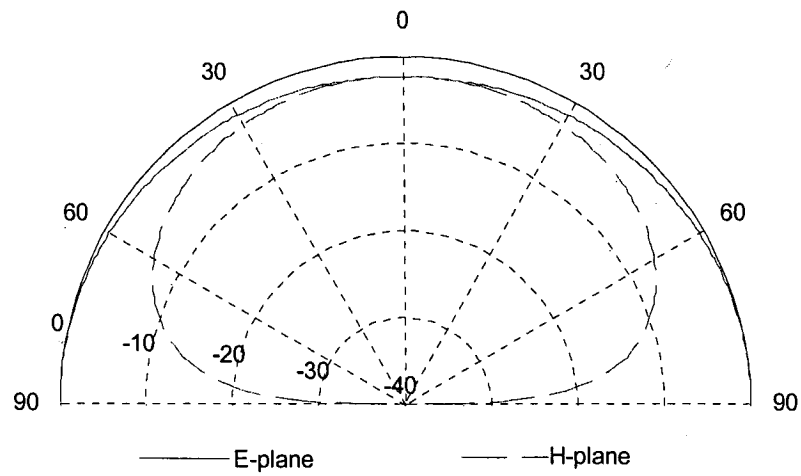

Fig. 5.8 **Calculated radiation patterns (in dB) of a hemispheroidal DRA excited by a slot aperture, with a = 2.975 cm, b/a = 3, L= 5.0 cm, W = 0.06 cm, ε_r = 6.49 and resonant frequency f_0 = 1.18 GHz.**

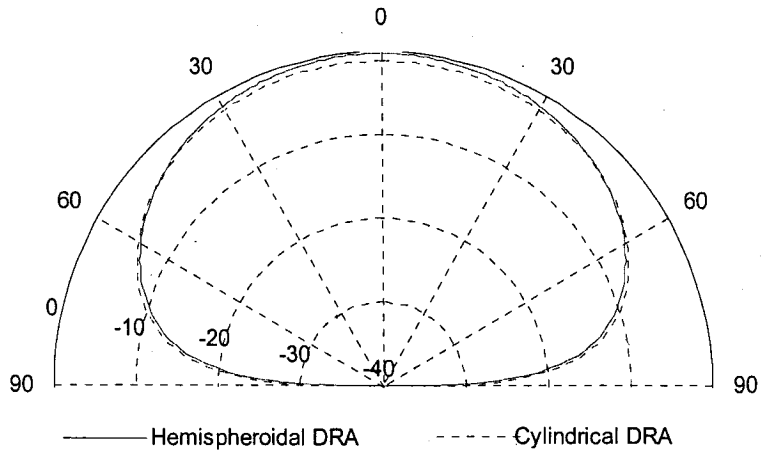

Fig. 5.9a **Radiation patterns (H-plane in dB) of a hemispheroidal DRA and a cylindrical DRA, both excited by a slot aperture, with a = 2.975 cm, b/a = h/r = 1.2, L= 5.0 cm, W = 0.06 cm, ε_r = 6.49 and f = 1.12 GHz. Solid line denotes results of hemispheroidal DRA of this work, and dash line denotes HFSS simulation results of a cylindrical DRA.**

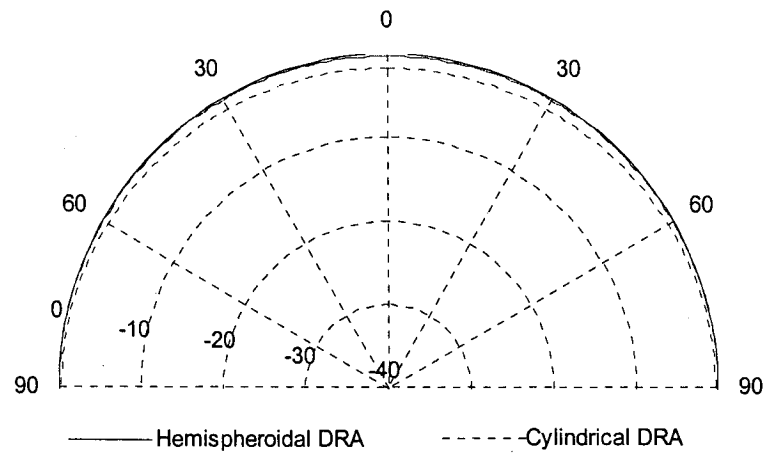

Fig. 5.9b **Radiation patterns (E-plane in dB) of a hemispheroidal DRA and a cylindrical DRA, both excited by a slot aperture, with a = 2.975 cm, b/a = h/r = 1.2, L= 5.0 cm, W = 0.06 cm, ε_r = 6.49 and f = 1.12 GHz. Solid line denotes results of hemispheroidal DRA of this work, and dash line denotes HFSS simulation results of a cylindrical DRA.**

Table 5.1 **Directivities of hemispheroidal DRA with a = 2.975cm, L = 5.0 cm, W = 0.06 cm, ε_r = 6.49 and different values of b/a (f_0 denotes resonant frequency).**

b/a	1.001	1.2	1.5	2.0
f_0 (GHz)	1.10	1.12	1.14	1.17
G_0 (dB)	5.83	5.78	5.67	5.50

5.3 Input Impedance

HFSS simulation results of the input impedance for different design parameters are presented. The resonant frequency is obtained from the input impedance. When the input reactance is equal to zero (X_{in} = 0) and the input resistance (R_{in}) is at its peak value, the corresponding frequency is the resonant frequency.

The results of input impedance of the hemispheroidal DRA with different values of b/a are shown in figures 5.10a-5.10b. It is noted that as the ratio of b/a increases, the input-impedance level decreases and the resonant frequency increases.

The input impedance of the hemispheroidal DRA excited by a slot aperture with different slot lengths are shown in figures 5.11a-5.11b. These figures show that as the

slot length decreases, the input-impedance level decreases, and the input-resistance peak shifts toward higher frequencies, to approach the free-source resonant frequency. These figures also show that the reactance part of the input impedance of the shortest slot becomes inductive, and is higher than the real part of the input impedance. This indicates the strong influence of the slot reactance on the input impedance of the antenna.

The input impedances of the hemispheroidal DRA with different values of dielectric constant are shown in figures 5.12a-5.12b. These results indicate that the resonant frequency decreases as the permittivity increases.

In addition, the simulation results of power distribution inside the hemispheroidal DRA are shown in figures 5.13a-5.13b. Three spherical surfaces (r = 5 mm, 15 mm, and 25 mm, r is the radius of the spherical surface) are chosen. The power distributions in both H-plane and E-plane on these surfaces are plotted.

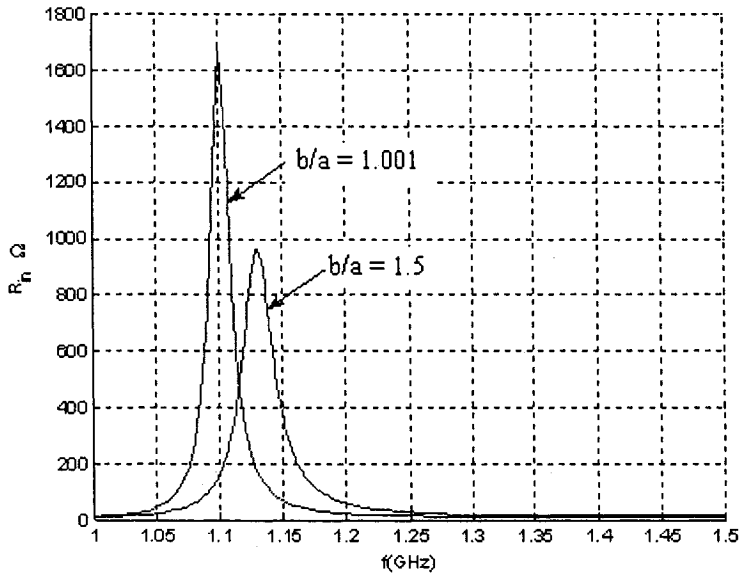

Fig. 5.10a **The real part, R_{in}, of the input impedance of a hemispheroidal DRA, excited by a slot aperture, with a = 2.975 cm, L = 5 cm, W = 0.06cm, ε_r = 6.49 and different values of b/a.**

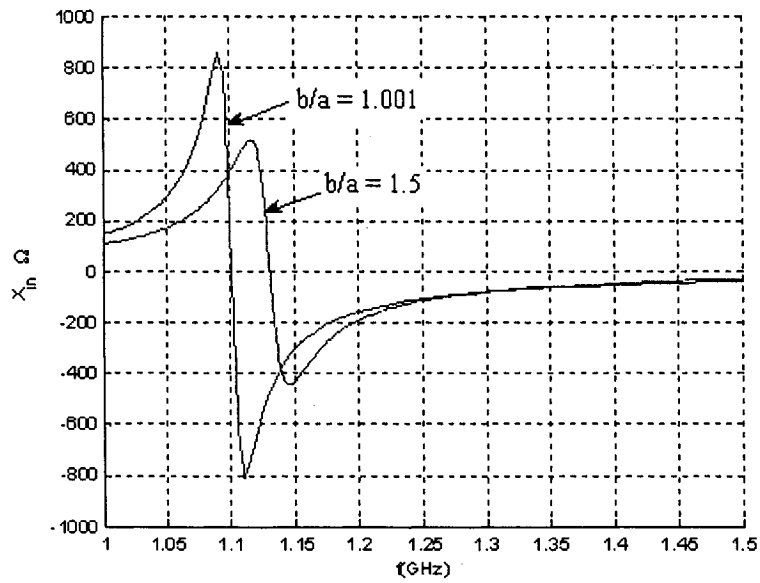

Fig. 5.10b **The imaginary part, X_{in}, of the input impedance of a hemispheroidal DRA, excited by a slot aperture, with a = 2.975 cm, L = 5 cm, W = 0.06cm, ε_r = 6.49 and different values of b/a.**

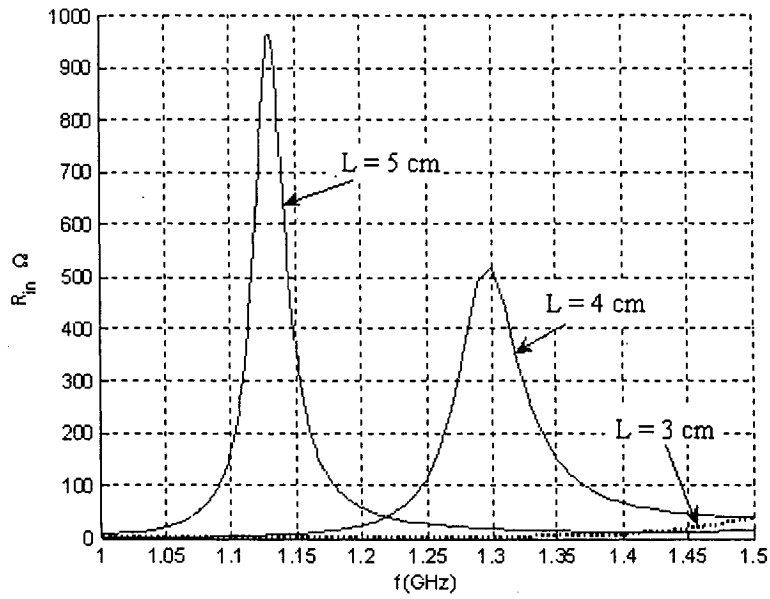

Fig. 5.11a **The real part, R_{in}, of the input impedance of a hemispheroidal DRA, excited by a slot aperture, with a = 2.975 cm, b/a =1.5, W = 0.06cm, ε_r = 6.49 and different slot lengths.**

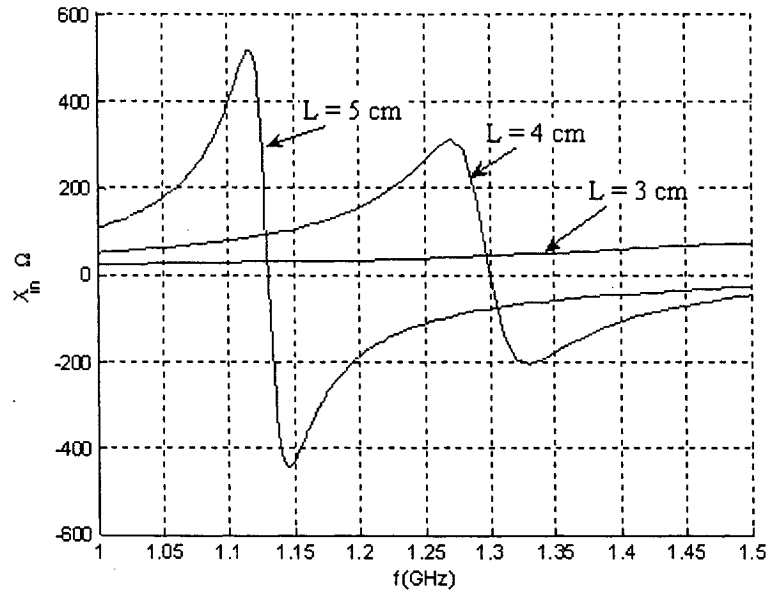

Fig. 5.11b **The imaginary part, X_{in}, of the input impedance of a hemispheroidal DRA, excited by a slot aperture, with a = 2.975 cm, b/a = 1.5, w = 0.06cm, ε_r = 6.49 and different slot lengths.**

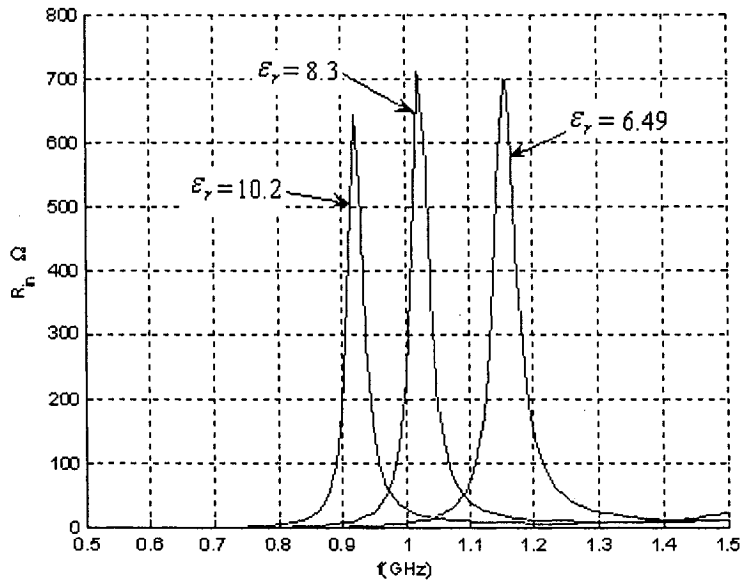

Fig. 5.12a **The real part, R_{in}, of the input impedance of a hemispheroidal DRA, excited by a slot aperture, with a = 2.975 cm, b/a = 1.15, w = 0.06cm, L= 5cm and different values of ε_r.**

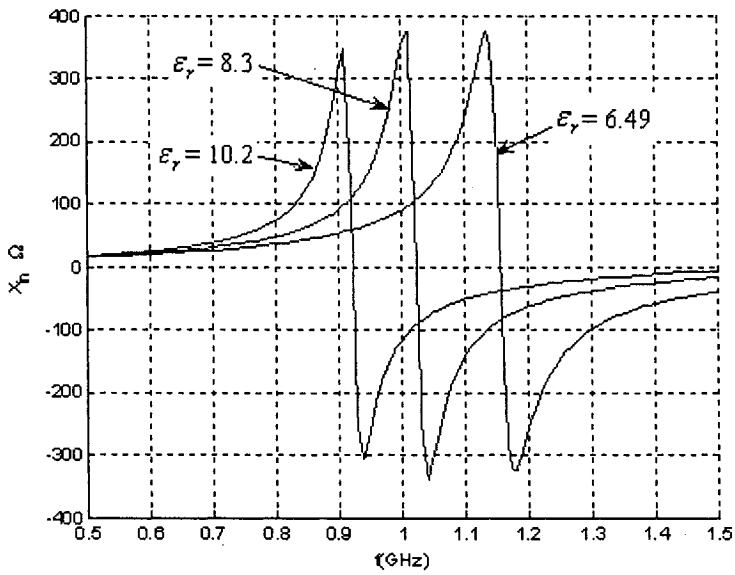

Fig. 5.12b **The imaginary part, X_{in}, of the input impedance of a hemispheroidal DRA, excited by a slot aperture, with a = 2.975 cm, b/a = 1.15, w = 0.06cm, L = 5cm and different values of ε_r.**

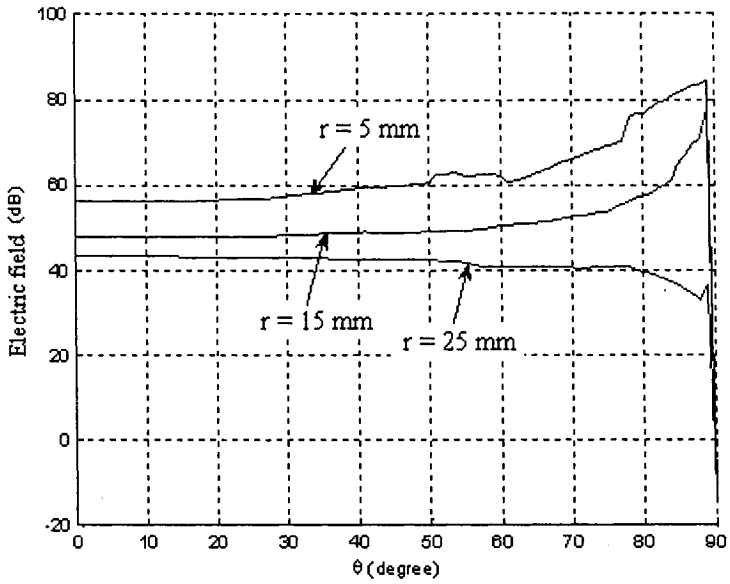

Fig. 5.13a **The electric field distributions (H-plane) inside a hemispheroidal DRA, excited by a slot aperture, with a = 2.975 cm, b/a = 1.5, w = 0.06cm, L = 5cm, f = 1.14GHz and ε_r = 6.49.**

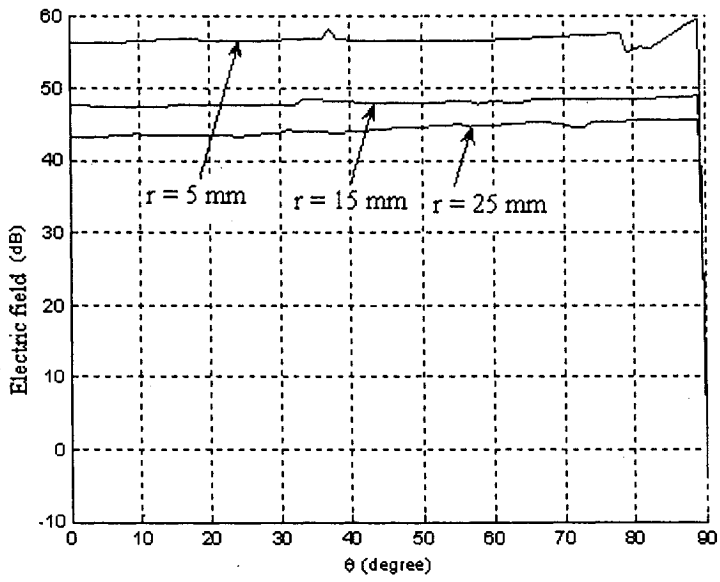

Fig. 5.13b **The electric field distributions (E-plane) inside a hemispheroidal DRA, excited by a slot aperture, with a = 2.975 cm, b/a = 1.5, w = 0.06cm, L = 5cm, f = 1.14GHz and ε_r = 6.49.**

Chapter 6
Conclusion

In this work, the problem of radiation from a prolate hemispheroidal dielectric resonator antenna, which is located above an infinite ground and excited by a slot aperture, has been investigated using the dyadic Green's function technique. The dyadic Green's functions have been constructed and the unknown scattering coefficients are obtained by enforcing the boundary conditions. Formulations of electromagnetic fields in their general forms were expressed in terms of dyadic Green's functions and a known current source. Also, simple and compact far field expressions for the electric field are derived for a prolate hemispheroidal DRA excited by a slot aperture.

Several radiation pattern results were obtained for different parameters. The effect of the slot length, the shape of the spheroid and dielectric constant on the radiation pattern were considered. The validity of the solution was examined by using HFSS simulation results. The results were in a very good agreement with HFSS simulation results. The solution was also examined for the case where the hemispheroid approaches the hemispherical shape ($b/a \approx 1$). The results were in a very good agreement with the known results for hemispherical DRA. Moreover, the input impedance is investigated using HFSS.

The solution for radiating by an oblate hemispheroidal DRA can be obtained from that of the prolate hemispheroidal DRA by replacing the prolate spheroidal wave functions with the oblate ones. In this work, only the radiation patterns of the prolate hemispheroidal DRA have been investigated. One potential extension of this study is the investigation of input impedance theoretically. Another potential study is the investigation of optimum designs for the hemispheroidal DRA, taking into account the shape of the hemispheroid, the dimension of the slot and dielectric constant.

Appendix A
Expressions of the Prolate Spheroidal Vector Wave Functions

$$\underset{o}{\boldsymbol{M}}_{e_{mn}}^{x(i)}(c;\eta,\xi,\phi)$$

$$\underset{o}{\boldsymbol{M}}_{e_{mn}\eta}^{x(i)} = -\frac{2(\xi^2-1)^{\frac{1}{2}}}{d(\xi^2-\eta^2)^{\frac{1}{2}}}\left[S_{mn}\frac{dR_{mn}^{(i)}}{d\xi}\sin\varphi\begin{matrix}\cos\\ \sin\end{matrix}m\varphi - \frac{m\xi}{\xi^2-1}S_{mn}R_{mn}^{(i)}\cos\varphi\begin{matrix}\sin\\ (-1)\cos\end{matrix}m\varphi\right] \quad \text{(A-1)}$$

$$\underset{o}{\boldsymbol{M}}_{e_{mn}\xi}^{x(i)} = \frac{2(1-\eta^2)^{\frac{1}{2}}}{d(\xi^2-\eta^2)^{\frac{1}{2}}}\left[\frac{dS_{mn}}{d\xi}R_{mn}^{(i)}\sin\varphi\begin{matrix}\cos\\ \sin\end{matrix}m\varphi + \frac{m\eta}{1-\eta^2}S_{mn}R_{mn}^{(i)}\cos\varphi\begin{matrix}\sin\\ (-1)\cos\end{matrix}m\varphi\right] \quad \text{(A-2)}$$

$$\underset{o}{\boldsymbol{M}}_{e_{mn}\phi}^{x(i)} = \frac{2}{d(\xi^2-\eta^2)}\left[\xi(1-\eta^2)\frac{dS_{mn}}{d\eta}R_{mn}^{(i)} + \eta(\xi^2-1)S_{mn}\frac{dR_{mn}^{(i)}}{d\xi}\right]\cos\varphi\begin{matrix}\cos\\ \sin\end{matrix}m\varphi \quad \text{(A-3)}$$

$$\underset{o}{\boldsymbol{M}}_{e_{mn}}^{y(i)}(c;\eta,\xi,\phi)$$

The expressions of the components are obtained from those of $\underset{o}{\boldsymbol{M}}_{e_{mn}}^{x(i)}(c;\eta,\xi,\phi)$ by replacing the factors $\cos\phi$ and $\sin\phi$ by $\sin\phi$ and $-\cos\phi$, respectively.

$$\underline{\boldsymbol{M}^{z(i)}_{e_{mn}}(c;\eta,\xi,\phi)}$$

$$\boldsymbol{M}^{z(i)}_{e_{mn}\eta} = \frac{2m\eta}{d(\xi^2-\eta^2)^{\frac{1}{2}}(1-\eta^2)^{\frac{1}{2}}} S_{mn} R^{(i)}_{mn} \begin{matrix} sin \\ (-1)cos \end{matrix} m\phi \tag{A-4}$$

$$\boldsymbol{M}^{z(i)}_{e_{mn}\xi} = \frac{2m\xi}{d(\xi^2-\eta^2)^{\frac{1}{2}}(\xi^2-1)^{\frac{1}{2}}} S_{mn} R^{(i)}_{mn} \begin{matrix} (-1)sin \\ cos \end{matrix} m\phi \tag{A-5}$$

$$\boldsymbol{M}^{z(i)}_{e_{mn}\phi} = \frac{2(1-\eta^2)^{\frac{1}{2}}(\xi^2-1)^{\frac{1}{2}}}{d(\xi^2-\eta^2)} [\eta \frac{dS_{mn}}{d\eta} R^{(i)}_{mn} - \xi S_{mn} \frac{dR^{(i)}_{mn}}{d\xi}] \begin{matrix} cos \\ sin \end{matrix} m\phi \tag{A-6}$$

$$\underline{\boldsymbol{N}^{x(i)}_{e_{mn}}(c;\eta,\xi,\phi)}$$

$$\begin{aligned} \boldsymbol{N}^{x(i)}_{e_{mn}\eta} = {} & \frac{4}{kd^2(\xi^2-\eta^2)^{\frac{1}{2}}} \{[\eta S_{mn} \frac{d}{d\xi}(\frac{(\xi^2-1)^{3/2}}{(\xi^2-\eta^2)} \cdot \frac{dR^{(i)}_{mn}}{d\xi}) - \frac{1}{(\xi^2-1)^{1/2}} \frac{dS_{mn}}{d\eta} R^{(i)}_{mn} \\ & + (1-\eta^2) \frac{dS_{mn}}{d\eta} \frac{d}{d\xi}(\frac{\xi(\xi^2-1)^{1/2} R^{(i)}_{mn}}{\xi^2-\eta^2}) - \frac{m^2 \eta S_{mn} R^{(i)}_{mn}}{(1-\eta^2)(\xi^2-1)^{1/2}}] \cos\phi \begin{matrix} cos \\ sin \end{matrix} m\phi \\ & + \frac{m}{(\xi^2-1)^{1/2}} [\frac{dS_{mn}}{d\eta} + \frac{\eta}{1-\eta^2} S_{mn}] \cdot R^{(i)}_{mn} \sin\phi \begin{matrix} sin \\ (-1)cos \end{matrix} m\phi \} \end{aligned} \tag{A-7}$$

$$\begin{aligned} \boldsymbol{N}^{x(i)}_{e_{mn}\xi} = {} & -\frac{4}{kd^2(\xi^2-\eta^2)^{\frac{1}{2}}} \{[\xi \frac{d}{d\eta}(\frac{(1-\eta^2)^{3/2}}{(\xi^2-\eta^2)} \cdot \frac{dS_{mn}}{d\eta}) - \frac{1}{(1-\eta^2)^{1/2}} S_{mn} \frac{dR^{(i)}_{mn}}{d\xi} \\ & + (\xi^2-1) \frac{d}{d\eta}(\frac{\eta(1-\eta^2)^{1/2} S_{mn}}{\xi^2-\eta^2}) \frac{dR^{(i)}_{mn}}{d\xi} - \frac{m^2 \xi S_{mn} R^{(i)}_{mn}}{(1-\eta^2)^{\frac{1}{2}}(\xi^2-1)}] \cos\phi \begin{matrix} cos \\ sin \end{matrix} m\phi \\ & + \frac{m}{(1-\eta^2)^{1/2}} S_{mn} [\frac{\xi}{\xi^2-1} R^{(i)}_{mn} - \frac{dR^{(i)}_{mn}}{d\xi}] \sin\phi \begin{matrix} sin \\ (-1)cos \end{matrix} m\phi \} \end{aligned} \tag{A-8}$$

$$
\begin{aligned}
\underset{o}{N}^{x(i)}_{e_{mn}\phi} = & \frac{4(1-\eta^2)^{1/2}(\xi^2-1)^{1/2}}{kd^2(\xi^2-\eta^2)}\{[\frac{1}{(\xi^2-1)^{1/2}}\frac{d}{d\eta}((1-\eta^2)^{1/2}\frac{dS_{mn}}{d\eta})R^{(i)}_{mn} \\
& + \frac{1}{(1-\eta^2)^{1/2}}S_{mn}\frac{d}{d\xi}((\xi^2-1)^{1/2}\frac{dR^{(i)}_{mn}}{d\xi})]\sin\phi \begin{matrix}\cos \\ \sin\end{matrix} m\phi \\
& + m[\frac{1}{(\xi^2-1)^{1/2}}\frac{d}{d\eta}(\frac{\eta}{(1-\eta^2)^{1/2}}S_{mn})R^{(i)}_{mn} \\
& - \frac{1}{(1-\eta^2)^{1/2}}S_{mn}\frac{d}{d\xi}(\frac{\xi}{(\xi^2-1)^{1/2}}R^{(i)}_{mn})]\cos\phi \begin{matrix}\sin \\ (-1)\cos\end{matrix} m\phi\}
\end{aligned}
\tag{A-9}
$$

$$\underset{o}{N}^{y(i)}_{e_{mn}}(c;\eta,\xi,\phi)$$

The expressions of the components are obtained from those of $\underset{o}{M}^{x(i)}_{e_{mn}}(c;\eta,\xi,\phi)$ by replacing the factors $\cos\phi$ and $\sin\phi$ by $\sin\phi$ and $-\cos\phi$, respectively.

$$\underset{o}{N}^{z(i)}_{e_{mn}}(c;\eta,\xi,\phi)$$

$$
\begin{aligned}
\underset{o}{N}^{z(i)}_{e_{mn}\eta} = & \frac{4(1-\eta^2)^{1/2}}{kd^2(\xi^2-\eta^2)^{1/2}}[\eta\frac{dS_{mn}}{d\eta}\frac{d}{d\xi}\left(\frac{\xi^2-1}{\xi^2-\eta^2}R^{(i)}_{mn}\right) \\
& - S_{mn}\frac{d}{d\xi}\left(\frac{\xi(\xi^2-1)}{\xi^2-\eta^2}\frac{dR^{(i)}_{mn}}{d\xi}\right) + \frac{m^2\xi}{(1-\eta^2)(\xi^2-1)}S_{mn}R^{(i)}_{mn}]\begin{matrix}\cos \\ \sin\end{matrix} m\varphi
\end{aligned}
\tag{A-10}
$$

$$
\begin{aligned}
\underset{o}{N}^{z(i)}_{e_{mn}\xi} = & \frac{4(\xi^2-1)^{1/2}}{kd^2(\xi^2-\eta^2)^{1/2}}[\xi\frac{d}{d\xi}\left(\frac{1-\eta^2}{\xi^2-\eta^2}S_{mn}\right)\frac{dR^{(i)}_{mn}}{d\xi} \\
& - \frac{d}{d\eta}\left(\frac{\eta(1-\eta^2)}{\xi^2-\eta^2}\frac{dS_{mn}}{d\eta}\right)R^{(i)}_{mn} + \frac{m^2\eta}{(1-\eta^2)(\xi^2-1)}S_{mn}R^{(i)}_{mn}]\begin{matrix}\cos \\ \sin\end{matrix} m\varphi
\end{aligned}
\tag{A-11}
$$

$$N_{\substack{e_{mn\varphi} \\ o}}^{z(i)} = \frac{4m(1-\eta^2)^{1/2}(\xi^2-1)^{1/2}}{kd^2(\xi^2-\eta^2)}\left[\frac{\xi}{\xi^2-1}\frac{dS_{mn}}{d\eta}R_{mn}^{(i)} + \frac{\eta}{1-\eta^2}S_{mn}\frac{dR_{mn}^{(i)}}{d\xi}\right]\begin{matrix}(-1)\sin \\ \cos\end{matrix} m\varphi \qquad \text{(A-12)}$$

Appendix B
Intermediate Coefficients $I_{t,l}^{mn}$ in Closed Form

B.1 For $m \geq 1$ and $(n-m) + t = odd$:

$$I_{t,0}^{mn} = I_{t,1}^{mn} = I_{t,2}^{mn} = I_{t,3}^{mn} = I_{t,10}^{mn} = I_{t,11}^{mn} = 0 \tag{B-1}$$

$$\begin{aligned} I_{t,4}^{mn} &= [N_1]^{-1} \int_{-1}^{+1} \eta(1-\eta^2)^{-1/2} S_{m,m+r}(c,\eta) P_{m-1+t}^{m-1}(\eta) d\eta \\ &= t d_{t-1}^{mn} + (2t+2m-1) \sum_{r=t+1}^{\infty}{}' d_r^{mn} \end{aligned} \tag{B-2}$$

$$\begin{aligned} I_{t,5}^{mn} &= [N_1]^{-1} \int_{-1}^{+1} \eta(1-\eta^2)^{1/2} S_{m,m+r}(c,\eta) P_{m-1+t}^{m-1}(\eta) d\eta \\ &= \frac{(t+2m-1)(t+2m)}{2t+2m+1} \left(\frac{t+2m+1}{2t+2m+3} d_{t+1}^{mn} \frac{t}{2t+2m+1} d_{t-1}^{mn} \right) \\ &\quad - \frac{t(t-1)}{2t+2m-3} \left(\frac{t+2m-1}{2t+2m-1} d_{t-1}^{mn} + \frac{t-2}{2t+2m-5} d_{t-3}^{mn} \right) \end{aligned} \tag{B-3}$$

$$\begin{aligned} I_{t,6}^{mn} &= [N_1]^{-1} \int_{-1}^{+1} \eta(1-\eta^2)^{3/2} S_{m,m+r}(c,\eta) P_{m-1+t}^{m-1}(\eta) d\eta \\ &= \frac{(t+2m-1)(t+2m)(t+2m+1)}{(2t+2m+1)(2t+2m+3)} \cdot \frac{(t+2m+2)(t+2m+3)}{2t+2m+5} \\ &\quad \times \left(\frac{d_{t+1}^{mn}}{2t+2m+3} - \frac{d_{t+1}^{mn}}{2t+2m+7} \right) - \frac{t(t-2m)}{2t+2m-3} \\ &\quad \times \frac{(t+2m-1)(t+2m)(t+2m+1)}{(2t+2m+1)(2t+2m+3)} \cdot \left(\frac{d_{t-1}^{mn}}{2t+2m-1} - \frac{d_{t+1}^{mn}}{2t+2m+3} \right) \\ &\quad - \frac{t(t-1)(t-2)(t+2m-1)(t+4m-1)}{(2t+2m-5)(2t+2m-3)(2t+2m+1)} + \left(\frac{d_{t-3}^{mn}}{2t+2m-5} - \frac{d_{t-1}^{mn}}{2t+2m-1} \right) \\ &\quad + \frac{t(t-1)(t-2)(t-3)(t-4)}{(2t+2m-7)(2t+2m-5)(2t+2m-3)} \cdot \left(\frac{d_{t-5}^{mn}}{2t+2m-9} - \frac{d_{t-3}^{mn}}{2t+2m-5} \right) \end{aligned} \tag{B-4}$$

$$I_{t,7}^{mn} = [N_1]^{-1} \int_{-1}^{+1} \eta(1-\eta^2)^{1/2} \frac{dS_{m,m+r}(c,\eta)}{d\eta} P_{m-1+t}^{m-1}(\eta) d\eta$$

$$= -t(t+m-1)d_{t-1}^{mn} + m(2t+2m-1) \sum_{r=t+1}^{\infty}{}' d_r^{mn} \qquad \text{(B-5)}$$

$$I_{t,8}^{mn} = [N_1]^{-1} \int_{-1}^{+1} (1-\eta^2)^{3/2} \frac{dS_{m,m+r}(c,\eta)}{d\eta} P_{m-1+t}^{m-1}(\eta) d\eta$$

$$= \frac{(t+2m-1)(t+2m)}{2t+2m+1} [\frac{(t+m+2)(t+2m+1)}{2t+2m+3}$$

$$\times d_{t+1}^{mn} - \frac{t(m+t-1)}{2t+2m-1} d_{t-1}^{mn}] - \frac{t(t-1)}{2t+2m-3} \qquad \text{(B-6)}$$

$$\times [\frac{(t+m)(t+2m-1)}{2t+2m-1} d_{t-1}^{mn} - \frac{(t-2)(t+m-3)}{2t+2m-5} d_{t-3}^{mn}]$$

$$I_{t,9}^{mn} = [N]^{-1} \int_{-1}^{+1} (1-\eta^2)^{5/2} \frac{dS_{m,m+r}(c,\eta)}{d\eta} P_{m-1+t}^{m-1}(\eta) d\eta$$

$$= I_{t,8}^{mn} - \{\frac{(t+2m-1)(t+2m)(t+2m+1)}{(2t+2m+1)(2t+2m+3)(2t+2m+5)} [\frac{(t+1)(t+2m+2)(t+2m+3)}{2(2t+2m+3)}$$

$$+ \frac{(t+2)((t+3)(t+2m+1)}{2(2t+2m+3)} d_{t+1}^{mn} + \frac{(t+2m+2)(t+2m+3)(t+2m+4)}{(2t+2m+7)} d_{t+1}^{mn}]$$

$$- \frac{t(t-2m)(t+2m-1)}{(2t+2m-3)(2t+2m+1)(2t+2m+3)} [(\frac{t(t+1)(t+2m-1)}{2(2t+2m-1)}$$

$$+ \frac{(t-1)(t+2m)(t+2m+1)}{2(2t+2m-1)}) d_{t-1}^{mn} + \frac{(t+2m)((t+2m+1)(t+m+2)}{(2t+2m+3)} d_{t+1}^{mn}]\}$$

$$+ \frac{m(t+2)(t+2m-1)(t+2m)(t+2m+1)}{(2t+2m+1)(2t+2m+3)^2} d_{t+1}^{mn}$$

$$+ \frac{t(t-1)(t-2)(t+4m-1)(t+2m-1)}{(t+2m-5)(2t+2m-3)(2t+2m-1)}) d_{t-1}^{mn} \frac{(t+m)}{(2t+2m+1)}$$

$$+ \frac{mt(t+2m-1)}{(2t+2m+3)} [\frac{t+1}{(2t+2m+1)} - \frac{t(t-2m)}{(2t+2m-3)(2t+2m-1)}] d_{t-1}^{mn}$$

$$+ \frac{t(t-1)}{2} \frac{(t-2)(t-3)(t+4m-1)(t+2m-1)}{(2t+2m-3)(2t+2m+1)(2t+2m-5)^2} d_{t-3}^{mn}$$

$$- \frac{t(t-1)(t-2)}{(2t+2m-3)(2t+2m-5)^2} [\frac{(t-3)(t-4)}{(2t+2m-7)}(t+m-2) + m(t-2)] d_{t-3}^{mn} \qquad \text{(B-7)}$$

$$+ \frac{t(t-1)(t-2)}{(2t+2m-5)} \frac{(t+2m-3)}{(2t+2m-3)(2t+2m+1)} [\frac{(t-2)(t-1)}{2(2t+2m-5)}$$

$$+ \frac{4m(2m-1)+(t-2m-1)(2m+1)}{2(2t+2m-5)}] d_{t-3}^{mn} - \frac{t(t-1)(t-2)(t-3)(t-4)}{(2t+2m-9)(2t+2m-7)(2t+2m-5)}$$

$$\times \frac{t+m-5}{2t+2m-3} d_{t-5}^{mn}$$

B.2: For $m \geq 1$ and $(n\text{-}m) + t = even$:

$$I_{t,4}^{mn} = I_{t,5}^{mn} = I_{t,6}^{mn} = I_{t,7}^{mn} = I_{t,8}^{mn} = I_{t,8}^{mn} = 0 \tag{B-8}$$

$$\begin{aligned} I_{t,0}^{mn} &= [N_1]^{-1} \int_{-1}^{+1} (1-\eta^2)^{-1/2} S_{m,m+r}(c,\eta) P_{m-1+t}^{m-1}(\eta) d\eta \\ &= (2t+2m-1) \sum_{r=t}^{\infty}{}' d_r^{mn} \end{aligned} \tag{B-9}$$

$$\begin{aligned} I_{t,1}^{mn} &= [N_1]^{-1} \int_{-1}^{+1} (1-\eta^2)^{1/2} S_{m,m+r}(c,\eta) P_{m-1+t}^{m-1}(\eta) d\eta \\ &= \frac{(t+2m-1)(t+2m)}{2t+2m+1} d_t^{mn} - \frac{t(t-1)}{2t+2m-3} d_{t-2}^{mn} \end{aligned} \tag{B-10}$$

$$\begin{aligned} I_{t,2}^{mn} &= [N_1]^{-1} \int_{-1}^{+1} (1-\eta^2)^{3/2} S_{m,m+r}(c,\eta) P_{m-1+t}^{m-1}(\eta) d\eta \\ &= \frac{(t+2m-1)(t+2m)(t+2m+1)(t+2m+2)}{(2t+2m+1)(2t+2m+3)} \\ &\quad \times \left[\frac{d_t^{mn}}{(2t+2m+1)} - \frac{d_{t+2}^{mn}}{(2t+2m+5)} \right] - \frac{2t(t-1)(t+2m)(t+2m-1)}{(2t+2m-3)(2t+2m+1)} \\ &\quad \times \left[\frac{d_{t-2}^{mn}}{(2t+2m-3)} - \frac{d_t^{mn}}{(2t+2m+1)} \right] + \frac{t(t-1)(t-2)(t-3)}{(2t+2m-3)(2t+2m-5)} \\ &\quad + \left[\frac{d_{t-4}^{mn}}{(2t+2m-7)} - \frac{d_{t-2}^{mn}}{(2t+2m-3)} \right] \end{aligned} \tag{B-11}$$

$$
\begin{aligned}
I_{t,3}^{mn} &= [N_1]^{-1}\int_{-1}^{+1}(1-\eta^2)^{5/2}S_{m,m+r}(c,\eta)P_{m-1+t}^{m-1}(\eta)d\eta \\
&= I_{t,2}^{mn} - \{\frac{(t+2m-1)(t+2m)}{(2t+2m+5)(2t+2m+1)}\cdot\frac{(t+2m+1)(t+2m+2)(t+2m+3)}{(2t+2m+3)} \\
&\times[\frac{(t+1)d_t^{mn}}{(2t+2m+1)(2t+2m+3)}+\frac{(2m+1)d_{t+2}^{mn}}{(2t+2m+3)(2t+2m+7)} \\
&-\frac{(2m+t+4)d_{t+4}^{mn}}{(2t+2m+7)(2t+2m+9)}]-\frac{t(t-2m)(t+2m-1)(t+2m)(t+2m+1)}{(2t+2m-3)(2t+2m+1)(2t+2m+3)}) \\
&\times[\frac{(2m+1)d_t^{mn}}{(2t+2m-1)(2t+2m+3)}-\frac{(t+2m+2)d_{t+2}^{mn}}{(2t+2m+3)(2t+2m+5)} \\
&-\frac{t(t-1)(t-2)(t+2m-1)(t+4m-1)}{(2t+2m-5)(2t+2m-3)(2t+2m+1)}\cdot\frac{(t-3)d_{t-4}^{mn}}{(2t+2m-7)(2t+2m-5)} \\
&+\frac{(2m+1)d_{t-2}^{mn}}{(2t+2m-5)(2t+2m-1)}-\frac{(2m+t)d_t^{mn}}{(2t+2m-1)(2t+2m+1)} \\
&+\frac{t(t-1)(t-2)(t-3)(t-4)}{(2t+2m-7)(2t+2m-5)(2t+2m-3)}\cdot\frac{(t-5)d_{t-6}^{mn}}{(2t+2m-11)(2t+2m-9)} \\
&+\frac{(2m+1)d_{t-4}^{mn}}{(2t+2m-9)(2t+2m-5)}-\frac{(2m+t-2)d_{t-2}^{mn}}{(2t+2m-5)(2t+2m-3)}]\}
\end{aligned}
\tag{B-12}
$$

$$
\begin{aligned}
I_{t,10}^{mn} &= \frac{1}{N_1}\int_{-1}^{+1}\eta(1-\eta^2)^{1/2}\frac{dS_{m,m+r}(c,\eta)}{d\eta}P_{m-1+t}^{m-1}(\eta)d\eta \\
&= \frac{t(t-1)(t+m-2)}{(2t+2m-3)}d_{t-2}^{mn}+m(2t+2m-1) \\
&\times\sum_{r=t}^{\infty}{}'d_r^{mn}-[\frac{t(t-1)}{2}+\frac{(t+2m)(t+2m-1)}{2(2t+2m+1)}]d_t^{mn}
\end{aligned}
\tag{B-13}
$$

$$
\begin{aligned}
I_{t,11}^{mn} &= \frac{1}{N_1}\int_{-1}^{+1}\eta(1-\eta^2)^{1/2}\frac{d\rho_{m+r}^{m}(c,\eta)}{d\eta}P_{m-1+t}^{m-1}(\eta)d\eta \\
&= \frac{(t+2m-1)(t+2m)}{(2t+2m+1)(2t+2m+3)}\cdot[(\frac{t(t+2m+1)(t+2m+2)}{2(2t+2m+1)} \\
&+\frac{(t+1)((t+2)(t+2m)}{2(2t+2m+1)})d_t^{mn}+\frac{(t+m+3)(t+2m+1)(t+2m+2)}{(2t+2m+5)}d_{t+2}^{mn}] \\
&-\frac{2t(t-1)}{(2t+2m-3)(2t+2m+1)}\cdot[(\frac{(t-2)(t+2m-1)(t+2m)}{2(2t+2m-3)} \\
&+\frac{(t-1)t(t+2m-2)}{2(2t+2m-3)})d_{t-2}^{mn}+\frac{(t+m+1)(t+2m-1)(t+2m)}{(2t+2m+1)}d_t^{mn}] \\
&+\frac{t(t-1)(t-2)(t-3)(t+m-1)}{(2t+2m-5)(2t+2m-3)^2}d_{t-2}^{mn}-\frac{m(t+1)(t+2m-1)(t+2m)}{(2t+2m+1)^2})d_t^{mn} \\
&-\frac{mt(t-1)}{(2t+2m+1)}\cdot[1-\frac{2(t-1)(2t+2m-1)}{(2t+2m-3)^2}]d_{t-2}^{mn} \\
&+\frac{t(t-1)(t-2)(t-3)(t+m-4)}{(2t+2m-7)(2t+2m-5)(2t+2m-3)}d_{t-4}^{mn}
\end{aligned}
\tag{B-14}
$$

B.3: For $m = 0$ and $(n - m) + t = odd$:

$$I_{t,1}^{0n}(c) = I_{t,2}^{0n}(c) = I_{t,3}^{0n}(c) = I_{t,10}^{0n}(c) = I_{t,11}^{0n}(c) = 0 \tag{B-15}$$

$$\begin{aligned} I_{t,5}^{0n} &= [N_2]^{-1} \int_{-1}^{+1} \eta(1-\eta^2)^{1/2} S_{0r}(c,\eta) P_{l+t}^{l}(\eta) d\eta \\ &= \frac{t+3}{2t+5}\left(\frac{d_{t+1}^{0n}}{2t+3} - \frac{d_{t+3}^{0n}}{2t+7}\right) + \frac{t}{2t+1}\left(\frac{d_{t-1}^{0n}}{2t-1} - \frac{d_{t+1}^{0n}}{2t+3}\right) \end{aligned} \tag{B-16}$$

$$\begin{aligned} I_{t,6}^{0n} &= [N_2]^{-1} \int_{-1}^{+1} \eta(1-\eta^2)^{3/2} S_{0r}(c,\eta) P_{l+t}^{l}(\eta) d\eta \\ &= \frac{(t+3)(t+4)(t+5)}{(2t+5)(2t+7)} \cdot \left[\frac{d_{t+1}^{0n}}{(2t+3)(2t+5)} - \frac{2d_{t+3}^{0n}}{(2t+5)(2t+9)}\right. \\ &\quad \left. + \frac{d_{t+5}^{0n}}{(2t+9)(2t+11)}\right] + \frac{3t(t+3)}{(2t+1)(2t+5)} \cdot \left[\frac{d_{t-1}^{0n}}{(2t-1)(2t+1)}\right. \\ &\quad \left. - \frac{2d_{t+1}^{0n}}{(2t+1)(2t+5)} + \frac{d_{t+3}^{0n}}{(2t+5)(2t+7)}\right] - \frac{t(t-1)(t-2)}{(2t-1)(2t+1)} \\ &\quad \times \left[\frac{d_{t-3}^{0n}}{(2t-5)(2t-3)} - \frac{2d_{t-1}^{0n}}{(2t-3)(2t+1)} + \frac{d_{t+1}^{0n}}{(2t+1)(2t+3)}\right] \end{aligned} \tag{B-17}$$

$$\begin{aligned} I_{t,7}^{0n} &= [N_2]^{-1} \int_{-1}^{+1} (1-\eta^2)^{1/2} \frac{dS_{0r}(c,\eta)}{d\eta} P_{l+t}^{l}(\eta) d\eta \\ &= d_{t+1}^{0n} \end{aligned} \tag{B-18}$$

$$\begin{aligned} I_{t,8}^{0n} &= [N_2]^{-1} \int_{-1}^{+1} (1-\eta^2)^{3/2} \frac{dS_{0r}(c,\eta)}{d\eta} P_{l+t}^{l}(\eta) d\eta \\ &= \frac{(t+3)(t+4)}{2t+5} \cdot \left(\frac{d_{t+1}^{0n}}{2t+3} - \frac{d_{t+3}^{0n}}{2t+7}\right) \\ &\quad - \frac{t(t-1)}{2t+1} \cdot \left(\frac{d_{t-1}^{0n}}{2t-1} - \frac{d_{t+1}^{0n}}{2t+3}\right) \end{aligned} \tag{B-19}$$

$$
\begin{aligned}
I_{t,9}^{0n} &= [N_2]^{-1}\int_{-1}^{+1}(1-\eta^2)^{5/2}\frac{dS_{0r}(c,\eta)}{d\eta}P_{l+t}^{l}(\eta)d\eta \\
&= I_{t,8}^{0n} - \frac{(t+3)(t+4)(t+5)}{(2t+5)(2t+7)}\cdot\Big[\frac{(t+1)d_{t+1}^{0n}}{(2t+3)(2t+5)} + \frac{1}{2t+7} \\
&\quad\times\Big(\frac{t+6}{2t+9} - \frac{t+1}{2t+5}\Big)d_{t+3}^{0n} - \frac{(t+6)d_{t+5}^{0n}}{(2t+11)(2t+9)} - \frac{t(t+3)}{2t+3} \\
&\quad\times\Big(\frac{t+4}{2t+5} - \frac{t-1}{2t+1}\Big)\cdot\Big[\frac{(t-1)d_{t-1}^{0n}}{(2t-1)(2t+1)} + \frac{1}{2t+3} \\
&\quad\times\Big(\frac{t+4}{2t+5} - \frac{t-1}{2t+1}\Big)d_{t+1}^{0n} - \frac{(t+4)d_{t+3}^{0n}}{(2t+7)(2t+5)}\Big] + \frac{t(t-1)(t-2)}{(2t+1)(2t-1)} \\
&\quad\times\Big[\frac{(t-3)d_{t-3}^{0n}}{(2t-5)(2t-3)} + \frac{1}{2t-1}\Big(\frac{t+2}{2t+1} - \frac{t-3}{2t-3}\Big)d_{t-1}^{0n} - \frac{(t+2)d_{t+1}^{0n}}{(2t+3)(2t+1)}\Big]
\end{aligned}
\tag{B-20}
$$

B.4: For $m = 0$ and $(n - m) + t = even$:

$$
I_{t,5}^{0n} = I_{t,6}^{0n} = I_{t,7}^{0n} = I_{t,8}^{0n} = I_{t,9}^{0n} = 0 \tag{B-21}
$$

$$
\begin{aligned}
I_{t,1}^{0n} &= [N_2]^{-1}\int_{-1}^{+1}(1-\eta^2)^{1/2}S_{0r}(c,\eta)P_{l+t}^{l}(\eta)d\eta \\
&= \frac{d_t^{0n}}{2t+1} - \frac{d_{t+2}^{0n}}{2t+5}
\end{aligned}
\tag{B-22}
$$

$$
\begin{aligned}
I_{t,2}^{0n} &= [N_2]^{-1}\int_{-1}^{+1}(1-\eta^2)^{3/2}S_{0r}(c,\eta)P_{l+t}^{l}(\eta)d\eta \\
&= \frac{(t+3)(t+4)}{2t+5}\Big[\frac{d_t^{0n}}{(2t+1)(2t+3)} - \frac{2d_{t+2}^{0n}}{(2t+3)(2t+7)} \\
&\quad + \frac{d_{t+4}^{0n}}{(2t+7)(2t+9)}\Big] - \frac{t(t-1)}{2t+1}\Big[\frac{d_{t-2}^{0n}}{(2t-3)(2t-1)} \\
&\quad - \frac{2d_t^{0n}}{(2t-1)(2t+3)} + \frac{d_{t+2}^{0n}}{(2t+3)(2t+5)}
\end{aligned}
\tag{B-23}
$$

$$
\begin{aligned}
I_{t,3}^{0n} &= [N_2]^{-1}\int_{-1}^{+1}(1-\eta^2)^{5/2}S_{0r}(c,\eta)P_{l+t}^{l}(\eta)d\eta \\
&= I_{t,2}^{0n} - \frac{(t+3)(t+4)(t+5)(t+6)}{(2t+5)(2t+7)(2t+9)}\cdot\left[\frac{d_{t+2}^{0n}}{(2t+5)(2t+7)}\right. \\
&\quad \left. -\frac{2d_{t+4}^{0n}}{(2t+7)(2t+11)} + \frac{d_{t+6}^{0n}}{(2t+11)(2t+13)}\right] - \frac{(t+3)(t+4)}{2t+5} \\
&\quad \times\left[\frac{(t+1)(t+5)}{(2t+5)(2t+7)} + \frac{3t}{(2t+1)(2t+5)}\right]\cdot\left[\frac{d_{t}^{0n}}{(2t+1)(2t+3)}\right. \\
&\quad \left. \times\frac{2d_{t+2}^{0n}}{(2t+3)(2t+7)} + \frac{d_{t+4}^{0n}}{(2t+7)(2t+9)}\right] - \frac{t(t-1)}{2t+1} \\
&\quad \times\left[\frac{3t(t+3)}{(2t+1)(2t+5)} - \frac{(t+2)(t-2)}{(2t+1)(2t-1)}\right]\cdot\left[\frac{d_{t-2}^{0n}}{(2t-3)(2t-1)}\right. \\
&\quad \left. -\frac{2d_{t}^{0n}}{(2t+3)(2t-1)} + \frac{d_{t+2}^{0n}}{(2t+3)(2t+5)}\right] + \frac{t(t-1)(t-2)(t-3)}{(2t+1)(2t-1)(2t-3)} \\
&\quad \times\left[\frac{d_{t-4}^{0n}}{(2t-7)(2t-5)} - \frac{2d_{t-2}^{0n}}{(2t-1)(2t-5)} + \frac{d_{t}^{0n}}{(2t+1)(2t-1)}\right]
\end{aligned}
\tag{B-24}
$$

$$
\begin{aligned}
I_{t,10}^{0n} &= [N_2]^{-1}\int_{-1}^{+1}\eta(1-\eta^2)^{1/2}\frac{dS_{0r}(c,\eta)}{d\eta}P_{l+t}^{l}(\eta)d\eta \\
&= \frac{t+3}{2t+5}d_{t+2}^{0n} + \frac{t}{2t+1}d_{t}^{0n}
\end{aligned}
\tag{B-25}
$$

$$
\begin{aligned}
I_{t,11}^{0n} &= \int_{-1}^{+1}\eta(1-\eta^2)^{3/2}\frac{dS_{0r}(c,\eta)}{d\eta}P_{l+t}^{l}(\eta)d\eta \\
&= \frac{(t+3)(t+4)(t+5)}{(2t+5)(2t+7)}\left(\frac{d_{t+2}^{0n}}{2t+5} - \frac{d_{t+4}^{0n}}{2t+9}\right. \\
&\quad + \frac{3t(t+3)}{(2t+1)(2t+5)}\left(\frac{d_{t}^{0n}}{2t+1} - \frac{d_{t+2}^{0n}}{2t+5}\right. \\
&\quad \left. - \frac{t(t-1)(t-2)}{(2t-1)(2t+1)}\left(\frac{d_{t-2}^{0n}}{2t-3} - \frac{d_{t}^{0n}}{2t+1}\right)\right)
\end{aligned}
\tag{B-26}
$$

where the normalized coefficients N_1 and N_2 are given by

$$N_1 = N_{m-1,m-1+t} = \frac{2}{2t+2m-1}\frac{(t+2m-2)!}{t!} \tag{B-27}$$

$$N_2 = N_{1,1+t} = \frac{2}{2t+3}\frac{(t+2)!}{t!} \tag{B-28}$$

Appendix C
Derivation of Far Field Expressions

C.1 The asymptotic forms of radial functions

The prolate radial functions have the asymptotic forms as

$$R_{mn}^{(1)}(c,\xi) \xrightarrow[c\xi\to\infty]{} \frac{1}{c\xi}\cos[c\xi - \frac{1}{2}(n+1)\pi] \tag{C-1}$$

$$R_{mn}^{\prime(1)}(c,\xi) \xrightarrow[c\xi\to\infty]{} -\frac{1}{c\xi^2}\cos[c\xi - \frac{1}{2}(n+1)\pi] - \frac{1}{\xi}\sin[c\xi - \frac{1}{2}(n+1)\pi] \tag{C-2}$$

$$R_{mn}^{(2)}(c,\xi) \xrightarrow[c\xi\to\infty]{} \frac{1}{c\xi}\sin[c\xi - \frac{1}{2}(n+1)\pi] \tag{C-3}$$

$$R_{mn}^{\prime(2)}(c,\xi) \xrightarrow[c\xi\to\infty]{} -\frac{1}{c\xi^2}\sin[c\xi - \frac{1}{2}(n+1)\pi] + \frac{1}{\xi}\cos[c\xi - \frac{1}{2}(n+1)\pi] \tag{C-4}$$

$$R_{mn}^{(3)}(c,\xi) \xrightarrow[c\xi\to\infty]{} R_{mn}^{(1)}(c,\xi) + iR_{mn}^{(2)}(c,\xi) = \frac{1}{c\xi}e^{i[c\xi - \frac{1}{2}(n+1)\pi]} \tag{C-5}$$

$$R_{mn}^{\prime(3)}(c,\xi) \xrightarrow[c\xi\to\infty]{} R_{mn}^{\prime(1)}(c,\xi) + iR_{mn}^{\prime(2)}(c,\xi) = -\frac{1}{\xi}(1+\frac{1}{c})e^{i[c\xi - \frac{1}{2}(n+1)\pi]} \tag{C-6}$$

C.2 The asymptotic forms of vector prolate wave functions

Substitute the asymptotic forms of the radial functions into the prolate vector wave functions in Appendix B. After some tedious manipulation, the following simplified forms can be obtained:

$$\underline{\underline{M_{\substack{e_{mn} \\ o}}^{x(3)}(c;\eta,\xi,\phi)}}$$

$$M_{\substack{e_{mn\eta} \\ o}}^{x(3)} = \frac{2S_{mn}}{d\xi}\cdot(\frac{1}{c}+1)\cdot e^{i[c\xi-\frac{1}{2}(n+1)\pi]}\ sin\varphi \begin{matrix} cos \\ sin \end{matrix} m\varphi \tag{C-7}$$

$$M_{\substack{e_{mn\varphi} \\ o}}^{x(3)} = \frac{-2\eta S_{mn}}{d\xi}\cdot(\frac{1}{c}-1)\cdot e^{i[c\xi-\frac{1}{2}(n+1)\pi]}\ cos\varphi \begin{matrix} cos \\ sin \end{matrix} m\varphi \tag{C-8}$$

$$M_{\substack{e_{mn\xi} \\ o}}^{x(3)} = \frac{2(1-\eta^2)^{\frac{1}{2}}}{cd\xi^2}\cdot[\frac{dS_{mn}}{d\eta}sin\varphi \begin{matrix} cos \\ sin \end{matrix} m\varphi + \frac{m\eta}{1-\eta^2}S_{mn}\ cos\varphi \begin{matrix} sin \\ (-1)cos \end{matrix} m\varphi]e^{i[c\xi-\frac{1}{2}(n+1)\pi]} \tag{C-9}$$

$$\underline{\underline{M_{\substack{e_{mn} \\ o}}^{y(3)}(c;\eta,\xi,\phi)}}$$

The expressions of the components are obtained from those of $M_{\substack{e_{mn} \\ o}}^{x(3)}(c;\eta,\xi,\phi)$ by replacing the factors $cos\phi$ and $sin\phi$ by $sin\phi$ and $-cos\phi$, respectively.

$$\underline{N_{\substack{e_{mn} \\ o}}^{x(3)}(c;\eta,\xi,\phi)}$$

$$N_{\substack{e_{mn}\eta \\ o}}^{x(3)} = \frac{2}{c^2 d\xi}\left\{\left[\frac{m}{\xi^2}\frac{dS_{mn}}{d\eta} + \frac{m\eta}{\xi^2(1-\eta^2)}S_{mn}\right]\cdot \sin\varphi \begin{matrix} sin \\ (-1)cos \end{matrix} m\varphi \right.$$
$$\left. -\left[(c+1)(1-\eta^2)\frac{dS_{mn}}{d\eta} + \left(c^2\eta^2 + \frac{m^2\eta}{\xi^2(1-\eta^2)}\right)\cdot S_{mn}\right]\cdot \cos\varphi \begin{matrix} cos \\ sin \end{matrix} m\varphi \right\}\cdot e^{i[c\xi - \frac{1}{2}(n+1)\pi]} \qquad \text{(C-10)}$$

$$N_{\substack{e_{mn}\varphi \\ o}}^{x(3)} = \frac{2}{c^2 d\xi}\left\{\left[\frac{\eta}{\xi^2}\frac{dS_{mn}}{d\eta} + (c^2 + \frac{m^2}{(1-\eta^2)\xi^2})S_{mn}\right]\cdot \sin\varphi \begin{matrix} cos \\ sin \end{matrix} m\varphi \right.$$
$$\left. +\left[\frac{m\eta}{\xi^2}\frac{dS_{mn}}{d\eta} + \frac{m^2\eta^2}{(1-\eta^2)\xi^2}\cdot S_{mn}\right]\cdot \cos\varphi \begin{matrix} sin \\ (-1)cos \end{matrix} m\varphi \right\}\cdot e^{i[c\xi - \frac{1}{2}(n+1)\pi]} \qquad \text{(C-11)}$$

$$N_{\substack{e_{mn}\xi \\ o}}^{x(3)} = -\frac{2}{c^2 d\xi^2}\left\{\left[\frac{\xi m^2 - (c+1)(1+\eta^2)\xi - m^2}{(1-\eta^2)^{\frac{1}{2}}\xi}\cdot S_{mn} - (c+1)\eta(1-\eta^2)^{\frac{1}{2}}\frac{dS_{mn}}{d\eta}\right]\right.$$
$$\left. \cdot \cos\varphi \begin{matrix} cos \\ sin \end{matrix} m\varphi + \frac{m + m\xi(c+1)}{(1-\eta^2)^{\frac{1}{2}}\xi}\cdot S_{mn}\cdot \sin\varphi \begin{matrix} sin \\ (-1)cos \end{matrix} m\varphi \right\}\cdot e^{i[c\xi - \frac{1}{2}(n+1)\pi]} \qquad \text{(C-12)}$$

$$\underline{N_{\substack{e_{mn} \\ o}}^{y(3)}(c;\eta,\xi,\phi)}$$

The expressions of the components are obtained from those of $N_{\substack{e_{mn} \\ o}}^{x(3)}(c;\eta,\xi,\phi)$ by replacing the factors $\cos\phi$ and $\sin\phi$ by $\sin\phi$ and $-\cos\phi$, respectively.

C.3 Far field expression

The far field expression of prolate hemi-spheroidal DRA can be obtained by substituting above expressions in C.2 into equation (3.2) through equation (3.13). The far field expressions are

$$E_\eta = \frac{-ik_2}{\pi d c_1^2 \xi}\sum_{n=0}^{\infty}\sum_{m=0}^{n}\Bigg\{(c_1^2 S_{mn} + c_1 S_{mn} + 1)\cdot e^{i[c_1\xi - \frac{1}{2}(n+1)\pi]} \cdot [A_e^{+xM}\cdot sin((m+1)\phi) - A_e^{-xM}\cdot sin((m-1)\phi) - A_o^{+xN}\cdot sin((m+1)\phi)\cdot(\rho_1+\rho_2) + A_o^{-xN}\cdot sin((m-1)\phi)\cdot(\rho_1-\rho_2)] \cdot \iiint_v \Gamma_{mn} M_x(\bar{r}')dv' \Bigg\} \quad \text{(C-13)}$$

$$E_\phi = \frac{-ik_2}{\pi d c_1^2 \xi}\sum_{n=0}^{\infty}\sum_{m=0}^{n}\Bigg\{(-c_1^2 \eta S_{mn} + c_1 \eta S_{mn} + 1)\cdot e^{i[c_1\xi - \frac{1}{2}(n+1)\pi]} \cdot [A_e^{+xM}\cdot cos((m+1)\phi) + A_e^{-xM}\cdot cos((m-1)\phi) - A_o^{+xN}\cdot cos((m+1)\phi)\cdot(\rho_3+\rho_4) + A_o^{-xN}\cdot cos((m-1)\phi)\cdot(\rho_3-\rho_4)] \cdot \iiint_v \Gamma_{mn} M_x(\bar{r}')dv' \Bigg\} \quad \text{(C-14)}$$

$$E_\xi = \frac{-ik_2}{2\pi d c_1^2 \xi^2}\sum_{n=0}^{\infty}\sum_{m=0}^{n}\Bigg\{[-c_1(1-\eta^2)^{1/2} + 2c_1 - 2]\cdot e^{i[c_1\xi - \frac{1}{2}(n+1)\pi]} \cdot [A_e^{+xM}\cdot sin((m+1)\phi)\cdot(\frac{dS_{mn}}{d\eta} + \frac{m\eta}{1-\eta^2}S_{mn}) - A_e^{-xM}\cdot sin((m-1)\phi)\cdot(\frac{dS_{mn}}{d\eta} - \frac{m\eta}{1-\eta^2}S_{mn}) - A_o^{+xN}\cdot sin((m+1)\phi)\cdot(\rho_5-\rho_6) + A_o^{-xN}\cdot sin((m-1)\phi)\cdot(\rho_5+\rho_6)] \cdot \iiint_v \Gamma_{mn} M_x(\bar{r}')dv' \Bigg\} \quad \text{(C-15)}$$

where the prime symbol denotes the source point location; M_x is the magnetic current distribution that is along x-axis. A_e^{+xM}, A_e^{-xM}, A_o^{+xN}, and A_o^{-xN} are scattering coefficients, which are already determined in section 3; Γ_{mn}, ρ_1, ρ_2, ρ_3, ρ_4, ρ_5, and ρ_6 are

$$\Gamma_{mn} = \frac{2-\delta_{m0}}{N_{mn}} \psi^{(1)}_{\substack{e_{mn} \\ o}}(c_2, \mathbf{r}') \tag{C-16}$$

$$\rho_1 = \frac{m}{\xi^2} \cdot \frac{dS_{mn}}{d\eta} + \frac{m\eta}{\xi^2(1-\eta^2)} S_{mn} \tag{C-17}$$

$$\rho_2 = (c_1+1)(1-\eta^2)\frac{dS_{mn}}{d\eta} + (c_1{}^2\eta^2 + \frac{m^2\eta}{\xi^2(1-\eta^2)} S_{mn} \tag{C-18}$$

$$\rho_3 = \frac{\eta}{\xi^2} \cdot \frac{dS_{mn}}{d\eta} + (c_1{}^2 + \frac{m^2}{\xi^2(1-\eta^2)}) S_{mn} \tag{C-19}$$

$$\rho_4 = \frac{m\eta}{\xi^2} \cdot \frac{dS_{mn}}{d\eta} + \frac{m\eta^2}{\xi^2(1-\eta^2)} S_{mn} \tag{C-20}$$

$$\rho_5 = -(c_1+1)\eta(1-\eta^2)^{\frac{1}{2}} \frac{dS_{mn}}{d\eta} + \frac{m^2(\xi-1)-(c_1+1)(1+\eta^2)\xi}{\xi^2(1-\eta^2)^{\frac{1}{2}}} S_{mn} \tag{C-21}$$

$$\rho_6 = \frac{m+m\xi(c_1+1)}{\xi(1-\eta^2)^{\frac{1}{2}}} S_{mn} \tag{C-22}$$

From equations (C-13), (C-14) and (C-15), it can be seen that the $\hat{\eta}$- and $\hat{\phi}$-components of electric field become dominant in the far field. The $\hat{\xi}$-component of electric field is very small because of the factor of $\frac{1}{\xi^2}$, and it can be ignored.

Appendix D
Tabulated Numerical Data of Spheroidal Functions

Shown and compared in Tables d.1 to d.7 are some of the numerical results computed using Matlab code and others from literatures.

Table D.1: Comparison of selected values of Eigenvalues λ_{mn} computed by Flammer, Li-Wei Li and this work.

c	(m,n)	Flammer [35]	Li-Wei li [36]	This work
1.0	(0,0)	(-1)3.1900	(-1)3.1900008	0.31900005514689
	(0,1)	(0)2.59308	(0)2.5930846	2.59308457997714
	(0,2)	(0)6.53347	(0)6.5334718	6.53347180052379
	(1,1)	(0)2.19555	(0)2.19555484	2.19554835541301
	(1,2)	(0)6.42470	(0)6.4246991	6.42469914377514
	(2,2)	(0)6.14095	(0)6.1409490	6.14094899185770
5.0	(0,0)	(0)4.19513	(0)4.1951289	4.19512887261635
	(0,1)	(1)1.291171	(1)1.2911703	12.91170324504386
	(0,2)	(1)2.017691	(1)2.0176915	20.17691472053328
	(1,1)	(0)5.35043	(0)5.3504223	5.35042229846410
	(1,2)	(1)1.464294	(1)1.4642956	14.64295624486815
	(2,2)	(0)8.74767	(0)8.7476743	8.74767425153947

Table D.2 Comparison of selected values of $S_{mn}^{(1)}(c,\eta)$ computed by Flammer, Li Wei Li and this work.

c	(m,n)	η	Flammer [35]	Li-Wei Li [36]	This work
1.0	(0,0)	0.5	(-1)9.9606	(-1)9.960611	0.96061108379212
	(0,1)		(-1)4.878	(-1)4.877753	0.48775317760058
	(0,2)		(-2)-9.876	(-2)-9.8751	-0.09875149920899
	(1,1)		(-1)8.450	(-1)8.45042	0.84504245525652
	(1,2)		(0)1.276	(0)1.276209	1.27620870646391
	(2,2)		(0)2.211	(0)2.21063	2.21063000478601
	(0,0)	1.0	(-1)8.481	(-1)8.48141	0.84814157331933
	(0,1)		(-1)9.046	(-1)9.04596	0.90459613933557
	(0,2)		(0)1.022	(0)1.022189	1.02218857040739
	(1,1)		0	0	0
	(1,2)		0	0	0
	(2,2)		0	0	0
5.0	(0,0)	0.5	(-1)5.742	(-1)5.74224	0.57422428737684
	(0,1)		(-1)3.104	(-1)3.10366	0.31036643299778
	(0,2)		(-1)3.844	(-1)3.84387	0.38438655216441
	(1,1)		(-1)5.602	(-1)5.60163	0.56016304181379
	(1,2)		(-1)8.957	(-1)8.95726	0.89572596758390
	(2,2)		(0)1.580	(0)1.580245	1.58024491766210
	(0,0)	1.0	(-2)5.024	(-2)5.0230	0.05022979252991
	(0,1)		(-2)9.161	(-2)9.1606	0.09160581033840
	(0,2)		(-1)6.018	(-1)6.01737	0.60173711860713
	(1,1)		0	0	0
	(1,2)		0	0	0
	(2,2)		0	0	0

Table D.3 Comparison of selected values of $S'^{(1)}_{mn}(c,\eta)$ computed by Zhang&Jin, Li-Wei Li and this work.

c	(m,n)	η	Zhang & Jin [37]	Li-Wei Li [36]	This work
1.0	(0,0)	0.5	(-1)-1.55623	(-1)-1.5562274	-0.15562274047848
	(0,1)		(-1)9.26953	(-1)9.2695348	0.92695348094307
	(0,2)		(0)1.576815	(0)1.5768153	1.57681528265636
	(1,1)		(-1)-6.46554	(-1)-6.4655371	-0.64655371248883
	(1,2)		(0)1.610924	(0)1.6109241	1.61092409312373
	(2,2)		(0)-3.103903	(0)-3.1039031	-3.10390311004353
	(0,0)	1.0	(-1)-2.88792	(-1)-2.8879218	-0.28879218232905
	(0,1)		(-1)7.20549	(-1)7.205408	0.72054908034118
	(0,2)		(0)2.828126	(0)2.8281258	2.82812581458354
	(1,1)		-∞	-∞	-∞
	(1,2)		-∞	-∞	-∞
	(2,2)		(0)-5.588624	(0)-5.5886245	-5.58862448342572
5.0	(0,0)	0.5	(0)-1.352776	(0)-1.3527760	-1.35277603152896
	(0,1)		(-3)-1.868	(-3)-1.8683473	-0.00186834720444
	(0,2)		(0)2.253880	(0)2.2538797	2.25387961398492
	(1,1)		(0)-1.390932	(0)-1.3909322	-1.39093219212983
	(1,2)		(-1)-1.82351	(-1)-1.8235108	-0.18235106920427
	(2,2)		(0)-4.407164	(0)-4.4071637	-4.40716378682281
	(0,0)	1.0	(-1)-5.22512	(-1)-5.2251218	-0.52251218017003
	(0,1)		(-1)5.53679	(-1)5.5367911	-0.55367910992443
	(0,2)		(0)-1.451115	(0)-1.4511146	-1.45111471943139
	(1,1)		-∞	-∞	-∞
	(1,2)		-∞	-∞	-∞
	(2,2)		(0)-1.242292	(0)-1.2422924	-1.24229244294798

Table D.4 Comparison of selected values of $R_{mn}^{(1)}(c,\xi)$ computed by Flammer, Li-Wei Li and this work.

c	(m,n)	ξ	Flammer [35]	Li-Wei Li [36]	This work
1.0	(0,0)	1.005	(-1)9.468	(-1)9.4675413	0.94675413010661
	(0,1)		(-1)3.153	(-1)3.1530632	0.31530631944421
	(0,2)		(-2)4.470	(-2)4.4699843	0.04469984508812
	(1,1)		(-2)3.270	(-2)3.2699111	0.03269911140717
	(1,2)		(-3)6.503	(-3)6.5032691	0.00650326911384
	(2,2)		(-4)6.612	(-4)6.6119132	6.6119132246e-004
	(0,0)	1.077	(-1)9.228	(-1)9.2275734	0.92275733533302
	(0,1)		(-1)3.328	(-1)3.3276892	0.33276892454286
	(0,2)		(-2)5.375	(-2)5.3727668	0.05372766940739
	(1,1)		(-1)1.287	(-1)1.2864554	0.12864554097870
	(1,2)		(-2)2.754	(-2)2.7536876	0.02753687595442
	(2,2)		(-2)1.044	(-2)1.0435256	0.01043525630813
5.0	(0,0)	1.005	(-1)5.313	(-1)5.3150158	0.53150157521257
	(0,1)		(-1)5.381	(-1)5.3812189	0.53812188654774
	(0,2)		(-1)4.952	(-1)4.9520455	0.49520458557214
	(1,1)		(-1)1.211	(-1)1.2109114	0.12109114094800
	(1,2)		(-2)9.035	(-2)9.0348283	0.09034828143914
	(2,2)		(-2)1.372	(-2)1.3718611	0.01371861106395
	(0,0)	1.077	(-1)1.869	(-1)1.8698828	0.18698828324163
	(0,1)		(-1)3.317	(-1)3.3163581	0.31363581293428
	(0,2)		(-1)3.976	(-1)3.9760946	0.39760949630322
	(1,1)		(-1)3.118	(-1)3.1169107	0.31169107001903
	(1,2)		(-1)2.803	(-1)2.8029786	0.28029785306548
	(2,2)		(-1)1.639	(-1)1.6392284	0.16392283606430

Table D.5 **Comparison of selected values of $R_{mn}^{\prime(1)}(c,\xi)$ computed by Flammer, Li-Wei Li and this work.**

c	(m,n)	ξ	Flammer [35]	Li-Wei Li [36]	This work
1.0	(0,0)	1.005	(-1)-3.242	(-1)-3.2420704	-0.3242070354076
	(0,1)		(-1)2.493	(-1)2.4924622	0.24924621817597
	(0,2)		(-1)1.224	(-1)1.2240951	0.12240951337462
	(1,1)		(0)3.271	(0)3.2714545	3.27145452188116
	(1,2)		(-1)6.575	(-1)6.5747943	0.65747942612200
	(2,2)		(-1)1.325	(-1)1.3247288	0.13247288100077
	(0,0)	1.077	(-1)3.422	(-1)3.4220489	-0.34220489171700
	(0,1)		(-1)2.357	(-1)2.3571202	0.23571201576769
	(0,2)		(-1)1.283	(-1)1.2827216	0.12827216088182
	(1,1)		(-1)8.384	(-1)8.3833553	0.83833553326184
	(1,2)		(-1)2.067	(-1)2.0673152	0.20673151792349
	(2,2)		(-1)1.389	(-1)1.3893377	0.13893377014625
5.0	(0,0)	1.005	(0)-5.696	(0)-5.6978496	-5.69784957817588
	(0,1)		(0)-3.329	(0)-3.3286265	-3.32862645265462
	(0,2)		(0)-1.230	(0)-1.2296344	-1.22963440659343
	(1,1)		(1)1.148	(1)1.1475032	11.47503186131254
	(1,2)		(0)8.774	(0)8.7739487	8.77394849601707
	(2,2)		(0)2.699	(0)2.6992089	2.69920891705825
	(0,0)	1.077	(0)-3.901	(0)-3.9024990	-3.90249900826638
	(0,1)		(0)-2.881	(0)-2.8807343	-2.88073428701833
	(0,2)		(0)-1.460	(0)-1.4595536	-1.45955369490267
	(1,1)		(-2)-2.580	(-2)-2.5861761	-0.02586176086985
	(1,2)		(-1)7.911	(-1)7.9105678	0.79105676105262
	(2,2)		(0)1.502	(0)1.5020973	1.50209730240341

Table D.6 Comparison of selected values of $R_{mn}^{(2)}(c,\xi)$ computed by Flammer, Li-Wei Li and this work.

c	(m,n)	ξ	Flammer [35]	Li-Wei Li [36]	This work
1.0	(0,0)	1.005	(0)-2.838	(0)-2.8378072	-2.83780723811360
	(0,1)		(0)-6.912	(0)-6.9118575	-6.91185750174113
	(0,2)		(1)-3.593	(1)-3.5925889	-35.92588874323741
	(1,1)		(1)-1.506	(1)-1.5055640	-15.05564000972804
	(1,2)		(1)-7.295	(1)-7.2952166	-72.95216566055947
	(2,2)		(2)-3.750	(2)-3.7497723	-3.74977223965e2
	(0,0)	1.077	(0)-1.356	(0)-1.3557080	-1.35570885304140
	(0,1)		(0)-2.920	(0)-2.9198450	-2.91984501408759
	(0,2)		(1)-1.056	(1)-1.0558461	-10.55846235872703
	(1,1)		(0)-3.432	(0)-3.4319411	-3.43194111712486
	(1,2)		(1)-1.275	(1)-1.2753532	-12.75353150221821
	(2,2)		(1)-2.156	(1)-2.1563195	-21.56319542332019
5.0	(0,0)	1.005	(-1)-3.052	(-1)-2.9785864	-0.29785863644297
	(0,1)		(-1)-4.293	(-1)-4.3050633	-0.43050632917237
	(0,2)		(-1)-7.388	(-1)-6.8154226	-0.68154230068294
	(1,1)		(-1)-9.101	(-1)-9.0913849	-0.90913849419465
	(1,2)		(0)-1.778	(0)-1.1775917	-1.17759159452534
	(2,2)		(0)-3.775	(0)-3.7497723	-3.75519370254124
	(0,0)	1.077	(-1)2.291	(-1)2.5395874	0.25395874252412
	(0,1)		(-1)1.594	(-1)1.5717657	0.15717657262933
	(0,2)		(-1)-1.340	(-2)-5.152477	-0.05152473999533
	(1,1)		(-1)-1.248	(-1)-1.2352925	-0.12352924529051
	(1,2)		(-1)-2.651	(-1)-2.6426695	-0.26426694752392
	(2,2)		(-1)-3.910	(-1)-3.9044210	-0.39044209641026

Table D.7 Comparison of selected values of $R_{mn}^{\prime(2)}(c,\xi)$ computed by Flammer, Li-Wei Li and this work.

c	(m,n)	ξ	Flammer [35]	Li-Wei Li [36]	This work
1.0	(0,0)	1.005	(2)1.063	(2)1.0633242	1.0633242286675e+2
	(0,1)		(2)3.109	(2)3.1089726	3.1089725468020e+2
	(0,2)		(3)2.133	(3)2.1331831	2.1331830724444e+3
	(1,1)		(3)1.544	(3)1.5442861	1.5442860578986e+3
	(1,2)		(3)7.963	(3)7.9630836	7.9630835695164+3
	(2,2)		(4)7.574	(4)7.5736490	7.5736490437915+4
	(0,0)	1.077	(0)7.279	(0)7.2789540	7.27895039446102
	(0,1)		(1)1.672	(1)1.6721910	16.72191032381964
	(0,2)		(1)9.116	(1)9.1171233	91.17123337841893
	(1,1)		(1)2.624	(1)2.6239981	26.23998046516048
	(1,2)		(2)1.313	(2)1.3132273	1.3132273059612e+2
	(2,2)		(2)3.121	(2)3.1210720	3.1210720043946e+2
5.0	(0,0)	1.005	(1)4.082	(1)4.0728531	40.7285310219949
	(0,1)		(1)3.973	(1)3.9736573	39.73657265798575
	(0,2)		(1)4.212	(1)4.1978593	41.97895810422797
	(1,1)		(1)7.849	(1)7.8599734	78.59973427066133
	(1,2)		(2)1.064	(2)1.0645467	1.0645467224624e+2
	(2,2)		(2)7.153	(2)7.1538382	7.1538381803708e+2
	(0,0)	1.077	(0)1.909	(0)1.3876869	1.38768690964025
	(0,1)		(0)2.523	(0)2.5436221	2.54362212146930
	(0,2)		(0)3.637	(0)3.334322	3.33432191815735
	(1,1)		(0)4.022	(0)4.0224111	4.02241109274360
	(1,2)		(0)3.713	(0)3.7157073	3.71570729779921
	(2,2)		(0)4.045	(0)4.0511312	4.05113119033999

References

[1] S. A. Long, M. W. McAllister, and L. C. Shen, "The resonant cylindrical dielectric cavity antenna," *IEEE Trans. On Antenna Propagat.*, AP-31, pp. 406-412, 1983.

[2] M. W. McAllister, S. A. Long, and G. L. Conway, "Rectangular dielectric-resonator antenna," *Electron, Letters,* 19, pp. 218-219, 1983.

[3] M. W. McAllister and S. A. Long, "Resonant hemispherical dielectric antenna," *Electron, Letters,* 20, pp. 657-659, 1984.

[4] A. A. Kishk, M. R. Zunoubi, and D. Kajfez, "A numerical study of a dielectric dis antenna above grounded dielectric substrate," *IEEE Trans. On Antenna Propagat.*, AP-41, No. 6, pp. 813-821, 1993.

[5] A. A. Kishk, A. Ittipiboon; Y. M. M. Antar and M. Cuhaci, " Dielectric resonator antennas fed by a slot in the ground plane of a microstripline," *Antennas and Propagation, 1993., Eighth International Conference on*, vol. 1, pp. 540-543, 1993.

[6] K. W. Leung, K. M. Luk, K. Y. Chow and E. K. N. Yung, "Bandwidth enhancement of dielectric resonator antenna by loading a low-profile dielectric disk of very high permittivity," *Electronics Letters* , vol. 33, pp. 725-726, April 1997.

[7] M. T. Lee, , K. M. Luk, E. K. N. Yung and K. W. Leung, "Circularly polarised dielectric resonator antenna with a microstrip feed," *Microwave Conference, Asia Pacific 1999,* vol. 3, pp. 722-723, 1999.

[8] K. W. Leung, W. C. Wong, K. M. Luk and E. K. N. Yung, "Circular-polarised dielectric resonator antenna excited by dual conformal strips," *Electronics Letters*, vol. 36, pp. 484-486, 2000.

[9] W. C. Wong, K. W. Leung, K. M. Luk and E. K. N. Yung, "Circular-polarized dielectric resonator antenna excited by dual conformal strips," *Antennas and Propagation Society International Symposium, 2000. IEEE*, vol.2, pp.1021-1025, July 2000.

[10] R. K. Mongia, A. Ittipiboon, Y. M. M. Antar, P. Bhartia and M. Cuhaci, "A half-split cylindrical dielectric resonator antenna using slot-coupling," *Microwave and Guided Wave Letters, IEEE* vol. 3, issue 2, Feb. 1993.

[11] K.W. Leung, K. M. Luk, K. Y. A. Lai and D. Lin, "Theory and experiment of a coaxial probe fed hemispherical dielectric resonator antenna," *IEEE Trans. On Antenna Propagat.* , vol. 41, pp. 1390-1398, Oct. 1993.

[12] K.W. Leung, K. K. Tse, K. M. Luk, and E. K. N. Yung, "Cross-polarization haracteristics of a probe-fed hemispherical dielectric resonator antenna,"*IEEE Trans. On Antenna Propagat.* , vol. 47, pp. 1228-1230, July 1999.

[13] K. W. Leung, K. Y. A. Lai, K. M. Luk and D. Lin, "Input impedance of aperture coupled hemispherical dielectric resonator antenna," *Electronics Letters* , vol. 29, pp. 1165-1167, June 1993.

[14] A. A. Kishk, G. Zhou and A. W. Glisson, "Analysis of dielectric-resonator antennas with emphasis on hemispherical structures," *Antennas and Propagation Magazine, IEEE* , vol. 36 , pp. 20-31, April 1994.

[15] M. Salameh, Y. M. M. Antar and G. Seguin, "Coplanar-waveguide-fed slot-coupled rectangular dielectric resonator antenna," *IEEE Trans. On Antenna Propagat.*, vol. 50 , pp. 1415-1419, Oct. 2002.

[16] M. B. Oliver, Y. M. M. Antar, R. K. Mongia and A Ittipiboon, "Circularly polarised rectangular dielectric resonator antenna," *Electronics Letters* ,vol. 31, pp. 418-419, March 1995.

[17] A. A. Kishk, "Wide-band truncated tetrahedron dielectric resonator antenna excited by a coaxial probe," *IEEE Trans. On Antenna Propagat.* Vol. 51, pp. 2913-2917, Oct. 2003.

[18] H. Y. Lo, K. W. Leung, K. M. Luk and E. K. N. Yung, "Low profile equilateral-triangular dielectric resonator antenna of very high permittivity," *Electronics Letters* , Vol. 35 , Issue: 25 , pp. 2164-2166 Dec. 1999

[19] L. J. Chu and J. A. Stratton, "Steady-state solutions of electromagnetic field problems: III. Forced oscillations of a prolate spheroid." *J. Appl. Phys.*, vol. 12, pp. 241-248, 1941.

[20] S. A. Schelkunoff, *Advanced Antenna Theory*. New York: Wiley, 1952.

[21] W. L. Weeks, *Electromagnetic Theory for Engineering Application*. New York: McGraw-Hill, 1964.

[22] L. Jen and C. S. Hu, "Spheroidal wave functions of large frequency parameters $c = kf$ and the radiation fields of a metallic prolate spheroid excited by any circumferential slot." *IEEE Trans. On Antenna Propagat.*, vol. AP-31, pp. 382-389, 1983.

[23] M. Zhang and A. R. Sebak, "Radiation characteristics of a slot antenna on a conducting prolate spheroid." *Can. J. Phys.*, vol. 75, pp. 376-385, 1997.

[24] M. Taguchi, S. Nonaka, and K. Tanaka, "Analysis of oblate spheroidal antenna." in *Proc. Antennas and Propogation Society International Symposium,* vol. 2, pp. 968-971. 1993.

[25] S. Asano and G. Yamamoto, "Light scattering by a spheroidal particle." *Appl. Opt.,* vol. 14, pp.29-49, 1975.

[26] B. P. Sinha and R. H. MacPhie, "Electromagnetic scattering by prolate spheroids for plane waves with arbitrary polarization and angle of incidence." *Radio Sci.,* vol. 12, pp. 171-184, 1977.

[27] B. P. Sinha and R. H. MacPhie, " Electromagnetic plane wave scattering by a system of two parallel conducting spheroids." *IEEE Trans. On Antenna Propagat.*, vol.. AP-31, pp. 294-304, 1983.

[28] M. F. R. Cooray and I. R. Ciric, "Electromagnetic wave scattering by a system of two spheroids of arbitrary orientation." *IEEE Trans. On Antenna Propagat.*, vol.. AP-37, pp. 608-618, 1989.

[29] M. F. R. Cooray and I. R. Ciric, "Scattering of electromagnetic waves by a system of two dielectric spheroids of arbitrary orientation." *IEEE Trans. On Antenna Propagat.*, vol.. AP-39, pp. 680-684, 1991.

[30] N. K. Uzunoglu and E. A. Angelikas, "Field distributions in a three-layer prolate spheroidal human body model for a loop antenna irradiation." *IEEE Trans. On Antenna Propagat.*, vol. AP-35, pp. 1180-1185, 1987.

[31] M. F. Iskander, P. W. Barber, C. H. Durney, and H. Massoudi, "Irradiation of prolate spheroidal models of humans in the near field of a short electric dipole." *IEEE Trans. Microwave Theory Tech.,* vol. 49, pp. 524-531, 2001.

[32] A. Lakhtakia, M. F. Iskander, C. H. Durney, and H. Massoudi, "Irradiation of prolate spheroidal models of humans and animals in the near field of a small loop antenna." *Radio Sci.,* vol. 17, pp. 77-84, 1982.

[33] R. Ruppin, "Calculation of electromagnetic energy absorption in prolate spheroids by the poit matching method." *IEEE Trans. Microwave Theory Tech.,* vol. MTT-26, pp. 87-90, 1978.

[34] J. A. Stratton, P. M. Morse, L. J. Chu, J. D. C. Little, and F. J. Corbato, *Spheroidal Wave Function,* New York: 1956.

[35] C. Flammer, *Spheroidal Wave Functions*, Stanford, CA: Stanford University Press, 1957.

[36] Le-Wei Li, X.K. Kang and M.S. Leong, *Spheroidal Wave Functions in Electromagnetic Theory,* John Wiley & Sons, Inc., 2002.

[37] Shanjie Zhang and Jianming Jin, *Computation of special functions*, John Wiley & Sons, INC., 1996.

[38] T. Do-Nhat and R. H. Macphie, "Accurate values of prolate spheroidal radial functions of the second kind." *Can. J. Phys.*, vol.75, pp. 671-675, 1997.

[39] W. W. Hansen, "A new type of expansion in radiation problems." *Phys. Rev.,* vol. 47, pp. 139-143, 1935.

[40] W. W. Hansen, "Directional characteristics of any antenna over a plane earth." *J. Appl. Phys.,* vol. 7, pp. 460-465, 1936.

[41] W. W. Hansen, "Transformations useful in certain antenna calculations." *J. Appl. Phys.,* vol. 8, pp. 282-286, 1937.

[42] J. A. Stratton, *Eletromagnetic Theory*, New York: McGraw-Hill, 1941.

[43] C. T. Tai, *Dyadic Green's Functions in Electromagnetic Theory*, 2nd ed. Piscataway, NJ: IEEE Press, 1994.

[44] Le-Wei Li, M.S. Leong, P-S Kooi, and T-S Yeo, "Sheroidal vector wave function expansion of dyadic Green's functions for a dielectric spheoid." *IEEE Trans. On Antenna Propagat.*, vol. 49, pp. 645-659, April 2001.

[45] C. A. Balanis, *Antenna Theory: Analysis and Design*, John Wiley & Sons, INC., 1996.

[46] A. J. Giarola, "Dyadic Green's functions in the prolate spheroidal coordinate systems." In 1995 IEEE APS International Symposium Digest, Newport Beach, CA, 1995, vol.2, pp. 826-829.

[47] J. T. St. Martin,Y. M. M. Antar, A. A. Kishk, A. Ittipiboon, and M. Cuhaci, "Dielectric-resonator antenna using aperture coupling," *Electronics Letters*, 26, No. 24, pp. 2015-2016, 1990.

[48] R. Kranenburg and S. A. Long, "Microstrip transmission line excitation of dielectric-resonator antennas," *Electronics Letters*, 24, No. 18, pp.1156-1157, 1988.

[49] R. Kranenburg, S. A. Long, and J. T. Williams, "Coplanar waveguide excitation of dielectric-resonator antennas," *IEEE Trans. On Antenna Propagat.*, AP-39, No. 1, pp 119-122,1991.